Technische Universität Dortmund

Fakultät für Chemie

Dissertation

zur Erlangung des akademischen Grades eines

Doktors der Naturwissenschaften

Imaging EphA3 Receptor Tyrosine Kinase Substrate Interaction

vorgelegt von

Jian Hou

aus Hunan, China

November 2012, Dortmund

1. Gutachter: Prof. Dr. Philippe I.H. Bastiaens

2. Gutachter: Prof. Dr. Roland Winter

Erklärung/Declaration

Die vorliegende Arbeit wurde in der Zeit von September 2007 bis September 2012 am Max-Planck-Institut für molekulare Physiologie in Dortmund unter der Anleitung von Prof. Dr. Philippe I.H. Bastiaens durchgeführt.

Hiermit versichere ich an Eides statt, dass ich die vorliegende Arbeit selbständig und nur mit den angegebenen Hilfsmitteln angefertigt habe

The present work was accomplished from September 2007 to September 2012 at Max-Planck-Institute for molecular physiology in Dortmund under the guidance of Prof. Dr. Philippe I.H. Bastiaens.

I hereby declare that I performed the work presented independently and did not use any other but the indicated aids.

Dortmund, November 2012

Jian Hou

Content

Abstract

Receptor tyrosine kinases (RTKs) function as key signaling molecules to influence several physiological processes such as cell growth, survival and migration. Crystal structure and biochemical evidence suggests that the kinase activity of some RTKs, like the Eph RTK family, is affected by the phosphorylation of several key tyrosine residues in the activation loop (AL) of the tyrosine kinase domain and in the conserved juxtamembrane segment (JMS). However, in living cells, little is known about this regulatory mechanism in which tyrosine phosphorylation affects the catalytic activity and substrate accessibility of RTKs in both space and time.

In this thesis, we used the EphA3 RTK as an example to investigate the JMS auto-inhibition involved in the Eph RTK activity regulatory mechanism. To achieve this, a generic cellular EphA3 RTK substrate interaction-imaging assay was developed that is based on Förster Resonance Energy Transfer as measured by Fluorescence Lifetime Imaging Microscopy (FRET-FLIM). A high affinity EphA3 peptide substrate was applied to increase the probability of kinase-substrate complexes forming. Using this assay, it was possible to quantitatively investigate the formation of steady-state enzyme-substrate (ES) complexes between the purified EphA3 catalytic domain fused to mCitrine and the Cy3.5 labeled peptide substrate. A kinase/phosphatase reaction cycle could be reconstituted that gave rise to stable ES-intermediates as measured by FRET-FLIM.

By using this ES imaging approach, EphA3 RTK (WT)-substrate interactions could be observed in EphA3-mCitrine expressing quiescent Cos-7 cells that had been microinjected with the Cy3.5-substrate. This suggests that a population of EphA3 receptors exists with a temporarily relieved JMS auto-repression in the absence of ephrin-A5 ligands. Stimulation with soluble ephrin-A5 ligands led to a detectable increase in ES-intermediates, that pointed

to an autocatalytic phosphorylation mechanism of JMS auto-repression relieve. To further study the role of JMS tyrosine phosphorylation on active site accessibility, the ES imaging approach was applied to analyze the active site accessibility of JMS regulation deficient mutants (MTs). Different substrate accessibilities were observed for these JMS regulation-deficient mutants (MTs), which revealed a possible function of JMS tyrosine phosphorylation in the regulation of the EphA3 RTK active site accessibility in living cells.

In this work, a generic living cell compatible FRET-FLIM approach has been developed that allows direct observation of kinase-substrate interactions and helps to elucidate conformational dynamics of EphA3 RTK in living cells. In principle, this assay could also be used to quantitatively address conformational dynamics of other RTKs in living cells.

Zusammenfassung

Rezeptortyrosinkinasen (RTKs) fungieren als Schlüsselmoleküle in der Signalübertragung und beeinflussen dadurch mehrere physiologische Prozesse der Zelle, wie beispielsweise Wachstum, Überleben und Migration. Kristallstrukturen wie auch biochemische Untersuchungen deuten darauf hin, dass die Aktivität einiger RTKs – darunter auch die Eph-RTKs – durch die Phosphorylierung mehrerer Tyrosinreste innerhalb des *activation loops* (AL) der Tyrosinkinasedomäne als auch innerhalb des konservierten Juxtamembransegment (JMS) gesteuert wird. Wie der RTK-Regulationsmechanismus durch Phosphorylierung in lebenden Zellen abläuft ist bis heute jedoch noch kaum bekannt. Ebenso wenig wurde bis jetzt der Effekt von Tyrosinphosphorylierungsreaktionen auf die katalytische Aktivität und die Substratzugänglichkeit von RTKs räumlich oder zeitlich quantifiziert.

In dieser Arbeit wurde am Beispiel der EphA3-RTK untersucht, welchen Einfluss die Autoinhibierung des JMS auf Aktivität und Regulation von Eph-RTKs hat. Dazu wurde ein allgemeiner Zell-Imaging Assay zur Messung der Interaktion der EphA3-Kinase mit ihrem Substrat entwickelt, welcher auf Förster-Resonanzenergietransfer (FRET) beruht und mithilfe von Fluoreszenzlebensdauer-Mikroskopie (FLIM) gemessen wurde. Um die Wahrscheinlichkeit der Bildung des Kinase-Substrat-Komplexes zu erhöhen, wurde ein hochaffines EphA3-Peptidsubtrat verwendet. Mithilfe dieses Assay war es möglich, quantitativ die Bildung des Fließgleichgewichts (*steady-state*) des Enzym-Substrat-Komplexes (ES) zwischen der aufgereinigten und mCitrine-markierten EphA3-Kinasedomäne und des Cy3.5-markiertem Substratpeptids zu erforschen. Auch unterschiedliche Phosphorylierungsstadien des Kinase/Phosphatase-Zyklus konnten mithilfe von FLIM-FRET beobachtet und ihr jeweiliger *steady-state* erforscht werden.

Des Weiteren war es durch diesen ES-Assay möglich, *steady-state*-Interaktionen von EphA3-RTK (WT) in lebenden Zellen zu untersuchen, indem unstimulierte Cos7-Zellen sowohl transient mit EphA3-mCitrine transfiziert als auch mit dem Cy3.5-markiertem Substratpeptid mikroinjiziert wurden. Daraus erschloss sich, dass bereits eine Population des EphA3-Rezeptors existiert, welche in Abwesenheit ihres ephrinA5-Liganden eine zeitweilig aufgehobene JMS Autorepression aufweisen. Stimulation mit freiem ephrinA5 führte zu einer detektierbaren Erhöhung des ES-Komplexes, was auf einen autokatalytischen Phosphorylierungsmechanismus des JMS hindeutet, welcher die Autorepression steuert. Zur weiteren Untersuchung der JMS-Tyrosinphosphorylierung auf die Zugänglichkeit des aktiven Zentrums, wurde der ES-Assay mit einer JMS-regulationsdefizienten Mutante (MT) durchgeführt. Die dabei gemachten Beobachtungen unterstreichen die These einer Regulation von EphA3 RTK durch die Tyrosinphosphorylierung des JMS in lebenden Zellen.

In dieser Arbeit wurde ein *in vivo*-kompatibler FLIM-FRET-Assay entwickelt, welcher die direkte Visualisierung von Kinase-Substrat-Interkationen ermöglicht und somit dazu beiträgt, das dynamische Verhalten von EphA3-RTKs in lebenden Zellen aufzuklären. Im Prinzip kann dieser Assay auch für die quantitative Analyse der Aktivitätsdynamiken anderer RTKs verwendet werden.

1 Introduction

Signaling pathways in living cells are organized in space and time. Their complexities are derived from a number of multilayered and interconnected regulatory mechanisms, such as post-translational modifications (PTMs) of proteins (Davis, Walker et al. 2008; Deribe, Pawson et al. 2010). In nature, there are various protein PTMs including the addition of simple chemical groups (phosphate, acetyl, methyl groups), more complex groups (sugars, lipids) and small polypeptides (ubiquitin, ubiquitin-like proteins). The covalent attachment of a phosphate group to proteins, also known as phosphorylation, remains the most dominant and best studied PTM occurring in living cells (Westheimer 1987; Deribe, Pawson et al. 2010).

The discovery of the reversible phosphorylation of protein as a regulatory mechanism began in the mid 1950's with the revolutionary work of Krebs and Fischer on glycogen phosphorylase kinase and phosphatase (Krebs and Fischer 1956; Krebs and Beavo 1979). This was followed by the identification of large amounts of serine/threonine protein kinases, further reiterating the fact that protein phosphorylation is a key step within a wide range of cellular events.

The specific phosphorylation of tyrosine residues was first identified by Tony Hunter while exploring the biochemical properties of the polyoma T antigen (Eckhart, Hutchinson et al. 1979; Hunter and Sefton 1980). Since then, tyrosine phosphorylation has been intensively investigated. Tyrosine phosphorylation dependent signaling pathways play a vital role in many cell-cell communication events, including those that regulate proliferation, differentiation and development, cell adhesion and retraction (Hunter 2009). A detailed explanation of the function of tyrosine kinases will be addressed in the following sections.

1.1 Tyrosine kinases

Protein tyrosine kinases (PTKs) are enzymes that are responsible for catalyzing the transfer of the γ–phosphate of magnesium adenosine triphosphate (MgATP) to the hydroxyl group of a tyrosine residue in a protein substrate. Of the approximately 2000 kinases found so far in the human genome, more than 90 are PTKs (Hunter 2009). According to previous reports, 51 out of the 90 tyrosine kinases are related to cancer either through mutation or abnormal expression (Hunter 2009). Tyrosine kinases are divided into two subclasses: receptor tyrosine kinases (RTKs), which are investigated in this thesis, and non-receptor tyrosine kinases (NRTKs). In general, RTKs possess a ligand binding domain in the extracellular region, a single-pass transmembrane helix, a cytoplasmic region that contains the protein tyrosine kinase (PTK) domain plus additional carboxyl (C-) terminal and juxtamembrane regulatory regions (Lemmon and Schlessinger 2010). RTKs can be activated through binding of their extracellular domain to certain protein ligands, such as growth factors and cytokines. Non-receptor tyrosine kinases lack a transmembrane domain; most of them are soluble intracellular proteins, but some of them attach to membranes via a membrane targeting posttranslational modification, for instance, c-Src is myristoylated at the N terminus, and can act as the catalytic subunit for receptors that lack their own catalytic domain (Hunter 2009; Lemmon and Schlessinger 2010; Patwardhan and Resh 2011).

1.1.1 Receptor tyrosine kinase subfamilies

Humans have 58 known RTKs, which are classified into 20 subfamilies (Figure 1.1), including the receptors for insulin, epidermal growth factor (EGF), fibroblast growth factor (FGF), platelet-derived growth factor (PDGF), vascular endothelial growth factor (VEGF), nerve growth factor (NGF), as well as the more recently identified and largest subfamily of RTKs, the Eph receptors (Hubbard and Till 2000; Lemmon and Schlessinger 2010). Four of

these RTKs are reported to lack catalytic activity (e.g. ErbB3) (Hunter 2009). The molecular mechanisms implicated in the activation of RTKs share common principles among the families but differ remarkably in their details. The activation of approximately half the RTK families (Figure 1.1) are thought to be well understood, but more biochemical and cell biological studies are needed to complement the picture. This encouraged us to establish the fluorescent imaging assay of kinase activity in this work. Below, I give an overview of RTK activity regulatory mechanisms that are under investigation in this thesis.

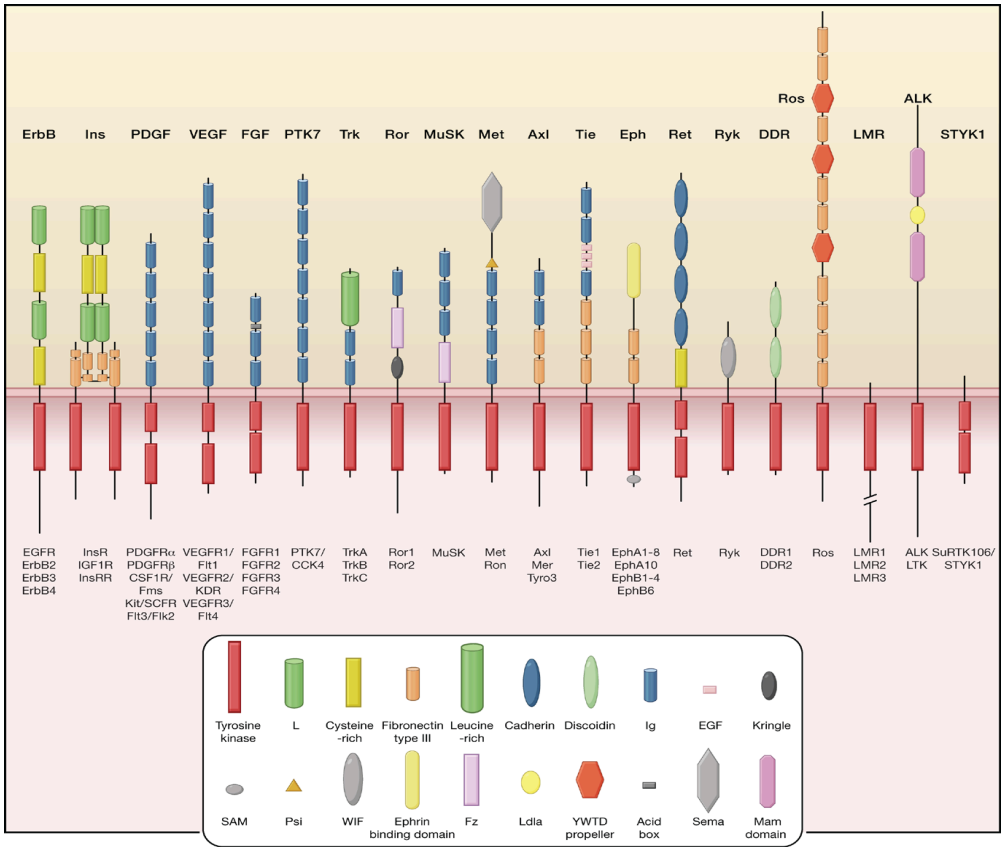

Figure 1.1 Schematic diagram of the domain organization for RTKs, adapted from (Lemmon and Schlessinger 2010). Human RTKs consist of 20 subfamilies, shown here with the family members listed under each receptor. The RTKs are divided into two parts by the horizontal line: the extracellular (top) and the cytoplasmic (bottom) part of the receptors. The legend of the domain type is on the bottom of the panel. The lengths of the receptors as indicated are only approximately to scale.

1.1.2 Structure and catalytic mechanism of the protein kinase

The first determination of the kinase structure in a fully active form was that of the cyclic adenosine monophosphate (cAMP) dependent protein kinase (cAPK) catalytic subunit by the pioneering work of Susan Taylor and colleagues (Knighton, Zheng et al. 1991). This protein serine threonine kinase (PSK), cAPK, contains a catalytic domain with a bi-lobal organization and a deep cleft between the two lobes. The smaller amino-terminal lobe (N-lobe) that consists of mainly anti-parallel β-sheets constitutes an unusual nucleotide-binding motif. The larger lobe (C-lobe), in contrast, is predominantly α-helical, with a single β-sheet at the domain interface and is primarily involved in peptide recognition and catalysis. The protein substrate and Mg-ATP bind at the cleft between two lobes (Knighton, Zheng et al. 1991; McDonald, Murray-Rust et al. 1995).

A few years later, the first insight into the catalytic mechanism of tyrosine kinases was gained by solving the domain structure of insulin receptor tyrosine kinase (IRK). This allowed structural features of PSK and PTK to be compared. Similar to cAPK, IRK also consisted of the characteristic bi-lobed protein kinase architecture. The N-lobe comprises a twisted β-sheet of five antiparallel β-strands and one α-helix and the larger C-lobe comprises eight α-helices and four β-strands (Hubbard, Wei et al. 1994). The N-terminal ATP binding lobes of IRK and cAPK show conserved features whereas significant differences are found in the activation loop in the larger C-lobe (Taylor, Radzio-Andzelm et al. 1995). A closer comparison of PTKs and PSKs indicates that PTKs have a deeper catalytic cleft than PSKs so that a Tyr residue can cross over the distance between the peptide backbone and γ-phosphate of ATP, whereas smaller side groups of Ser and Thr residues cannot. This consequently results in the protein kinase tyrosine or serine/threonine specificity (Hubbard, Wei et al. 1994; Taylor, Radzio-Andzelm et al. 1995; Ubersax and Ferrell Jr 2007).

The reported c-Src kinase crystal structure further proved the common catalytic mechanism of protein kinases (Xu, Harrison et al. 1997). The tyrosine kinase catalytic site lies in a cleft between two lobes. These lobes move relative toward each other opening or closing the cleft. In the open form, ATP can access the catalytic site and ADP can be released; the closed form is necessary to bring tyrosine residues into the catalytically active state (Roskoski 2004).

The structural studies about cAPK suggested that several key residues near the site of phosphoryl transfer might play an important role in catalytic function. As shown in Figure 1.2, Asp-184 interacts with the essential Mg^{2+}, which chelates the β- and γ-phosphates of ATP and may position the terminal phosphate for direct transfer to the hydroxyl acceptor or mask the charge of γ-phosphate. Lys-72 will further interact with α- and β-phosphates of ATP and facilitate phosphoryl group transfer without influencing ATP binding. Asp-166 may direct the hydroxyl group to attack the γ-phosphate of ATP. Some other residues like Lys-168 and Thr-201 are also involved in forming the P+1 binding cleft (Adams 2001).

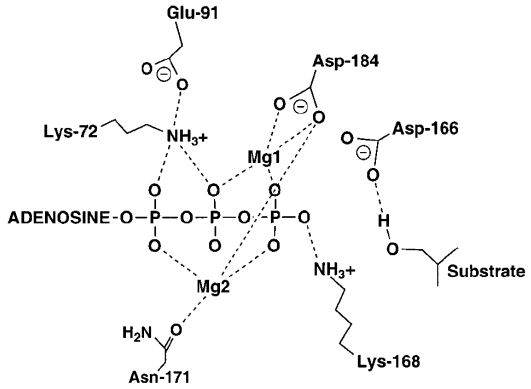

Figure 1.2 Key residue interactions in the active site of cAPK, adapted from (Adams 2001). This diagram is based on the cAPK ternary complex with ATP and PKI (peptide inhibitor) and a binary complex of PKA with a substrate peptide.

According to the apo IRK structure, Hubbard et. al also proposed a novel *cis*-inhibition *trans*-activation mechanism. The tyrosine at position 1162 plays a key role in insulin receptor kinase activation. When Tyr1162 occupies the active site, both substrate and ATP-binding site are inaccessible. The binding of insulin to the receptor triggers the conformational change, thus *trans*-autophosphorylation can occur when Tyr1162 is flipped out. In consequence, the tyrosine on the activation loop is phosphorylated and the equilibrium is shifted towards a non-inhibition stage with a significantly increased kinase activity (Hubbard, Wei et al. 1994; Hubbard and Till 2000).

1.2 Regulation of protein tyrosine phosphorylation

The fine-tuned cellular equilibrium of protein tyrosine phosphorylation is maintained by the opposing action of protein tyrosine kinases (PTKs) and protein tyrosine phosphatases (PTPs) that catalyze phosphorylation and dephosphorylation, respectively. The realization that disrupting the equilibrium of cellular tyrosine phosphorylation causes a wide range of human diseases vividly exemplifies the importance of tightly controlling the activities of both PTKs and PTPs (Tiganis and Bennett 2007). To achieve this equilibrium, kinases and phosphatases are regulated at both protein and activity levels by a range of mechanisms. At the protein level, they are negatively regulated by the E3 ubiquitin ligase, which leads to protein ubiquitylation and subsequent degradation by the proteasome. Their activity can be modulated, in other words they can be activated or inactivated reversibly (case by case differently) via other kinases/phosphatases.

Furthermore, the localization of RTKs and PTPs was also implied in the regulation of tyrosine phosphorylation both in space and time (Grecco, Schmick et al. 2011). In living cells, upon ligand stimulation, plasma membrane anchored RTKs produce the phosphorylated soluble protein tyrosine substrates in absence of PTP activity near the

plasma membrane region. Those pTyr-substrates diffuse towards the cytoplasm where they can be dephosphorylated by the cytosolic PTPs and generate the protein substrate phosphorylation flux. In this thesis, the cyclic reaction-diffusion system is investigated with a novel fluorescent kinase activity-imaging assay.

1.2.1 Tyrosine phosphatases

Tyrosine-specific protein phosphatases catalyze the removal of a phosphate group attached to a tyrosine residue. The first PTP was characterized in 1988 and a recent report suggested that a total of 107 PTPs are encoded in the human genome (Ostman, Hellberg et al. 2006). In general, PTPs are classified into three sub-families: classical PTPs, dual specificity PTPs (DSPs) and low molecular weight PTPs (LMW-PTPs) (Purushottam, Nai-Mu et al. 2005). Classical PTPs comprise the largest subfamily of PTPs and are further divided into receptor-like group and non-receptor group.

1.2.1.1 Protein tyrosine phosphatase structure and function

The dynamics of RTKs activity are regulated by the opposing PTP activity. The three-dimensional structures of more than 20 PTPs have been reported, which extended our understanding of the mechanism of PTP catalysis and substrate recognition. The PTPs are composed of β-barrels flanked by α-helices on both sides. The diversity in structure within the PTP family mainly results from the variety of non-catalytic sequences attached to the N- or C-terminus of the catalytic domain, such as SH2 domains, PDZ domains, and extracellular ligand binding domains (Barford, Flint et al. 1994). Despite the diversity in amino acid sequences and the variation in substrate specificity, their catalytic domains share some structural features that are crucial for catalysis among all PTPs, including the active site P-loop formed by the $C(X)_5R$ sequence motif and the general acid-containing surface loop (Zhang 2002).

PTPs share a common catalytic mechanism, so that the one for PTP1B is likely representative for most PTPs. The pTyr residue of the substrate is stabilized by hydrogen bonds to the residues of the phosphate-binding loop (P-loop) and a highly conserved arginine group. The bound phosphate is further stabilized by a nearby α-helix dipole, located amino-terminal to the P-loop, and the active site arginine (Zhang 2002). The substrate binding consequently promotes a conformational change of the WPD loop (a catalytically essential loop region), which brings Asp181 closely to the substrate and forms a hydrogen bond with the phenolic oxygen atom of pTyr to provide the general acid function (Zhang 2002; Bialy and Waldmann 2005). The key step of covalent catalysis is a nucleophilic attack by a deprotonated cysteine residue (Cys215), which results in the formation of a thiophosphoryl enzyme intermediate. Mutagenesis evidence has indicated that substitution of the active-site cysteine totally abolishes enzymatic activity (Zhang 2002). It has been shown now in several cases that the activation of RTK produces hydrogen peroxide which can inhibit PTPs by reversible oxidation of reactive cysteines in the catalytic cleft, and therefore provides a negative feed back loop (Grecco, Schmick et al. 2011).

Furthermore, the acidic Asp181 stabilizes the formation of a negative charge by protonation. In the second step, aspartic acid plays the role of a general base by deprotonating the water molecule, which attacks the thiophosphoryl intermediate to release the free phosphate and regenerate the active enzyme (Bialy and Waldmann 2005; Purushottam, Nai-Mu et al. 2005). Mutation of the critical aspartate residue (Asp181) in the WPD loop of PTP1B to alanine (D-A substrate trapping mutant) resulted in the dramatic decrease in k_{cat} without affecting the K_m for the peptide substrate. Therefore, this mutant has been applied in PTP substrate identification and inhibitor screening (Tiganis and Bennett 2007).

1.2.1.2 Phosphatase inhibitors

One way to regulate PTP activity is to block its catalysis by adding inhibitors, which is applied in this work to modulate the tyrosine phosphorylation equilibrium. The PTP catalytic site is highly conserved, making it difficult to obtain selective PTP inhibitors. Futhermore, a single PTP may regulate multiple signaling pathways, or a key pathway may be controlled by several PTPs (Zhang 2002). Thus, targeting a particular PTP may give rise to unwanted side effects or modulating a particular pathway may need targeting of several PTPs (Purushottam, Nai-Mu et al. 2005).

Structure-based design together with a library screening approach was used to identify highly potent and selective PTP inhibitors. The active sites of PTPs contain two negative charges at physiological pH to accommodate pTyr. Most of active-site-directed PTP inhibitors reported to date are non-hydrolyzable pTyr mimics possessing a high charge density to serve as competitive inhibitors (Vintonyak, Antonchick et al. 2009). However, this conserved mechanism reduces selectivity and often causes the potent inhibition of multiple phosphatases. Besides, such molecules generally show limited cell membrane permeability, which restrict their bioavailability for small-molecule therapeutics.

To overcome the current limitations, several small-molecule inhibitors that occupy the allosteric site and stabilize an inactive conformation of PTP1B were developed by researchers at Sunesis Pharmaceuticals in 2004 (Wiesmann, Barr et al. 2004). Compared to the pTyr binding site, the allosteric site is not well conserved among phosphatases and is less charged, which provides a promising strategy for the design of potent and specific PTP inhibitors with acceptable pharmacological properties (Zhang and Zhang 2007).

In this work, we are interested in generating strong perturbations to cyclic phosphorylation reaction by RTKs and PTPs. Generic PTP inhibitors like vanadate and pervanadate (the

complexes of vanadate with hydrogen peroxide) are used for this purpose. Vanadate has been known as a competitive inhibitor for the protein-tyrosine phosphatase, in contrast, pervanadate inhibits PTPs by irreversibly oxidizing the catalytic cysteine of PTPs (Huyer, Liu et al. 1997). Common buffer ingredients such as EDTA and reducing agent can affect these inhibitors' potencies so that the application of these inhibitors in assays should be conducted carefully.

1.2.2 Regulatory mechanisms of receptor tyrosine kinase activity

RTKs are activated through the binding of their cognate protein ligands on the extracellular domain. In the absence of ligand, RTKs are inactive and adopt a monomeric/dimeric form on the cell surface dependent on the type of RTKs. For example, EGFR (epidermal growth factor receptor) adopts an inactive monomeric conformation in the absence of ligand binding (Jura, Zhang et al. 2011). The juxtamembrane segment (JMS) of the EGFR brings two kinase domains together in an asymmetric arrangement upon binding of EGF ligands *(Macdonald-Obermann and Pike 2009; Jura, Zhang et al. 2011)*. It has been suggested that ligand binding stabilizes the dimeric structure that leads to efficient *trans* phosphorylation of Tyr residues in the cytoplasmic domains of the dimer (McDonald, Murray-Rust et al. 1995; Hubbard 2004).

The activation loop in the tyrosine kinase domain of RTKs is a critical structural element in the regulation of catalytic activity (Hubbard 2004). This polypeptide segment consists of about 20–25 residues and contains 1–3 Tyr phosphorylation sites. It is known that this loop contributes residues both for catalysis and for substrate-peptide binding and the phosphorylation of those residues is a general mechanism of catalytic enhancement in RTKs (Zhang, Gureasko et al. 2006). When tyrosine residues are unphosphorylated, the loop is not positioned optimally for phosphoryl transfer (Hubbard 2004). *Trans* phosphorylation of

the activation loop results in a change that adjusts the loop into a catalytically competent conformation. The unphosphorylated kinase domain typically exhibits low basal activity. However, its fluctuation might be relevant to the accessibility of the kinase active site, which is addressed in this thesis.

It has been reported that constitutively (ligand-independent) activation of many receptor tyrosine kinases could lead to disease states including various cancers. This underscores the importance of maintaining a low basal phosphorylation level (Hubbard 2004). There are 107 protein phosphatases that can remove phosphate from pTyr in proteins that contribute to maintaining the low basal level of phosphorylation in receptor tyrosine kinases (Zhang 2002). On the other hand, RTKs have evolved various auto-inhibitory mechanisms to suppress basal-level activity, such as the JMS restricting the basal activity of Eph RTKs, which are relevant to this work and will be further discussed in section 1.4.

1.2.3 Spatiotemporal organization of tyrosine phosphorylation

Living cells are isolated by the plasma membrane from the extracellular environment. Transmembrane proteins like RTKs initiate reaction cascades that mediate the transmission of signals across the plasma membrane barrier (Grecco, Schmick et al. 2011). In general, the membrane-bound RTK undergoes upon ligand stimulation an allosteric change affecting enzymatic activity or binding affinity for other downstream molecules, conveying signals into the cytoplasm (Smock and Gierasch 2009; Lemmon and Schlessinger 2010).

The signal propagation into the cytoplasm by phosphorylation of soluble tyrosine containing substrates is tightly controlled by reaction-diffusion systems that generate a local environment of activated substrates (Grecco, Schmick et al. 2011). The opposing tyrosine kinase/phosphatase activities regulate the tyrosine phosphorylation signaling. The catalytic activity of fully active PTPs is much higher than that of tyrosine kinases, which

constrain the effective transfer of exterior signals via phosphorylation in the cytoplasm (Grecco, Schmick et al. 2011). However, the membrane-tethered RTKs together with cytosolic PTPs can form a cyclic reaction and generate a membrane-proximal gradient of phosphorylated substrate that extends into the cytoplasm (Figure 1.3) (Brown and Kholodenko 1999; Kholodenko 2006; Grecco, Schmick et al. 2011).

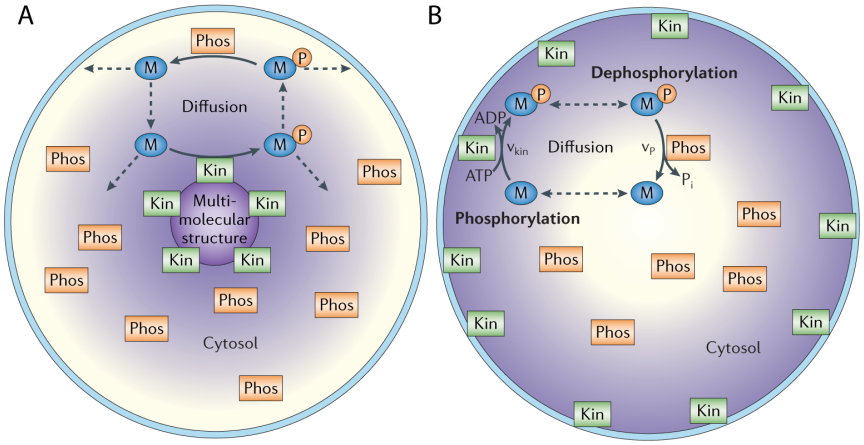

Figure 1.3 Spatial segregation of two opposing enzymes in a protein-modification cycle generates intracellular gradients, adapted from (Kholodenko 2006). Kinases (Kin) localize to (A) supra-molecular structures or (B) the cell membrane, whereas phosphatases (Phos) are homogeneously distributed in the cytoplasm. The concentration gradients are presented by color intensity.

The temporal response dynamics of tyrosine phosphorylation has been extensively studied, but owing to classical biochemical approaches such as Western-blotting that were applied lack spatial information. Advances in quantitative fluorescence microscopic techniques allowed the in depth investigation of the temporal and spatial organization of tyrosine phosphorylation. Using acceptor labeled anti-pTyr antibodies, the lateral spreading of phosphorylation patterns upon EGF stimulation in EGFR expressing cells, has been quantitatively investigated using FRET-FLIM techniques (Verveer, Wouters et al. 2000).

Furthermore, genetically encoded FRET based kinase activity reporters enable the observation of the spatiotemporal distribution of tyrosine phosphorylation in living cells.

The availability of quantitative microscopic imaging approaches allows us to investigate not only the real-time phosphorylation events but also map where they are localized within the cell and how this is regulated. Using FRET-FLIM, the activity, trafficking, and functions of EphA3 controlled by PTP1B have been demonstrated (Nievergall, Janes et al. 2010). It was suggested that the phosphorylation of EphA3, which was investigated in this work, is regulated by the endocytosis events, which transmit signals from the plasma membrane to other cytosolic compartments and generate the localized phosphorylation environment. A similar mechanism was suggested for EGFR, where the rapid endocytosis upon ligand addition is thought to control the magnitude and the specificity of the response (Wiley and Burke 2001).

1.3 Kinase and substrate interaction

1.3.1 Substrate specificity

It has been estimated that 30% of all cellular proteins contain at least one phosphorylated residue and that there are about 700,000 potential phosphorylation sites (P-sites) available to any given kinase (Ubersax and Ferrell Jr 2007). How can protein tyrosine kinases recognize their substrate proteins within such a rich cellular protein background and target specific phosphorylation sites within substrates? Or is there no specificity for kinase?

The general understanding at the end of the 1980's was that protein tyrosine kinases are highly unselective, displaying little individual specificity for their substrates (Cheng, Matsuura et al. 1993). For instance, the peptide derived from the Src kinase autophosphorylation site can be indiscriminately phosphorylated by many tyrosine kinases

and even appeared to be a better substrate for certain non-src family kinases such as EGFR (Cheng, Matsuura et al. 1993). This non-specificity also applies to the protein substrates of the protein tyrosine kinases. For example, several cytoskeletal proteins including tubulin and tau proteins can be phosphorylated *in vitro* by different protein tyrosine kinases, for example EGFR, IRK and Src (Cheng, Matsuura et al. 1993).

There are evidences suggesting that kinases achieve their substrate specificity via different mechanisms. First, the kinase and substrate have complementary sequences that interact based on charge, hydrogen bonding or hydrophobic interactions, which provide the first level of substrate specificity to the kinase. Second, the docking motifs and targeting subunits of the kinases, such as the D-domain for MAPK and the hydrophobic path of the yeast S-phase cyclin Clb5, further improve the substrate specificity of kinases (Ubersax and Ferrell Jr 2007). The third level is gained from the localization of protein kinases to individual subcellular compartments or structures. A localized kinase can accelerate the reaction rate by increasing the local concentration of the reactants and enhance substrate specificity by limiting the number of substrates to which a kinas has access (Ubersax and Ferrell Jr 2007).

With those mechanisms, the kinase substrate specificity seems to be corroborated, especially for protein substrates. Whereas, weak binding affinities and transient interactions between kinases and the peptide substrates still be major obstacles to achieve high specificity for *in vitro*, and *in vivo*, kinase activity assay (Parang and Cole 2002; Tarrant and Cole 2009). The high *Km*-value of the kinase peptide substrate is one of the major challenges for the development of many kinase substrate interaction assays, which will be addressed in this thesis.

1.3.2 Kinase phosphorylation kinetics

In general, the kinase enzymatic reaction follows Michaelis-Menten kinetics: a substrate (S) binds reversibly to a kinase (E) to form an enzyme-substrate complex (ES) that undergoes a phosphorylation reaction to form a product (P).

$$E + S \underset{k_{-1}}{\overset{k_1}{\rightleftharpoons}} ES \xrightarrow{k_{cat}} E + P$$

Under certain conditions, such as the enzyme concentration being much less than the substrate concentration ([E]<<[S]), the rate of product formation is given by the Michaelis-Menten equation,

$$v = \frac{V_{max}[S]}{[S]+K_M} \ , \ V_{max} = k_{cat}[E]_0 \qquad \text{Eq. 1}$$

According to the Michaelis-Menten equation (Eq.1), the rate of product formation v is dependent on the substrate concentration [S], the maximum rate $V_{\max}$ achieved by the system at saturating substrate concentrations, the enzyme concentration $[E]_0$ and the Michaelis constant K_M which is the substrate concentration at which the reaction rate is half of $V_{\max}$. In a conventional Lineweaver-Burk plot, $1/v$ versus $1/[S]$ follows a linear relation (Kou, Cherayil et al. 2005).

However, the reactions catalyzed by protein kinases require both ATP and a substrate protein (peptide) and therefore undergo a bisubstrate kinetic mechanism, which is more complicated. As shown in Figure 1.4, the kinetic pathway for substrate phosphorylation by a protein kinase consists of three fundamental steps: substrate binding (k_2, k_{-2}), the phosphoryl transfer step (k_3, k_{-3}) and irreversible, net product release (k_4) (Lieser, Aubol et al. 2005). The reaction rate is dependent on the substrate concentration so that k_{cat} (turnover number) and K_M can be determined by biochemical techniques. For substrate

recognition, K_M ($K_M = \frac{k_{-2}(k_3+k_4)+k_3k_4}{k_2(k_3+k_{-3}+k_4)}$) includes all the rate constants in the reaction scheme in Figure 1.4, while the real substrate affinity term ($k_{-2}/k_2=K_d$) is different to K_M (Lieser, Aubol et al. 2005). For kinase, for which the phosphoryl transfer is the rate-limiting step, K_M usually is less than K_d. Commonly K_M is referred to as the apparent affinity and could also reflect the intrinsic stability of the enzyme substrate complex (Adams 2001).

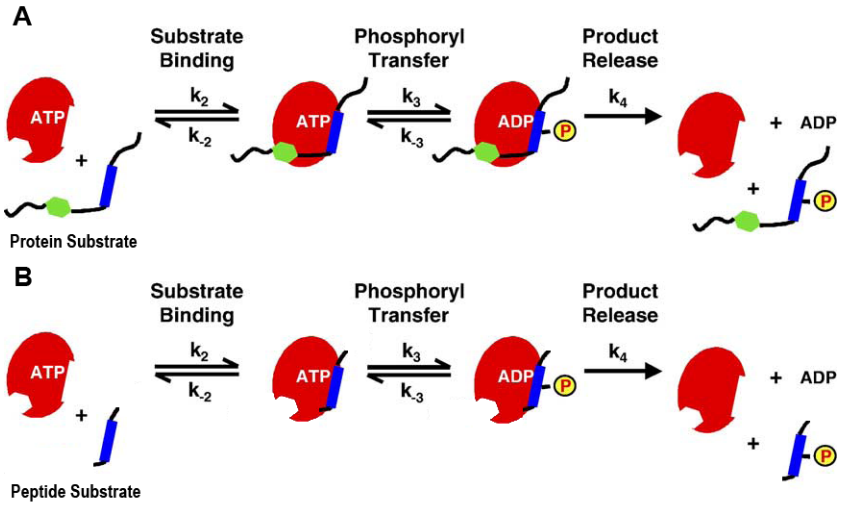

Figure 1.4 Substrate phosphorylation by protein kinases, adapted from (Lieser, Aubol et al. 2005). A) Kinetic pathway for protein substrate phosphorylation by a protein. Three steps important for catalysis are included: substrate binding (k_2, k_{-2}), phosphoryl transfer (k_3, k_{-3}), and irreversible, net product release (k_4). Proximal (blue) and distal (green) binding motifs for the protein substrate are shown. B) As compared to the protein substrate, the peptide substrate has a lack of the distal contact.

The cellular concentration of protein tyrosine kinases and substrates is typically below the K_M (in millimolar range). Catalytic conversion of substrate in cells by the kinases relies on two principal factors: proper subcellular co-localization and molecular interaction between the kinase and substrate (Lieser, Aubol et al. 2005). The docking interaction mediated by distal sites can significantly enhance the stability of the enzyme-substrate complex (lower K_d) and overall catalytic efficiency (K_{cat}/K_M) (Figure 1.4A) (Taylor and Ghosh 2006). On the

other hand, peptides derived from consensus sequences of protein substrates have remarkably low affinity for the kinase (with a K_d in millimolar range) and their phosphoryl transfer rate is very fast, compared to full-length protein substrates (Taylor and Ghosh 2006). Differences of about two orders of magnitude between the K_m's for full-length proteins and derived peptide substrates are very common because of the participation of residues outside the limited consensus sequence for substrate recognition (Figure 1.4 B) (Lieser, Aubol et al. 2005). Nevertheless, the latest reported good ($Km \approx 30\mu M$) peptide substrate sequence (Tara, John et al. 2009) was used in this thesis to enable the formation of EphA3 RTK substrate complex at a relatively low substrate concentration.

1.4 Eph receptor tyrosine kinase

In this thesis, the EphA3 catalytic activity regulatory mechanisms were investigated using FRET-FLIM. Erythropoietin-producing hepatocellular (Eph) receptors are the largest subfamily of RTKs in the animal kingdom, and together with their Eph receptor-interacting (ephrin) ligands, have been implicated in the modulation of cell contact dependent signaling and patterning in normal and oncogenic development (Pasquale 2008). Ephs and ephrins are both classified based on their sequence similarity and ligand affinity into two subclasses A- and B- (Figure 1.5). In humans, nine EphA (EphA1–8 and EphA10) receptors together with six GPI-anchored ephrin-A ligands (ephrinA1-6) and five EphB (EphB1–EphB4, EphB6) receptors with three transmembrane ephrin-B (ephrinB1-3) ligands were reported (Pitulescu and Adams 2010; Janes, Nievergall et al. 2012). In general, A-type receptors typically bind to A-type ligands, and B-type receptors bind to B-type ligands. However, there is also limited cross-binding between members of the two classes, for instance, EphA4, which can bind both A-type and most B-type ligands (Kullander and Klein 2002).

Eph–ephrin complexes undergo bidirectional signals: forward signals that depend on Eph kinase activity propagate in the receptor-expressing cell, and reverse signals that depend on Src family kinases and propagate in the ephrin-expressing cell (Figure 1.5) (Pasquale 2010). Eph receptors and ephrins can also signal independently of each other, through the crosstalk with other signaling systems, such as EGFR. In some cases, Eph receptors can simply act as ligands for ephrins without any requirement for Eph receptor signaling, suggesting that the system does not always function bidirectionally (Klein 2009).

The dominating feature of Eph/ephrin to modulate cell morphology and position focuses on their capacity to direct cell adhesion and repulsion in a cell-contact dependent manner. Early experiments suggested that Eph receptors and ephrins use some common signaling effectors, such as Src family kinases and Ras/Rho family GTPases, which are particularly important for the organization of the actin cytoskeleton and cell adhesion (Pitulescu and Adams 2010).

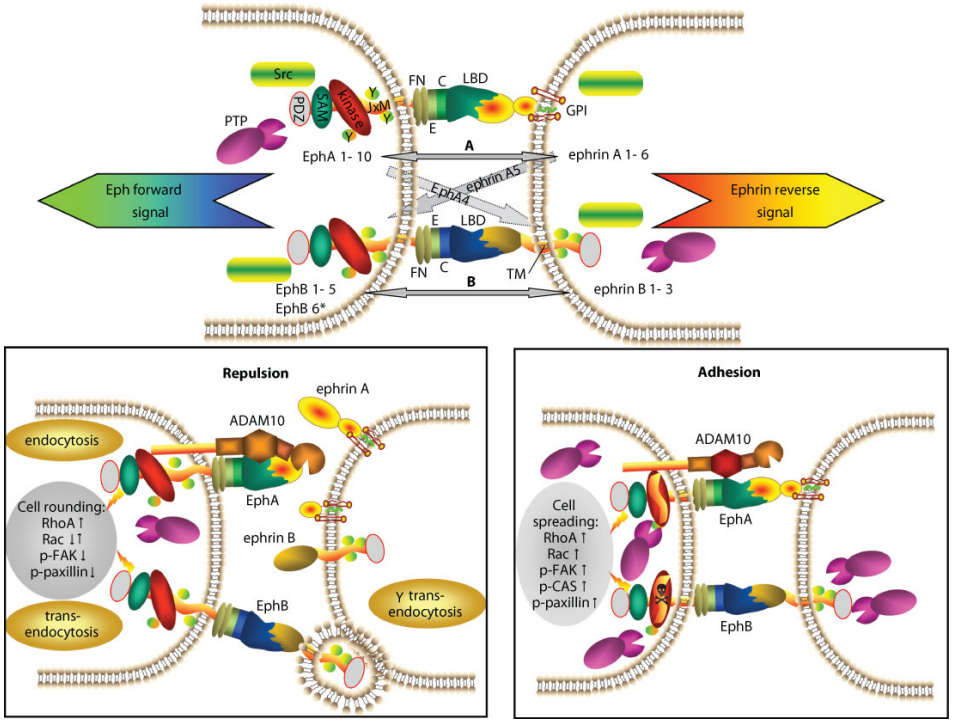

Figure 1.5 Structural and functional features Eph/ephrin, adapted from(Lackmann and Boyd 2008). Structural modules of EphA receptors (EphA1 to EphA10) include the N-terminal ligand-binding domain [(LBD): EphA, green; EphB, blue], cysteine-rich domain (C), EGF-like motif (E), fibronectin-type III motifs (FN), regulatory juxtamembrane domains (JXM) containing two tyrosine (Y) phosphorylation/SH2 domain–binding sites, kinase domain, sterile-alpha-motif interaction domain (SAM), and PDZ-binding motif. Solid arrows indicate Eph/ephrin interactions within the A and B subfamilies, whereas broken arrows indicate those across Eph/ephrin subfamilies. Eph forward and ephrin reverse signaling in opposing cells is positively modulated by Src kinase and down modulated by PTP activities. Cell rounding and cell repulsion rely on active Eph kinases, pY-mediated downstream signaling, and abrogation of the Eph-ephrin tether between cells: Possible mechanisms include (ADAM10) metalloprotease-mediated shedding of Eph-bound ephrin and endocytosis of this complex or transendocytosis of intact EphB/ephrin B complexes into either cell. Eph downstream signaling components affecting cell morphology include RhoA, Rac, focal adhesion kinase (p-FAK), paxillin, Crk-associated substrate (CAS): (p-), phosphorylated;(↑), increase; (↑↓), transient increase; (↓), decrease.

1.4.1 Eph-ephrin signaling

In this work, soluble ephrin-A5-Fc ligands were used to stimulate the EphA3 RTK modulating the phosphorylation of EphA3. Detailed features of the Eph-ephrin signaling are therefore discussed in this section.

Delicately coordinated spatial and temporal regulation of Eph receptor and ephrin expression controls many processes that are critical for development and tissue homeostasis, including the formation of tissue boundaries, assembly of intricate neuronal circuits, remodeling of blood vessels and organ size (Pasquale 2010). Therefore, elucidating the mechanism of action of the Eph receptors and the regulation of their signaling networks are important for understanding developmental processes (Pasquale 2008).

Upon confrontation of Ephs with ephrins on two opposing cells, the initially adhesive event commonly becomes repulsive, leading to the segregation of the two cells. Paradoxically, Eph/ephrin interactions were also shown to induce cell-cell adhesion under some

conditions. The major determinant of this important switch in cellular interaction is the degree of Eph- and ephrin-clustering, activation and phosphorylation (Janes, Nievergall et al. 2012).

Prior to ephrin contact, Ephs are largely distributed across the plasma membrane and display minimal kinase activity, which however may become observable under over-expression conditions (Janes, Nievergall et al. 2012). Several reports suggest that clustering is crucial for tyrosine phosphorylation mediated Eph and ephrin signaling as well as on phospho-tyrosine (pTyr) independent functions such as cell adhesion and migration (Lackmann and Boyd 2008). Furthermore, the degree of Eph/ephrin clustering may not only affect signal strength but may also differentially regulate downstream pathways thus leading to variable outputs.

The activity of Eph RTKs is regulated by the phosphorylation of an activation loop tyrosine as well as two juxtamembrane tyrosines. The JMS does not only modulate the activity of the kinase domain but also provides SH2 domain–docking sites for downstream signaling molecules. Obviously, the ability to activate downstream pathways is dependent on Eph tyrosine kinase signaling capacity, and modulating the ratio of kinase-active to kinase-inactive receptors will switch responses from repulsion to adhesion. Much evidence has been provided that Eph/ephrin signaling pathway is regulated by PTPs. SHIP2 (Src Homology Inositol Phosphatase-2) inhibits the ligand-induced Eph receptor endocytosis by suppressing PI3K signaling and is a negative regulator of ligand-induced Eph receptor endocytosis (Zhuang, Hunter et al. 2007). The application of siRNA knockdown of SHIP2 could increase EphA2 internalization in cultured cells whereas overexpression of SHIP2 or the addition of PI3K inhibitor had the opposite effect (Zhuang, Hunter et al. 2007; Pitulescu and Adams 2010). Recent results have demonstrated that in tumor cells the balance

between the Eph receptor tyrosine kinase and the corresponding tyrosine phosphatase activity provides a molecular switch that dynamically shifts the response to ephrin ligand from cell-cell repulsion to adhesion (Wimmer-Kleikamp, Nievergall et al. 2008). Further evidences have shown that direct interaction between PTP1B and EphA3 negatively regulates ephrinA5 induced EphA3 phosphorylation and consequently effects EphA3 trafficking and downstream biological responses (Nievergall, Janes et al. 2010).

Two general mechanisms have been proposed that achieve controlled termination of Eph-ephrin–mediated cell-cell contacts (Lackmann and Boyd 2008). The first one involves rapid endocytosis, also termed as *trans-endocytosis*. During this process, the intact Eph receptor-ligand complex together with patches of the surrounding plasma membrane can be internalized into the receptor- or ephrin-expressing cells to terminate Eph/ephrin-mediated cell interactions (Pitulescu and Adams 2010). The second mechanism involves regulated cleavage of ephrin ligands by transmembrane proteases following cell-cell contacts (Janes, Saha et al. 2005). As for EphA/ephrinA mediated cell-cell contacts, ephrin-shedding by the transmembrane metalloprotease ADAM10 (a Disintegrin and Metalloprotease 10), releases the molecular tether between the opposing cells (Figure 1.5). Notably, this process is tightly regulated: the intact Eph-ephrin complex is crucial to provide the high-affinity binding site for ADAM10, which then adapts its protease domain into a conformation that yields efficient cleavage of only Eph-bound ephrin (Janes, Saha et al. 2005; Lackmann and Boyd 2008).

1.4.2 Structure and function of Eph receptor tyrosine kinases

The current model of Eph RTKs activity regulation based on crystal structure and biochemical evidences is described below. The regulatory mechanism of EphA3 RTK kinase activity in living cells was investigated and described in this thesis.

Like other RTKs, the Eph receptors are type-I transmembrane proteins (Figure 1.1). Conserved structural features are shared by most of the members of Eph RTK family (Figure 1.5). The extracellular region of the Eph protein comprises a highly conserved N-terminal ligand-binding domain (LBD), a cysteine-rich domain and two fibronectin III domains whereas the cytoplasmic side contains a juxtamembrane region, a kinase domain that catalyzes tyrosine phosphorylation of protein substrates including the Eph receptors themselves, a sterile-α-domain (SAM) and a PSD95/Dlg/ZO1 (PDZ)-binding motif (Figure 1.5) (Himanen and Nikolov 2003). The extracellular and cytosolic regions are connected by a transmembrane helix.

Overall kinase domain (KD) structures of EphB2, A4, and A3 adopt the canonical protein kinase bilobal fold (Davis, Walker et al. 2008). The N-lobe comprises a twisted five strand anti-parallel β-sheet and a single helix αC, whereas the C-lobe is mostly α-helical. The N- and C-lobes are connected by the hinge, which is known to allow for a range of conformations, with the catalytically competent conformation generally corresponding to a closed conformation (Wiesner, Wybenga-Groot et al. 2006).

Activation of all Eph RTKs follows some general principles. Ligand binding leads to the interaction of two catalytically repressed kinase domains and to an adaptive change towards a conformation favoring phosphorylation in *trans*. This results in phosphorylation within the regulatory sequence of the monomer that triggers the activation of the catalytic domain. The active kinase can then phosphorylate other molecules, such as kinase domains of nearby receptors, initiating downstream signaling cascades (Himanen and Nikolov 2003). Oligomerization rather than dimerization is required for receptor stimulation, as soluble ligand ectodomains do not efficiently activate receptors unless clustered by cross-linking (Binns, Taylor et al. 2000).

Full activation of the protein tyrosine kinase domain of the receptor requires the autophosphorylation of tyrosine residues in the JMS. The JMS contains two tyrosine residues (tyrosines 596 and 602 of EphA3 and A4; tyrosines 604 and 610 of EphB2), which are embedded in a characteristic and conserved sequence motif of approximately 10 amino acid (Davis, Walker et al. 2008). These tyrosine residues are major sites for autophosphorylation that regulate the kinase activity via autorepression. When juxtamembrane tyrosine residues are phosphorylated, the JMS is released from the interaction with the kinase domain, which allows the kinase domain to convert into its active state (Kullander and Klein 2002). Replacement of the two juxtamembrane tyrosine residues with phenylalanine residues (2YF) in EphB2 leads to the loss of SH2-domain recruitment and ligand-stimulated tyrosine kinase activity, respectively (Hubbard 2004). *In vitro* biochemical studies of the EphA4 cytoplasmic domain demonstrated the requirement of pTyr residues in the JMS for kinase activation, which suggested that juxtamembrane phosphorylation is modulating activation-loop (AL) phosphorylation (Binns, Taylor et al. 2000).

EphA3 shares some common features with other Eph RTKs family members. Its JMS is also involved in the regulation of kinase activities. The JMS regulation-deficient mutant 2YF mimics the dephosphorylated (odered) JMS, which represses the ordering of the AL, and inhibits the kinase activity. Another mutant 2YE mimics the phosphorylated JMS (tyrosine to glutamic acid substitution, 2YE) features a disordered JMS and the relieved AL that allows the catalytic conversion of the substrate (Davis, Walker et al. 2008). Previous results have suggested that for EphB2 and A4 kinase the phenylalanine substitution of the second tyrosine in juxtamembrane (Y_{JX2}) affects the kinase activity more than that of the first tyrosine in juxtamembrane (Y_{JX1}). However, for EphA3 the phenylalanine substitution of Y_{jx1} seems to be more effective than that of Y_{jx2} according to the *in vitro* kinase activity assay and

the auto phosphorylation level indicated by Western blotting (Davis, Walker et al. 2008; Shi, Yue et al. 2010). Does the current model of the Eph RTK family kinase activity regulation apply to EphA3? And does EphA3 follow the same regulatory model in living cells? To address these questions, the influence of the JMS on the regulatory mechanism of the EphA3 kinase activity in living cells was investigated and described in this thesis.

1.5 Visualization of protein dynamics

In living cells, protein functions are highly dynamic both in space and time. Advanced fluorescence microscopic techniques are highly sensitive, have a large dynamic range, allow the simultaneous detection of multiple components, exhibit excellent spatial and temporal resolution, and are largely noninvasive (Bastiaens and Pepperkok 2000; Verveer, Rocks et al. 2006). Those features made them suitable for the observation of the spatio-temporal behavior of proteins. However, due to the diffraction limit of optical microscopes, the highest resolution of light microscopy is orders of magnitude larger than the protein size (Huang, Bates et al. 2009). The co-localization observed in the fluorescent microscopy image cannot confirm protein-protein interactions. Therefore, the combination of fluorescence microscope with the other advanced fluorescent techniques such as Förster Resonance Energy Transfer (FRET), Fluorescence Correlation Spectroscopy (FCS) and Fluorescence Recovery After Photo-bleaching (FRAP) (Giepmans, Adams et al. 2006) is required to fill the gap and allow the direct observation of specific protein dynamics in living cells.

1.5.1 Förster Resonance Energy Transfer

In this work, Förster resonance energy transfer (FRET) was applied to visualize EphA3 RTK dynamic behavior in living cells. FRET, a well-established spectroscopic phenomenon, was first described in 1948 (Förster 1948; Clegg 2009). It is a non-radiative process, by which

energy is transferred from a donor fluorophore to an acceptor fluorophore. The efficiency of the transfer depends on the spectral overlap of the donor emission and acceptor excitation (Figure 1.6A), the relative orientation and distance of the fluorophore's transition dipoles (Komatsu, Aoki et al. 2011). The rate of energy transfer is given by

$$k_T(r) = \frac{1}{\tau_D}\left(\frac{R_0}{r}\right)^6 \qquad \text{Eq. 2}$$

Here, r is the distance between the donor (D) and the acceptor (A), and τ_D is the lifetime of the donor in the absence of energy transfer (Lakowicz 2006). R_0, usually between 4 to 7nm, is the characteristic distance at where the FRET efficiency is 50% and is known as "Förster radius" (Figure 1.6B), which is different for different FRET pairs and can be determined by the equation

$$R_0^6 = 8.79\times10^{-25} n^{-4} Q_D \kappa^2 J(\overline{v}) cm^6 \qquad \text{Eq. 3}$$

Q_D represents the quantum yield of the donor, n is the refractive index of the medium, κ^2 is the relative orientation factor between the two fluorophore dipole moments, $J(\overline{v})$ is the spectral overlap integral between the donor fluorescence and the absorbance of the acceptor (Figure 1.6A) (Lakowicz 2006; Clegg 2009).

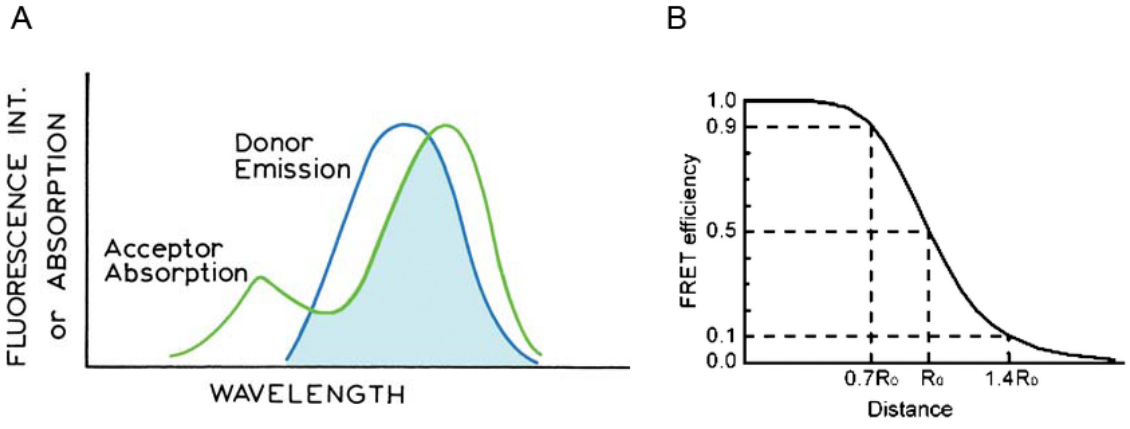

Figure 1.6 Factors affect FRET efficiency, adapted from (Lakowicz 2006; Li, Pham et al. 2006) A) Spectra overlap integral between the donor emission and the acceptor absorption. B) The FRET efficiency is 50% when the distance equals to the Förster radius (R_0). FRET efficiencies ranging from 10% to 90% correspond to distances from 1.4 R_0 to 0.7 R_0.

The efficiency of energy transfer is defined by the equation

$$E_{FRET} = \frac{R_0^6}{R_0^6 + r^6} \qquad \text{Eq. 4}$$

According to the factors included in those equations, modulation of the distance or relative orientation between the fluorophores affect the FRET efficiency (E_{FRET}), which is revealed experimentally by observing the fluorescence intensity (I) or related lifetime (τ) of the donor in the absence of the acceptor (D) or in the presence of the acceptor (DA) (Lakowicz 2006; Wang, Shyy et al. 2008).

$$E = 1 - \frac{I_{DA}}{I_D} = 1 - \frac{\tau_{DA}}{\tau_D} \qquad \text{Eq. 5}$$

1.5.2 Principles of fluorescence lifetime imaging microscopy (FLIM)

FRET can be measured by several techniques such as the sensitized donor intensity, acceptor photo bleaching and FLIM according to Eq. 5. When the energy transfer from a fluorescent donor to a matched acceptor introduces an additional deactivation pathway for the donor's excited state, the donor's fluorescence intensity as well as fluorescence lifetime is reduced (Verveer, Rocks et al. 2006). FLIM is a powerful analytical tool for the quantitative mapping of fluorescent probes that report local biochemical dynamics. The fluorescence lifetime is an intrinsic fluorescence parameter that is independent of the local concentrations of fluorescence probes and the light path (Bastiaens and Pepperkok 2000; Gerritsen, Agronskaia et al. 2009). Therefore, compared to the intensity-based methods, FLIM provides more reliable signals and it is more feasible for living cells FRET

measurement (Verveer, Rocks et al. 2006; Gerritsen, Agronskaia et al. 2009), despite its instrument requirements.

As the fluorescence lifetimes are in the nanosecond range, detection systems with a high temporal resolution are required to resolve and quantify fluorescence decays (Gerritsen, Agronskaia et al. 2009). At present, two main techniques have been applied for the measurement of fluorescence lifetimes: time domain and frequency domain methods (Figure 1.7). In frequency domain methods, the fluorescence lifetime is derived from the phase shift and demodulation of the fluorescent light with respect to a modulated excitation source (Figure 1.7A) (Gerritsen, Agronskaia et al. 2009). In time domain methods, the specimen is excited with a pulse light with its duration much shorter than the emission lifetime of the fluorescence probe and fluorescence intensity decays are recorded to calculate the fluorescence lifetime (Figure 1.7B) (Wang, Shyy et al. 2008).

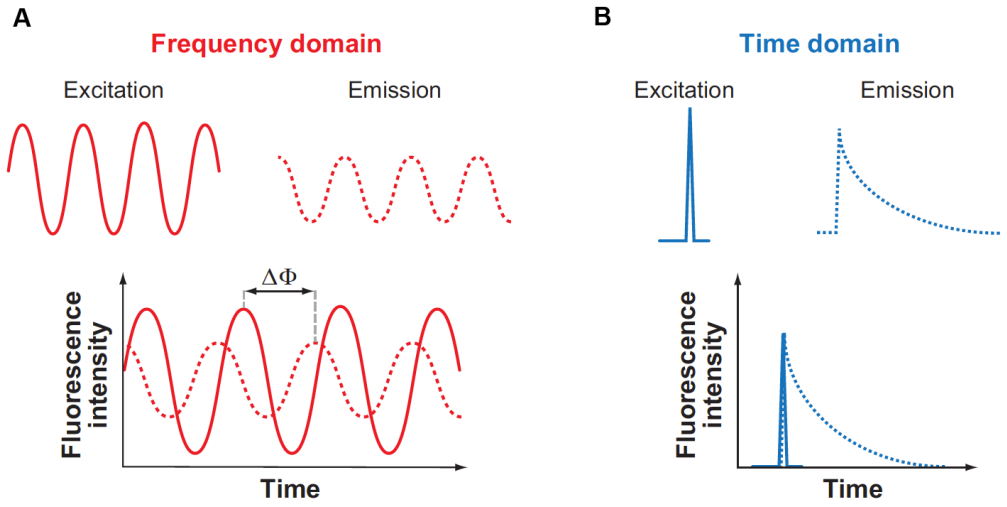

Figure 1.7 Principles of fluorescence lifetime measurements, adapted from (Wang, Shyy et al. 2008) A) Frequency domain: Both the excitation and emission lights are in sinusoidal format with the same frequency. The phase-shift between the excitation and emission lights is used to calculate the fluorescence lifetime. B) Time domain: The specimen is excited with a very short pulse light and

the captured time trace of the emission fluorescence intensity is used to calculate the fluorescence lifetime characteristics.

Fluorescence lifetime imaging can be integrated both with wide field and with confocal scanning microscopes and the most common implementation in time-domain FLIM is based on time-correlated single photon counting (TCSPC) (Lakowicz 2006; Gerritsen, Agronskaia et al. 2009). In TCSPC typically picoseconds excitation pulse lasers are used to excite fluorescent probes and the time delays between the excitation pulse and the detection of a single-photon are recorded. The fluorescence emitted by the specimen is selected by an emission filter and detected by a fast detector (an avalanche photodiode (APD), for example) that is capable to detect single photons. Care must be taken that the count rate of the experiment is sufficiently low to prevent pulse-pileup due to the dead time of the time-to amplitude converter (TAC) and detector. The signal from TAC is further digitized and the event is stored in a multichannel analyzer (MCA). By repeating this process, MCA accumulates the histogram of the arrival time of photon, which represents the fluorescence decay curve of the specimen. In general, the decay curve recorded by TCSPC can be fitted to an (multi) exponential decay employing a deconvolution to account for the instrument response function (IRF) (Lakowicz 2006; Gerritsen, Agronskaia et al. 2009).

1.5.3 Enzyme substrate imaging

In this thesis, we used EphA3 as an example to investigate RTKs kinase activity regulatory mechanism. Current biosensors do not allow us to directly observe the kinase substrate interaction and investigate the regulation of kinase active site accessibility in living cells. An recently developed enzyme-substrate (ES) interaction imaging assay (Yudushkin, Schleifenbaum et al. 2007) provides an opportunity to investigate the kinase activity regulatory mechanisms in depth in living cells.

The design of FRET based enzyme substrate imaging as reporter for enzyme activity is in theory straightforward. Once a suitable enzyme substrate has been identified, a compatible FRET-dye pair can be attached to both the enzyme and substrate, which should result in a detectable change in FRET signal when ES intermediate is formed.

The first experimental example of the ES imaging was the visualization of PTP1B activity based on the spatially resolved ES interactions in living cells (Yudushkin, Schleifenbaum et al. 2007). The formation of the ES complex consisting of the GFP tagged PTP1B (donor) and the chromophore conjugated PTP1B substrate (acceptor) was triggered by uncaging a photoactivatable group from the phosphate moiety. Subsequently, the fluorescence lifetime of the donor decreased significantly. Since only the donor tagged enzyme is detectable, a very specific readout for this enzyme is provided. This allows filtering the enzyme of interest out from a complicated endogenous enzymes background. When normalized over the amount of donor in a region of interest, the fluorescent lifetime is a direct readout for the amount of ES complex (Schultz 2007). The larger amount of ES complex then indicates regions with less enzyme activity and vice versa, giving us a rough map of enzyme activity (Schultz 2007; Yudushkin, Schleifenbaum et al. 2007).

The kinase catalysis process is divided into several steps including substrate binding, phosphoryl transfer, and product release. Therefore, in the ES imaging assay for the EphA3 kinase, the FRET signal fluctuation reflects kinase substrate binding affinity adjustment and changes of catalytic activity due to the tyrosine phosphorylation that is involved in the regulatory mechanism, and the association/ disassociation of the kinase substrate. Previous work from Thies Klüßendorf (Klüßendorf 2011) suggested the possibility of imaging the transient ERK2-substrate interactions with an genetically encoded ERK2 ES sensor. However, no attempts to establish ES imaging for RTKs have been published so far.

Therefore, the EphA3 RTK ES imaging assay established in this thesis is the first example of an RTK ES imaging assay and was developed by using the crystal structure based activity regulation model and a relatively good ($Km \approx 30\mu M$) substrate.

As discussed previously, the tyrosine phosphorylation level is maintained by the continuous opposing activities of RTKs and PTPs. The balance between EphA3 kinase and opposing PTP1B activity is likely to be a critical regulatory mechanism for EphA3-mediated cell positioning during tumor development and progression (Nievergall, Janes et al. 2010). EphA3 RTK possesses a highly conserved JMS that regulates the accessibility of its active site and kinase activity by the auto-phosphorylation of two tyrosine residues within the JMS (Davis, Walker et al. 2008). However, most of the evidences about the JMS involved regulatory mechanism were obtained from *in vitro* experiments, while the detailed principles in living cells are still concealed up to date. Therefore, it is important to develop an ES imaging assay for RTK to investigate features of JMS regulatory mechanism of EphA3 RTK substrate accessibility and kinase activity in living cells.

To achieve is, this work comprised the following aspects:

1. Establish a fast and efficient protein expression and purification system, which enabled us to obtain proteins with high quality for biochemical assay.
2. Characterize the recombinant EphA3c-mCitrine (EphA3c-mCit) and substrate interactions by FRET-FLIM in a simple purified system, thus proving the principle of ES imaging assay for RTKs.
3. Reconstitute the kinase/phosphatase cyclic reaction and monitor different substrate phosphorylation steady-states *in vitro* by FRET-FLIM.
4. Compare the steady-state substrate accessibility between the wild type (WT) and JMS regulation-deficient mutants (MTs) of EphA3 RTK in living cells.

5. Investigate EphA3 kinase substrate interactions upon ephrin A5 ligand stimulation in living cells.
6. Observe different responses from the WT and MTs of EphA3 RTK substrate interactions upon the phosphatase inhibitor perturbation in living cells.

2 Methods

2.1 Molecular Cloning

Basic methods of DNA handling and manipulation were performed according to the molecular cloning laboratory manual (Sambrook and Russell.W 2001) if not mentioned otherwise.

Bacterial culture and storage

A single transformed colony from LB agar plate (in the presence of appropriate antibiotic) is inoculated in 10ml LB liquid medium (with appropriate antibiotic) at 37°C and 200rpm if not stated otherwise. After 6-10 h, the culture in log phase can be stored in aliquots of LB medium containing 20% (v/v) sterile glycerol at -80°C. The pre-culture from 10 ml was used to scale up to the desired volume of main culture.

Plasmid preparation (mini and midi prep)

The QIAprep Spin Miniprep Kit and Midiprep kit were used for routine molecular biology applications. Plasmid DNA was prepared according to the QIAprep Spin Miniprep and Midiprep manual. In brief, overnight bacterial cultures from 10 ml LB medium (100ml for Midiprep) were harvested by centrifugation at 5000rpm for 15 min, RT. The cell pellets were resuspended in buffer P1 (with RNAase). Buffer P2 and N3 were used sequentially for cell lysate and neutralizing the solution. Spin columns containing a silica gel membrane were used to concentrate the plasmid DNA that was eluted in an EB buffer of the desired volume.

Polymerase Chain Reaction (PCR)

Phusion High Fidelity DNA Polymerase (NEB) was used for DNA amplification if not mentioned. The highest fidelity, increased processivity and product yields made Phusion

DNA Polymerases one of the best available proofreading polymerases. Experiments were set up according to the handbook provided by the manufacture as shown in Table 2.1. The PCR mixture mentioned above was incubated in a PCR master cycler epgradient (Eppendorf AG) using PCR program as described in Table 2.1.

Table 2.1 Preparation of PCR reaction mixture and PCR program

Pipetting instructions (in order)

Component	Volume /50 µl reaction	Volume/20 µl reaction	Final Conc.
ddH_2O	add to 50 µl	add to 20 µl	
5x Phusion HF Buffer	10 µl	4 µl	1x
10 mM dNTPs	1 µl	0.4 µl	200 µM each
Primer F	2.5 µl	1 µl	0.5 µM
Primer R	2.5 µl	1 µl	0.5 µM
Template DNA	1 µl	1 µl	25-200pg/reaction
Phusion DNA polymerase	0.5 µl	0.2 µl	0.02U/µl

Cycling instructions

Cycle step	Temp.	Time	Number of cycles
Initial denaturation	98°C	30 s	1
Denaturation	98°C	5-10 s	
Annealing	45-72°C	10-30 s	25-35
Extension	72°C	15-30 s /1 kb	
Final extension	72°C	5-10 min	1
Storage	4°C	hold	1

Colony PCR is designed to quickly screen for plasmid inserts directly from *E. coli* colonies. This technique can be used to determine insert size and/or orientation in the vector in a short time. Taq DNA polymerase (NEB), which is considerably cheaper than Phusion polymerase (NEB), is chosen for this application. In short, the master pre-mixture of the reaction solution without template is prepared according to the protocols provided by the company. Colonies from the agar plate were selected and suspended in 20 µl the master

pre-mixture. 10 minutes initial denaturation time was used for sufficient cell breakage and DNA denaturation. The extension time and annealing temperature were chosen according to the template and primers.

Dephosphorylation of 5'-phosphorylated DNA Fragments

To prevent self-ligation of vector DNA during the ligation of two DNA fragments, the5'-phosphorylated ends of the digested vector DNA were dephosphorylated with calf-intestinal alkaline phosphatase (CIP). Since the buffer used in PCR amplification is quite similar to the suggested buffer for CIP, 1U CIP was added directly into the tube with PCR reaction mixtures. Reactions were incubated at least 1h at 37°C to achieve complete digestion and the DNA subsequently purified by PCR purification kit.

PCR purification and gel extraction

The QIAquick PCR Purication Kit or QIAquick Gel Extraction Kit was used to remove the contaminants. Both kits are designed for the fast purification of DNA fragments in a range of 100 bp to 10 kb from PCR/enzymatic reactions or from agarose gels. In both cases, DNA binds to a silica membrane in the presence of high salt concentrations, while contaminants were washed out. Excising DNA fragments from an agarose gel and a further melting step were required for the gel extraction kit. The rest was performed according to the manufacturer's manual.

Restriction enzyme digestion

Restriction enzyme digestion was used for sub-cloning. Both vector and purified PCR product were digested with the appropriate restriction enzymes. Digestions of DNA fragments were performed as recommended by the manufacturer at 37°C for at least 2 h (or overnight in some cases) to achieve complete digestion. An example is shown in Table 2.2. The reaction was stopped by the addition of a DNA loading buffer. Fragments produced by

restriction enzyme digestion were purified using agarose gel electrophoresis and a gel extraction kit.

Table 2.2 Restriction enzyme digestions.

Component	Volume /20 µl reaction	Volume /50 µl reaction
ddH_2O	add to 20 µl	add to 50 µl
10xBuffer (NEB1/2/3/4)	2 µl	5 µl
DNA	2 µg accordingly	5 µg accordingly
Enzyme 1(20 U/µL)	0.2µl	0.5µl
Enzyme 2 (10 U/µL)	0.4µl	1 µl

DNA electrophoresis

Electrophoresis through agarose gel is used to separate, identify, and purify DNA fragments. The double-stranded DNA (dsDNA) migrates through the gel matrix at rates that are inversely proportional to the $\log_{10}$ of the number of base pairs (Sambrook and Russell.W 2001). The location of the DNA within the gel can be determined directly by staining with a low concentration of fluorescent dyes, such as 20,000× diluted RedSafe Dye. Bands containing as little as 20 pg of dsDNA can be detected by direct examination of the gel in UV. If necessary, these bands of DNA can be extracted from the gel and used for further experiments. In detail, 1× TAE buffer supplemented with 5 µl RedSafe /100 ml gel was used to prepare the agarose gel and running buffer. Electrophoresis took place at a constant voltage of 90 V for about 30 mins. Samples were prepared by mixing DNA with 5× DNA loading buffer (QIAgen). The concentration of agarose gel was chosen according to the size of DNA fragments.

DNA Ligation

Usually 25 ng vector DNAs were ligated with a 2-3 fold molar ratio of DNA insert fragments according to the manual provided by the manufactures. The appropriate amounts of vector and insert DNA were supplemented with 5 µl 2×Quick Ligation Reaction Buffer (aliquot and

avoid thaw-freeze cycle) and 1 U Quick T4 DNA Ligase (NEB) and ddH_2O was added to a final volume of 10 µl. The reaction was incubated at RT for 5-15 min (16°C for 4 hours or 4°C overnight) and then transformed into E. coli XL-10 Gold chemical competent cells.

Chemical Transformation

1. The 5 µl ligation mixture containing approximately 25 ng of the desired plasmid DNA to was added to 100 µl chemical competent cells. The mixture was incubated on ice for 30 mins without shaking.
2. The cells were heat shocked at 42° C for 45 seconds and immediately cooled on ice for 2 min.
3. 500 µl of LB or SOC medium was added to the cells.
4. It was shaken at 37°C for 1 hour at 200rpm.
5. Cells were collected by spinning at 5000 rmp for 1 minute to discard the supernatant and cells resuspended in 100 µl of fresh LB medium were spread on LB agar plates supplemented with the appropriate antibiotics.
6. Plates were inverted and incubated overnight (12-16 hours) at 37°C.

Transformation by electroporation

1. 50 µl electro-competent *E. coli* XL-10 Gold were mixed with 50 µl ice-cold 10 % glycerol and 5.0 µl recombinant DNA in a chilled electroporation cuvette (0.2 µm path length).
2. A high voltage pulse was applied using the Gene Pulser & Pulse controller from Biorad (conditions: 25 µF, 800 Ω, 1.3 V). Time constants shown by the device should be between 4 and 6 ms.
3. 1 mL of SOC medium was immediately added to the cuvette and the mixture was transferred to a 15 ml falcon tube to grow the culture at 37°C for 1 h on a shaker.

4. 100 µL cell suspensions were spread on agar plates containing the appropriate antibiotics.
5. Plates were inverted and incubated overnight (12-16 hours) at 37°C.

DNA sequencing

Sequencing PCRs were performed using the BigDye Terminator Cycle Sequencing Kit. 200-300 ng plasmid DNA, 4.0 µl ready reaction premix, 2.0 µl BigDye Sequencing buffer and 1.0 µl primer (25 pmol/µl) were replenished with ddH_2O to a final volume of 20 µl. After initial denaturation at 96°C for 1 min, PCR cycles consisted of denaturation at 96°C for 10 sec, 5 sec annealing at 50°C (adjust according to the primer's Tm value) and extension at 60°C for 4min. Cycle number was 25 and finished PCR reactions were stored to 4°C. PCR products were further purified by the DyeEx 2.0 Spin kit according to the manufacturer's manual. Purified reactions were dried in a vacuum centrifuge and then sent to in house DNA sequencing facility for readout.

Sequence and Ligation Independent Cloning (SLIC)

Compared to the assembly of recombinant DNA by restriction enzyme cutting and re-ligation, SLIC has important advantages in that it does not require specific sequences and it will not introduce extra unnecessary amino acid into the protein sequence (Li and Elledge 2007). It also allows the assembly of the vector DNA with (multiple) DNA fragments using *in vitro* or *in vivo* RecA dependent homologous recombination (Li and Elledge 2007). Here we applied the simplified protocol depending on *in vivo* homologous recombination system to achieve the acceptable efficiency with low cost.

1. The plasmid was linearized by desired restriction enzyme, treated with CIP phosphatase and purified by gel extraction. The PCR was performed with specially

designed primers to produce the insert fragment with at least 15bp-identified sequence (both 3' and 5'-end) as the target vector.

2. 50 ng of the plasmids were mixed with desired inserts with 1:10 molar ratio. The mixture was used to transform *E.coli* XL-10 gold chemical competent cell directly according to the standard protocol.
3. Positive colonies were identified by colony PCR, resulting in 20-50% positive insertion.

2.2 Construction of vectors

2.2.1 SLIC Vectors for recombinant protein expression

The pET24a (+) plasmid (Novagen, Germany) was used as a backbone and modified for recombinant protein expression. NaeI (for N1 vector) or SfoI (for C1 vector) sites in the original vector were silenced via site direct mutation. TEV protease recognizing site, 6×His tag and an extra NaeI or SfoI resctriction site were assembled by PCR and introduced to the vector by sequence and ligation independent cloning (SLIC) strategy. The fluorescent protein (FP) was further cloned into the basic pET24a-LIC-N1/C1 vectors by ligation independent strategy (Figure 2.1).

These vectors enable the expression and purification of the recombinant protein with only one extra glycine after TEV protease digestion. The sequence encoding the intracellular domain of EphA3 (EphA3c, amino acids 577–947) was subcloned from pET28a-LIC-EphA3c (provided by S. Dhe-Paganon, Structural Genomics Consortium, University of Toronto) into the pET24a-LIC N1, C1 and pET24a-mCitrine-N1, C1 vectors by SLIC. The sequence encoding PTP1B catalytic domain (amino acids 1-298) was subcloned from the PTP1B-GFP vector (provided by Ivan Yuduskin, Dortmund, MPI) into pET24a-LIC N1, C1 by SLIC. The sequence encoding the EphA3c OPTYF substrate peptide (KQWDNYEFIW) and 9 Arginine

repeats was introduced to the C-terminus of mCherry in pET24a-LIC-mCherry-C1 vector by SLIC (Figure 3.1a).

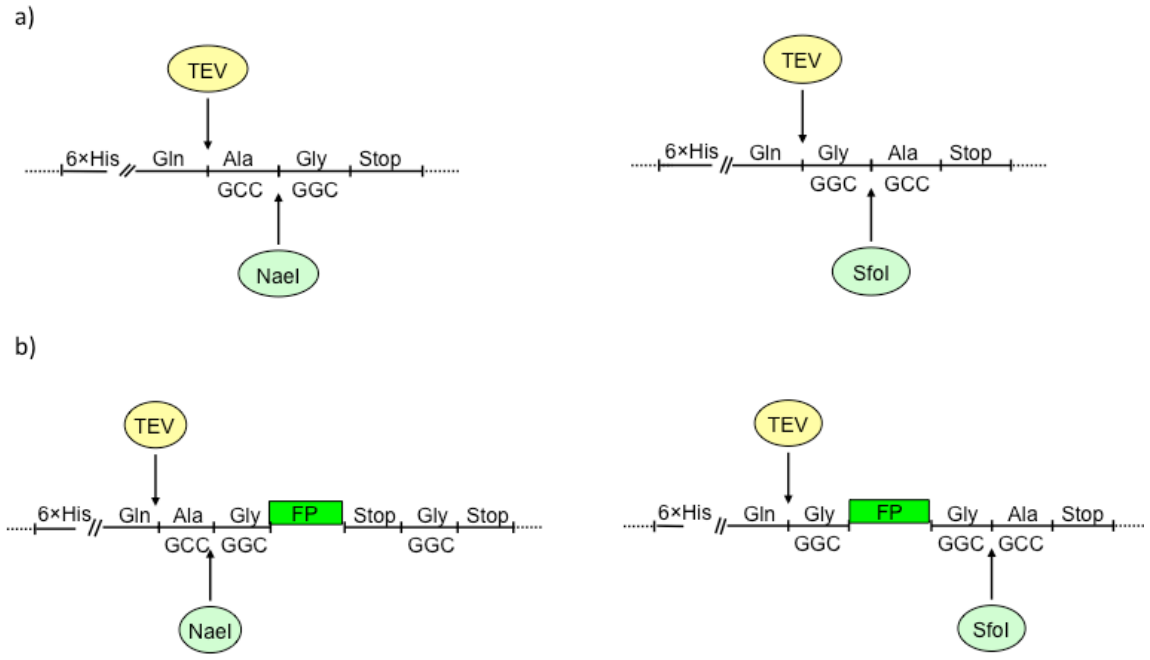

Figure 2.1 Schematic structure of SLIC vector. a) pET24a-LIC-N1/C1, basic vector for cloning. b) pET24a-LIC-FP-N1/C1 vectors, fluorescent proteins (FP) could be fused to the N- or C- terminus of the target protein. FP could be replaced by monomeric EGFP, Cherry and Citrine for different applications.

The sequence and ligation independent cloning (SLIC) allows assembly of DNA fragments without the insertion of extra amino acids. In this system, with the combination of TEV protease the affinity tag used for purification could be removed. Only one glycine or alanine remained, having minimum effects on the function of the purified protein. Furthermore, this cloning strategy does not require specific sequences or expensive enzymes to facilitate the homologous recombination. Ideally, it is suitable for all the routine molecular biology cloning work in the lab.

However, in this particular case, several issues should be addressed. Firstly, the high background of self-ligated plasmids increased the difficulty in identifying the successful insertion. Another SLIC vector was generated containing necessary sequences for "blue-white" screening to assist in the identification of positive colonies. Nevertheless, the extra work required to insert this sequence should be considered. Secondly, the best condition required for TEV protease digestion might not be suitable for some proteins to maintain their stability (Kapust, Tozser et al. 2002). In our case, only about 50% digested protein could be recovered owing to the insufficient digestion. Thirdly, most of the time, few extra amino acids at N- or C- terminus of proteins have only limited effects on their functions *in vitro* (Cabrita, Dai et al. 2006).

Given these facts, the SLIC based protein expression system generated here has the advantage of producing non-modified recombinant protein with high yield.

2.2.2 Vectors for mammalian cell expression

Plasmids pmEGFP-N1and C1 from Clontech were modified by our lab to achieve a group of derivatives such as pmCitrine-N1, C1 and pmCherry-N1, C1 that were used in this project. The full length EphA3 receptor kinase (gift from Prof. Dr. Martin Lackmann, Monash University, Australia) was subcloned into pmCitrine-N1 vector using EcoRI and AgeI restriction sites. The site direct mutation PCR was applied to create EphA3 RTK with different active state, such as, pmCitrine-N1-EphA3 (tyrosine to phenylalanine substitution, 2YF) and pmCitrine-N1-EphA3 (tyrosine to glutamic acid substitution, 2YE) mutants (Figure 3.1 a). The DNA sequence of these mutants was identified by DNA sequencing.

2.3 Protein purification and characterization

Protein expression and purification (EphA3c-mCitrine as an example)

1. Transform BL21 (DE3) Rosseta cells with plasmid pET24a-LIC-EphA3c-mCitrine and select on a LB agar plate with 30 mg/L kanamycin (Kan) and 34 mg/L chloramphenicol (Cam). ***Day 1***
2. Pick a single colony from the agar plate using a sterile nano pipette tip and inoculate it into 10 ml of LB liquid medium containing 30 mg/L Kan and 34 mg/L Cam, 37°C at 200 rpm shaking overnight. ***Day 2***
3. Inoculate this pre-culture into 1 L of TB medium with 30 mg/L Kan and 34 mg/L Cam and grow cells in 2 L flasks at 37°C, 180 rpm shaker until the absorbance at 600 nm (OD_{600}) reaches 0.6-0.8 (about 5-7 hours).
4. Cool down the flask on ice till approximately 16°C and induce the protein expression with 0.05-0.1 mM of IPTG.
5. Return the flask to the shaker (180 rpm) at 12°C overnight (12-16 hours). ***Day 3***
6. Harvest cells by centrifugation in the centrifuge Sorvall RC 6+ at 5000 rpm, 4°C for 30 minutes.
7. Discard the supernatant carefully and wash the cells with buffer A once and transfer the pellets to a 50ml falcon tube which can be frozen and stored in -80°C for later use.
8. Resuspend the cell pellet in 30 mL ice-cold lysis Buffer (50 ml buffer A + 10 µl 5 mg/ml DNaseI+ 1mM TCEP+1 mM PMSF + 1 tablet of protein inhibitor+10mM Imidazole+10mM $MgCl_2$). The supplement reagent should be added freshly.
9. Pass the cell suspensions through the chilled pressure chamber of microfluidizer several times at 40,000 psi until no obvious particles are visible.
10. Centrifuge the cell lysate in the Sorvall RC-5B refrigerated super speed centrifuge at 18,000 rpm for 4°C 1 hour.

11. Carefully transfer and filter the supernatant through a 0.45 μm low protein-binding syringe filter (Millipore).
12. Pre-equilibrate Histrap HP (1 ml) column with cold buffer A (all the buffer used for the following experiment of protein purification has to be vacuum filtered and degased) by Äkta purifier (1 ml/min).
13. Load the filtered cell lysate to the column via the built-in injection pump of Äkta purifier (1 ml/min flow rate and 4°C have been used if not indicated otherwise).
14. Wash the column with at least 5 column volumes (CV) of buffer A (or till the OD_{280} reaches the baseline).
15. Wash the column with 5 CV of 4% buffer B (buffer A + 500 mM imidazole) to reduce the non-specific bound protein.
16. Elute the target protein with buffer B gradient 4% to 50% in 20 CV and collect the fraction 2 ml/ tube according to the absorbance at 280 nm or/and 520 nm (for mCitrine fused protein). Apply SDS-PAGE to identify the fraction of interest.
17. Clean the column with 5 CV 100% buffer B, 5 CV ddH_2O sequentially and store in 20% ethanol.
18. Collect the fractions of interest and dialyze the sample against buffer for TEV protease (20 mM Tris-HCl, pH 8.0, 100 mM NaCl, 1 mM DTT). Add TEV protease at 1:20 molar ratio to the protein in the dialysis membrane tubing (10 kDa cut off). Perform dialysis was performed at 4°C with magnetic constant low-speed stirring-bar. ***Day 4***
19. Transfer the solution from the dialysis tube to a high-speed centrifugation tube and remove the precipitations by centrifugation at 12,000 rpm, 4°C for 15 minutes.
20. Add 5 mM $MgCl_2$ and 10 mM imidazole to the supernatant. Load the cleavage mixture onto the Histrap HP (1 ml) column again to remove the free 6×His tag peptide and uncleaved protein.

21. Collect the flow through and concentrate to the desired volume (usually about 2 ml) in buffer C using 15 ml Amicon concentrator (Millipore).
22. Introduce 10 mM ATP and 10 mM of $MgCl_2$ to achieve fully auto phosphorylated EphA3c-mCitrine; use 1: 40 molar ratio of recombinant PTP1Bc to produce fully dephosphorylated EphA3c-mCitrine. Perform both reactions at 4°C overnight. ***Day 5***
23. Centrifuge the sample in a refrigerated centrifuge (Eppendorf 5417R) at 14,000 rpm, 4°C for 15 minutes.
24. Pre-equilibrate gel filtration column (Hiload 16/60 Superdex-200, prep grade) with buffer C in advance and carefully load the supernatant with back filled loading loop (2 ml).
25. Separate the fractions (2 ml/tube) according to the apparent molecule weight. Apply OD_{280} (or OD_{520} for mCitrine) and SDS-PAGE to identify the protein of interest.
26. Concentrate the sample to about 4 mg/ml and divide it in aliquots for snap-frozen in liquid nitrogen. Store the protein at -80°C. ***Day 6***

SDS-Polyacrylamide Gel Electrophoresis (SDS-PAGE) of proteins

For analytical electrophorese of proteins carried out in polyacrylamide gels, proteins should be denatured into their individual polypeptide subunits and with minimized aggregation. Most of time, the strongly anionic detergent SDS is used together with a reducing agent, such as DTT, β-mercaptoethanol, and heated up to dissociate the proteins before loading onto the gel. The proteins bind SDS and are negatively charged which enable the SDS-protein complex to migrate through polyacrylamide gels in accordance with the size of the polypeptide (Sambrook and Russell.W 2001).

The widely used discontinuous buffer system was able to concentrate all of the complexes into a very small volume so that the resolution of SDS-PAGE improved. The effective range

of separation of SDS-PAGE depends on the pore size, which is affected by the concentration of polyacrylamide used to cast the gel and the amount of cross-linking. The acrylamide concentration of the resolving gel was adjusted from 10 to 15 % (v/v) according to the molecular weight of the protein of interest.

1. Assemble the Bio-Rad casting apparatus with glass plates according to the manufacturer's instructions. Prepare the resolving gel by mixing the components as shown in Table 2.3 sequentially. Ammonium persulfate (APS) and N,N,N',N'-tetramethylethylenediamine (TEMED) should be added as the last step in order to start polymerization.

2. Pour the acrylamide solution into the gap between the glass plates. Leave about 1.5-2 cm space for the stacking gel. Add ddH_2O on the top of the resolving gel to make a smooth interface. Place the gel in a vertical position at room temperature until the resolving gel is polymerized (about 20 minutes).

3. Wash the top of the gel several times with ddH_2O to remove any unpolymerized acrylamide. Remove remaining ddH_2O with the edge of a paper towel.

4. Prepare the stacking gel as Table 2.3. Polymerization will begin when TEMED has been added. Without delay, swirl the mixture rapidly and pour it directly onto the surface of the polymerized resolving gel till the top.

5. Immediately inset a clean comb into the stacking gel solution, being careful to avoid trapping air bubbles. Place the gel in a vertical position at room temperature until the resolving gel is polymerized (about 20 minutes). The prepared gel can be stored in a plastic pocket with the wet paper towel in the fridge for one week.

6. Prepare the protein samples in the appropriate volume with 5×SDS gel-loading buffer and heat them to 95°C for 3 minutes to denature the proteins.

7. Carefully remove the comb from the gel before use. Wash the wells with ddH_2O to remove any unpolymerized acrylamide. Mount the gel in the eclectrophoresis apparatus. Add Tris-glycine electrophoresis buffer to the top (inner chamber) and half of the bottom reservoirs.

8. Load samples with desired volume in a predetermined order into wells. Unused wells are filled up with 1×SDS gel-loading buffer.

9. Connect the electrophoresis apparatus to a Bio-Rad power supply and ensure the negative electrode is connected to the middle of the chamber. Apply 90 V for 10 minutes and increase the voltage to 150V untill the bromophenol blue reaches the bottom of the resolving gel (about 1-1.5 hour).

10. Carefully transfer the gel to a clean chamber for following experiment such as coomassie brilliant blue staining or western blotting.

11. Results are documented by Gel-Doc XR system.

Table 2.3 Solution for preparing 2 pieces of SDS-PAGE gel (Sambrook and Russell.W 2001)

Components\ Volume	10 ml (Resolving gel)			4 ml (Stacking gel)
	10% gel	12% gel	15% gel	5% gel
H_2O	4	3.3	2.3	2.7
30% acrylamide mix	3.3	4	5	0.67
1.5 M Tris (pH8.8)	2.5	2.5	2.5	0.5
10% SDS	0.1	0.1	0.1	0.04
10% APS	0.1	0.1	0.1	0.04
TEMED	0.004	0.004	0.004	0.004

Western blotting

In western blotting, electrophoretically separated components during discontinuous, denaturing SDS-PAGE are transferred from a gel to a solid support, such as polyvinylidene difluoride (PVDF) membrane in this case. Unoccupied binding sites of the membrane were blocked by blocking buffer (licor) and the immobilized proteins were probed with antibodies that react specifically with antigenic epitopes displayed by the target. Therefore, western blotting is very useful for identification and quantitation of specific proteins in complex mixtures like cell lysates. Semi-dry blotting was performed for most of the experiments.

1. PVDF membrane and filter paper were cut in appropriate size as the gel. PVDF membrane was activated in 100% methanol 2-3 minutes in advance.

2. The filter paper and the gel from SDS-PAGE were equilibrated with ice-cold transfer buffer to avoid deforming.

3. These materials were ordered as follows: cathode (-), 2× filter paper, SDS-PAGE gel, PVDF membrane, the other 2× filter paper and anode (+). Air bubbles between each layer were removed completely.

4. The extra transfer buffer was drained from the plate to avoid electrical shortcut. A constant voltage of 30V was applied to the gel sandwiches for 30 minutes.

5. After blotting, the membrane was blocked with 5 ml Li-cor blocking buffer at room temperature for 1 hour (shaker).

6. Primary antibody was diluted into 1 ml blocking buffer with the ratio recommended by the manufacturer's instruction. PVDF membrane was incubated with 1 ml diluted primary antibody in a self heat-sealed plastic envelop at 4°C overnight.

7. The PVDF membrane was washed with 1×TBST buffer for 3 times (5 minutes each time).

8. The PVDF membrane was further incubated with desired Li-cor Infar-red fluorescent-labeled secondary antibodies (diluted into 5 ml blocking buffer according to the manufacturers' recommendation) in the black box at room temperature for 45 minutes.

9. The PVDF membrane was intensively washed 3 times (10 minutes each on the shaker) and stored in PBS at 4°C before next step.

10. The result was readout by Odyssey Imaging System.

Enzyme activity assay

The recombinant phosphatase was characterized by the hydrolysis of pNPP conducted in 96-well plates in a final reaction volume of 100 µl as described elsewhere (Peters, Branner et al. 2003). The reaction was monitored by measuring the increase in absorbance at 405 nm due to the production of p-nitrophenol (Peters, Branner et al. 2003). The absorbance was measured in a 96 plates reader. Enzyme dilutions were prepared by diluting the enzyme stock solution in a 1:100 assay. Both the diluted enzyme solution and the buffer containing pNPP at various concentrations were incubated for at least 15 min at 30 °C. The reaction was initiated by adding an appropriate amount of PTP1Bc and terminated by the addition of 10 µl 4.5M NaOH containing 50% Ethanol.

A continuous enzyme-coupled kinase assay was performed to measure the kinase activity of EphA3 catalytic domain as described with minor modifications (Zhang, Gureasko et al. 2006). The ATP concentration was kept at 0.5 mM in all the assays. The buffer used contained 10 mM $MgCl_2$, 20 mM Tris, pH 7.5. The substrate peptide was using the OPTYF (KQWDNYEFIW). The concentration of the EphA3c (-mCitrine) protein used in the assay was in the range from 3.5 to 14 mM.

Intensity based FRET observation by fluorescence spectrometry

The intensity based observation of FRET signal was performed with Fluorometer. Transient ES interactions were determined in time-based experiments with fixed excitation (470nm) and emission wavelength (529nm). 49 µl of the pre-mixture containing purified EphA3c-mCitrine, Mg^{2+} and ATP were transferred into a fluorescent cuvette and placed into the sample chamber of the PTI fluorescent spectrometer. Spectroscopic measurements were taken for several minutes to record the baseline. Data acquisition was paused and 1 µl concentrated Cy3.5-substrate was added into the cuvette to start the phosphorylation reaction. Data acquisition was continued immediately.

The steady state ES complex emission scanning was performed similarly. In the 50µl cuvette, 5µM of purified recombinant EphA3c-mCit, 35 µM Cy3.5-substrate and a mixture of the two in the presence of 10mM AMPPNP were excited with 470 nm and emission wavelength changed from 520 to 620 nm respectively.

2.4 Generation of the Cy3.5-labeled EphA3 substrate

The Cy3.5-labeled EphA3 substrate Ac-K(Cy3.5)QWDNYEFIW-OH was synthesized as described with some modifications (Tara, John et al. 2009) in collaboration with Dr. Yongxiang Chen from Department of Chemical Biology, Max-Planck Institute of Molecular Physiology. Fmoc-Trp(Boc)-OH (1.0 eq.) was firstly attached to the trityl resin (initial

loading 1.75 mmol/g) in the presence of 2.0 eq. N,N-Diisopropylethylamine (DIPEA) in DMF/DCM (1:1 v/v) for 3 h followed by treatment with a solution of DMF/DCM/DIPEA/MeOH (1:1:0.3:0.7 v/v) for half an hour. The resulting loading was ca. 1.0 mmol/g measured by means of UV spectroscopy and 100 mg resin (0.1 mmol) loaded with Fmoc-Trp(Boc)-OH was used for peptide synthesis. The subsequent N-terminal peptide chain elongation was achieved by a standard Fmoc strategy using the commercially available amino acid building blocks. The Fmoc cleavage was achieved by shaking the resin five times for 10 min with a solution of piperidine/DMF (1:4 v/v). Each residue was coupled with 4.0 eq. Fmoc protected amino acid, 3.6 eq. HBTU, 4.0 eq. HOBt and 8.0 eq. DIPEA in DMF for 2 h. The acetyl group was finally added to the N-terminus employing a solution of Ac_2O/Pyridine/DCM (1:2:7 v/v). After drying in vacuum overnight, the resin was treated with 15 mL of trifluoroaceticacid/phenol/water/thioanisole/1,2-ethanedithiol (82.5:5:5:5:2.5v/v) solution to release the peptide while removing all of the side-chain protection groups. After the removal of trifluoroaceticacid by using argon flushing, the product was subsequently precipitated with diethyl ether. After purification by preparative HPLC, the pure peptide Ac-KQWDNYEFIW-OH (26.8 mg, 0.018mmol, 18%) was obtained. High resolution LC-MS was applied to identify the purity and molecular weight of the peptide, as shown in the S. Figure 1. (HR-ESIMS: *m/z*: calcd for $C_{72}H_{92}N_{15}O_{19}$: 1470.66939 $[M+H]^+$, found 1470.66919 $[M+H]^+$)

2.0 mg peptide (Ac-KQWDNYEFIW-OH) was then dissolved in 500 μL DMSO, followed by the addition of 2.0 mg Cy3.5-NHS-ester mono reactive dye and 15 µL triethylamine. The product was further purified by HPLC to obtain 1.6 mg Ac-K(Cy3.5)QWDNYEFIW-OH, as shown in S. Figure 2. (ESI-MS: m/z: calcd for $C_{111}H_{129}N_{17}O_{32}S_4$: 1170.39 $[M+2H]^+$, found 1170.47 $[M+2H]^+$).

2.5 Cell culture and microscopy

Cell culture

For routine passaging, cells were grown in a 10 cm petri dish and passaged when sub-confluent monolayers had formed. Passaging was undertaken by washing in PBS and detachment achieved with 2 ml of a 0.1% (w/v) Trypsin solution (PAN) and 0.02% EDTA at 37°C. Detached cells were resuspended with another 8 ml of full cell culture medium and inoculated to 35 mm MatTek dish or 10 cm petri dish for the following experiments.

Transient transfection

Fugene6/9/extreme (different batch) transfection reagent (Roche biochemical) was used for transient transfection of cell lines according to the manufacturer's instructions. In short, 3 µl of Fugene reagent was diluted into 97 µl of serum free DMEM and the mixture was incubated at room temperature for 5 minutes. 1 µg of plasmid DNA was added into the mixture and incubated for 15minutes. The mixture was added into the 35 mm MatTek dish (1×10^5 cells/dish split 1 day before, to achieve 60-70% confluent) drop wise. To ensure the optimal protein expression level, transient transfected cells were usually prepared 16 to 24 hours before the following experiments.

Starvation and stimulation

All transient transfected cells were serum starved in DMEM with 0.5 % FCS for at least 4 hours prior to stimulation. To facilitate the formation of clustered oligomeric ligands, 2 µl 1 µg/µl ephrin-A5-Fc was incubated (30 minutes at room temperature) at 1/8 molar ratio (unless otherwise stated) with 0.75 µl 1 µg/µl anti-human Fc antibody (R&D) and 37.25 µl PBS buffer. Stimulation of cells was undertaken in imaging medium (1 ml) in the presence of 2 µg/ml preclustered ephrin-A5 ligand as previously described (Wimmer-Kleikamp, Nievergall et al. 2008).

Microinjection

Microinjection is one of the key methods for the introduction of non-permeable molecules into cells. It allows single cell investigation to study complex cellular events and signal dynamics *in vivo*. However, the successful micromanipulation has to be done with great care. These steps consist of the preparation of suitable micro-capillary, angle adjustment of the manipulator, fine adjustment and focusing of the capillary and so on.

1. Injection needles were prepared from borosilicate glass capillaries, using a micropipette puller with optimized condition (P=500, heat=496/490, pull=40, vel=70, time=250).

2. Probes (Cy3.5-substrate) destined for microinjection were diluted in buffer (PBS) to a final concentration of 650μM.

3. The probes were centrifuged at 13000 g, 4°C for 15 min, the supernatant was immediately divided into small aliquots and the aliquot should be freshly spin for 10 minutes every time before the injection.

4. An Olympus FV1000 confocal microscope equipped with 63×oil objective, climate chambers (5% CO_2, 37°C) and automated micromanipulator (Inject Man II, Eppendorf, Germany) was used for microinjection.

5. The self-made capillary was back filled with desired probes using capillary loader and the liquid was pushed to the tip by shaking the hand. The injection angle was adjusted to 45° and the capillary was mounted to the capillary holder with matched adaptor (according to the diameter of the capillary).

6. A MatTak dish containing adherent cells was placed under the microscope. Focused the microscope on cells near the middle of the dish, and then focused approximately 300 μm above the cells.

7. The loaded capillary was first moved in coarse speed mode with help of the joystick to a position above the center of the petri dish. The movement of the capillary was monitored with the eyepieces. The capillary was lowed down until the visible tip was about 2-3 mm above the surface of the culture medium.

8. The Pc (compensation pressure) that can introduce continuous slow visible (in correspond fluorescence channel) outflow from the tip was chosen so that the unnecessary clog in the needle could be avoided. To start with, this condition (Pi (injection pressure)=180 hPa, Ti (injection time) =0.4 second, pc=50 hPa) was used for the Femto Jet with the combination of the capillary mention above.

9. The tip of the capillary was located by moving the joystick back and forth in the Y-axis while observing for the "shadow" through the microscope eyepiece. Centered the shadow, and brought the tip of the capillary down towards the focal plane of the microscope by slowly turning the joystick clockwise.

10. When the capillary touched the surface of the media, a reflection of light occurred. Switched to the fine speed mode and focused the microscope again on the cells. Brought the tip of capillary down towards the focal plane of the microscope and set a Z limit far above the cell for a test injection to ensure the sample could flow out from the tip as expected.

11. Canceled the Z limit and carefully lowered the capillary until the tip just touched the top of the region to be injected (both the cell and the tip are on focus). Set the Z limit again and rose up the capillary about 1-2 μm above the Z limit.

12. Simply by pressing the joystick button, automated injection was performed with the parameters set before.

13. Injected cells were kept on stage or in the incubator for at least 30 minutes before further experiments.

Fluorescence lifetime imaging microscopy (FLIM) and data processing

The FLIM set-up used in the presented work is a commercial integrated instrument as described elsewhere (Chandra, Grecco et al. 2012). In brief, the instrument is based on a vibrationally isolated, inverted microscope (Olympus FluoView FV1000 laser scanning confocal microscope) equipped with a time-correlated single-photon counting module (LSM Upgrade Kit, Picoquant). The microscopy stage was enclosed within a thermostatic incubation chamber that was heated to 37°C during live cells experiments. For detection of mCitrine, the sample was excited using a 470 nm diode laser (LDH 470, Picoquant) at 40MHz repetition. Fluorescence signal was collected through an oil immersion objective (60×/1.35 UPlanSApo, Olympus) (40×/1.2 NA air objective, for *in vitro* sample) and spectrally filtered using a narrow-band emission filter (HQ 525/15, Chroma). Photons were detected using a single-photon counting avalanche photodiode (PDM Series, MPD) and timed using a single-photon counting module (PicoHarp 300, Picoquant).

The FLIM data were analyzed with a custom developed software (Walther, Papke et al. 2011). All the time correlated single photo-counting (TCSPC) histograms were fitted by double exponential decay model including the instrumental response function (IRF). For

image processing operations, FLIM images were exported as 32 bit floating point TIFF files. In ImagJ, the mask according to the donor intensity was created and the background value was converted to “Not a Number” (NaN). Background was removed by multiplying the image with the created mask using the function “image calculator”. The average fluorescence lifetime (τ_{av}) of ROI was recalculated to compare the cells with or without microinjection of substrate. A pseudo color was applied to the intensity image and a customized lookup table (LUT) applied to the FLIM images with desired range as indicated in the LUT shown on figures respectively.

3 Results

3.1 Characterization of EphA3 kinase and substrate interaction in vitro

3.1.1 Preparation of recombinant protein for biochemical assays

The recombinant proteins used in this project were purified as described in section 2.3. In brief, the proteins were purified by a nickel-column (His-trap HP, 1/5ml) via the N-terminal fused 6×His-tag. Incubation with 10mM Mg^{2+} and 10mM ATP overnight is required for EphA3 kinase related proteins. The His-tag was removed by His-tag linked TEV protease digestion and excessive TEV protease was removed by passing the protein extract through the nickel-column again. The flow-through was collected and concentrated for further purification with a size-exclusion column (G200 or G75 chose accordingly) to improve the purity, which was checked by SDS-PAGE (Figure 3.1b). Purified protein was snap-frozen in liquid nitrogen and stored at -80°C for future experiments.

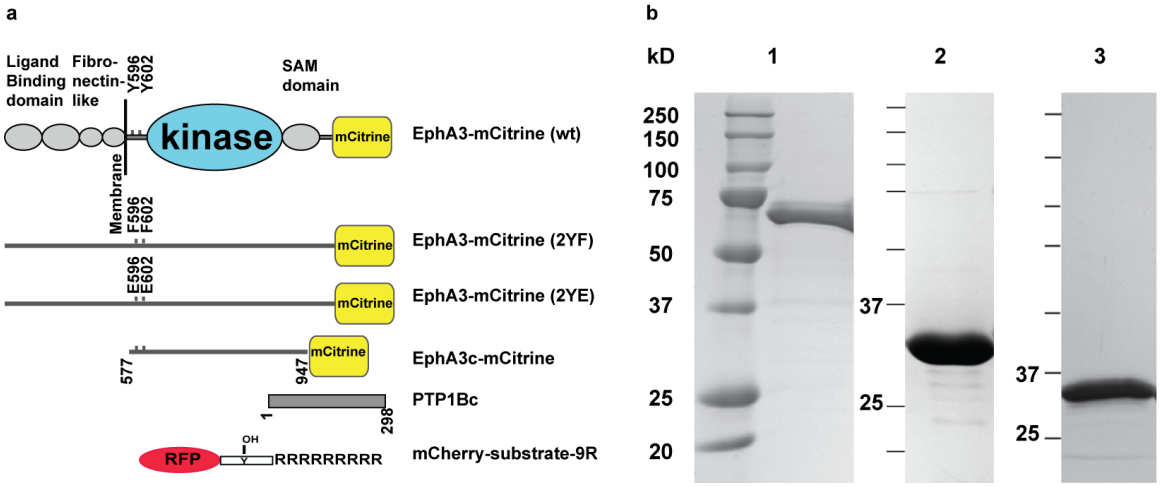

Figure 3.1 Recombinant proteins for the enzyme substrate interaction assay. a) The diagram of the EphA3 RTK-mCitrine WT, 2YF and 2YE mutants constructs; purified recombinant protein (EphA3c-mCit, PTP1Bc, and mCherry-substrate-9R). b) SDS-PAGE for the purified protein in (a). Lane1, EphA3c-mCitrine: EphA3c, amino acids 577–947, fused with mCitrine from C-terminal; lane2, PTP1Bc: PTP1B catalytic domain, amino acids 1-298; lane3, mCherry-substrate-9R, a poly

arginine peptide was fused to the C-terminal of the substrate to enable the cell penetration. Precision plus protein dual color standards purchased from Bio-Rad was applied to indicate the molecular weight of purified proteins.

3.1.2 Acceptor tagged substrate phosphorylation in vitro

The catalytic function of purified EphA3c-mCit (the catalytic kinase domain of EphA3 fused to the mCitrine and pre-activated (by ATP incubation and ATP was removed as described in method) if not indicated otherwise) was demonstrated by its ability to phosphorylate both mCherry-substrate and Cy3.5-substrate. By incubating purified recombinant EphA3c-mCitrine protein with mCherry-substrate in the presence of Mg^{2+} and ATP, the phosphate group is transferred to the tyrosine residue in the substrate region. The additional negative charge of the phosphate allows the separation of the phosphorylated mCherry-substrate from the unphorsphorylated one on native PAGE-Gel (Figure 3.2a). In general, the protein tyrosine kinase phosphorylation reaction is a rapid process. The result from Western blotting suggests that the substrate could be phosphorylated by EphA3c-mCitrine (Figure 3.2b) and the reaction was nearly completed after one minute (Figure 3.2c).

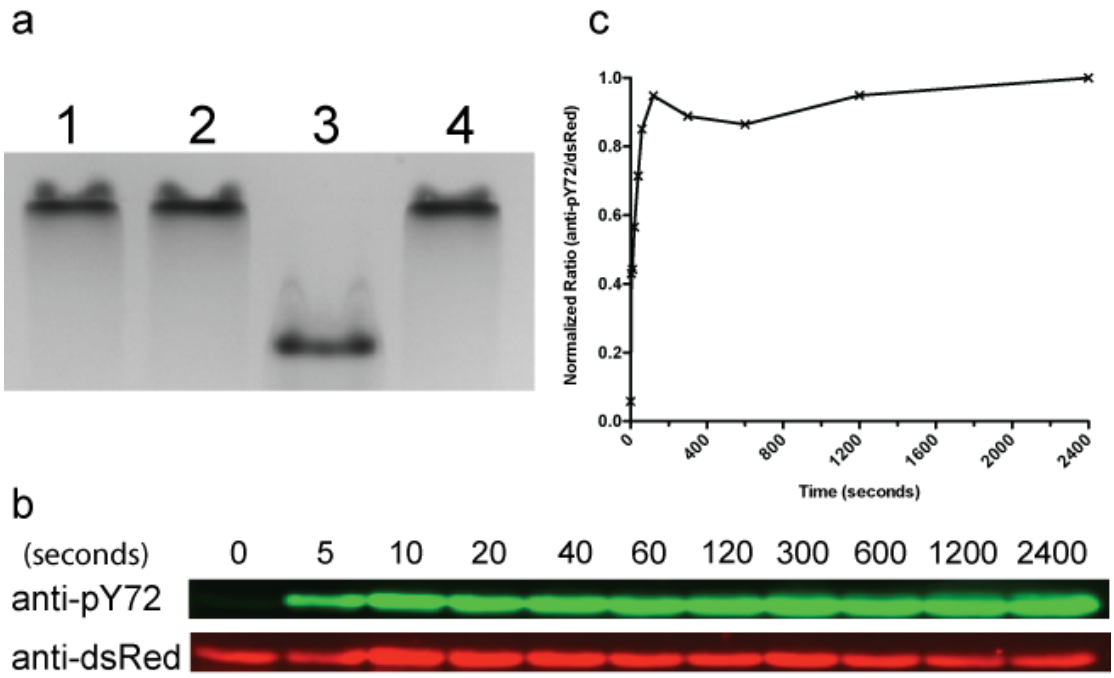

Figure 3.2 Characterization of EphA3c-mCitrine phosphorylation reactions with mCherry-substrate. a) 7.5% native gel was used to separate the phosphorylated and non-phosphorylated form of mCherry-substrate; 1, mCherry-Substrate; 2, mCherry-Substrate+ATP; 3, mCherry-Substrate+kinase+ATP; 4, mCherry-Substrate+Phosphatase. b) Western-blotting demonstrates the rapid phosphorylation reaction; Preheated 5×SDS loading buffer was used to quench the reaction samples in the following time points 0, 5, 10, 20, 40, 60, 120, 300, 600, 1200 and 2400 seconds. Antibodies recognizing mCherry and phosphorylated tyrosine residues were used to quantify the total amount of substrate and the phosphorylated portion respectively. ImageJ was used to quantify each band for densitometry analysis and the density ratio between the phosphorylated protein and total protein was plotted accordingly as shown in panel c.

The molecular weight of Cy3.5-substrate peptide (2339.79 Da) restricted us from using either western-blotting (the peptide is too small for SDS-PAGE and it can get through the PVDF membrane) or ESI-MS (the instrumental detection limitation of m/z is 2000) to observe the phosphorylation reaction. Furthermore, signals from phosphopeptides are generally weaker, as they are negatively charged and poorly ionized by electrospray MS.

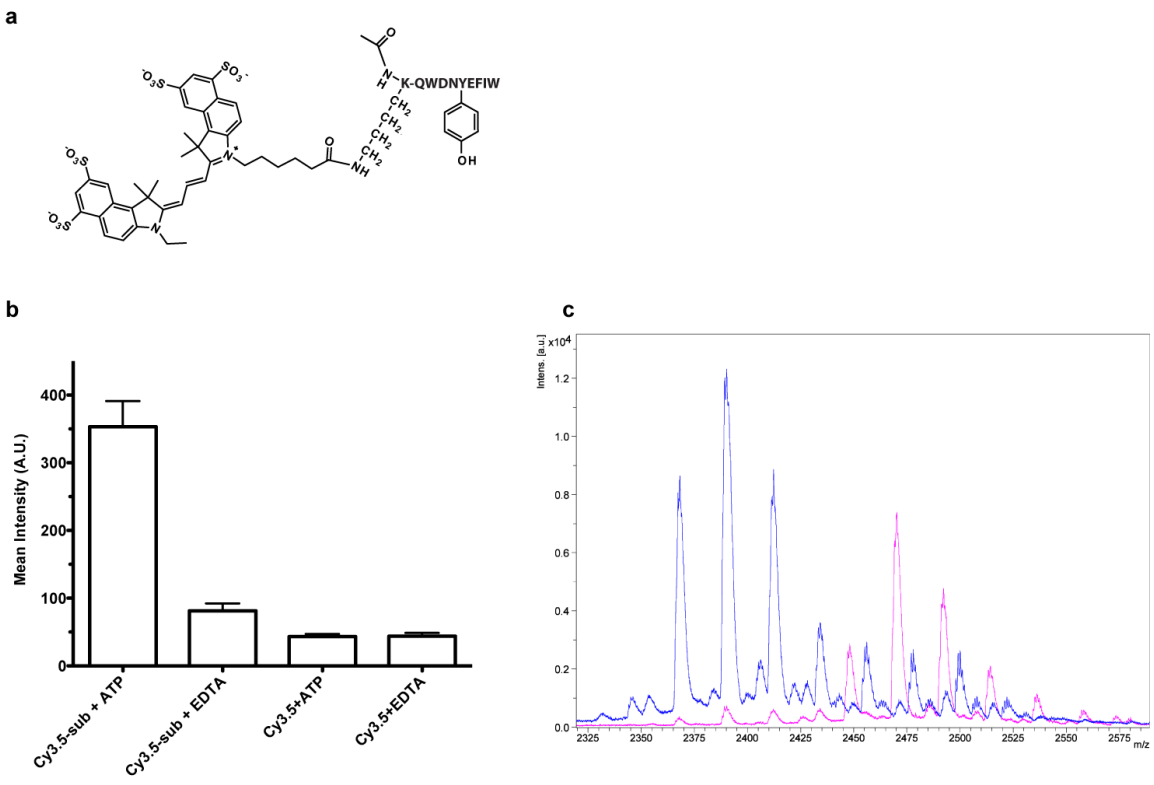

Figure 3.3, Determination of the phosphorylation of Cy3.5-substrate. a) The molecular structure of Cy3.5-substrate (OPTYF peptide sequence is KQWDNYEFIW) and the calculated molecular weight is 2340.58Da. b) Depicted are the fluorescence intensities (in arbitrary units (A.U.)) as function of the indicated condition with the mixture of recombinant EphA3c-mCit and Cy3.5-substrate or Cy3.5 as control in the presence of ATP or EDTA accordingly. Error bars indicate SD from 3 measurements. c) The sample as described above in the presence of ATP (red) or EDTA (blue) was determined by MALDI spectra. The extra phosphate group is attached to the labeled substrate. MALDI spectra were recorded on a Voyager-DE Pro Biospectrometry workstation from Applied Biosystems (Weiterstadt, Germany). Reaction products mixed with an equal volume of sample matrix (10 mg/mL 2,5-dihydroxybenzoic acid in water/acetonitril (1:1) containing 0.1 % (v/v) TFA). The mixture was quickly spotted on a MALDI sample plate, air-dried and spectra were measured with the following device settings: acceleration voltage = 25 kV, grid voltage = 93%, extraction delay time = 750 ns and guide wire = 0.3%. The laser intensity was manually adjusted during the measurements in order to obtain optimal signal to noise ratios (data obtained with the assistance of Long Yi).

As the substrate is conjugated with Cy3.5 dye (Figure 3.3a), anti-pTyr antibodies (pY72) linked proteinG glass beads were used to pull down the phosphorylated substrate by

centrifugation. After intensive washing steps, only the phosphorylated Cy3.5-substrate peptides would still bind to glass beads, which could be visualized using fluorescence microscopy. The fluorescence images were further quantified by ImageJ and plotted respectively. The phosphorylated Cy3.5-subtrates could be immunoprecipitated and detected as strong fluorescence intensity, whereas no significant signals were observed for the non-phosphorylated Cy3.5-substrate or free Cy3.5 dye (Figure 3.3b). Furthermore, the phosphorylation of Cy3.5-substrate by EphA3c-mCit was also examined by MALDI-TOF mass spectrometry (Figure 3.3c). The system error from this instrument limited the precise determination of the absolute molecular weight of the phosphorylated Cy3.5-substrate. However, the observed relative molecular weight shift upon phosphorylation (80 Da extra for the additional phosphate group) confirmed the phosphorylation of the Cy3.5-substrate and is consistent with the results obtained by the pull-down assay.

3.1.3 Detection of the stable ES-intermediate between EphA3c-mCitrine and acceptor tagged substrate peptide in vitro

The kinase phosphorylation reaction requires both ATP and a protein (peptide) substrate containing tyrosine residue so that the ternary complex can form and transfer the phosphate group from ATP to tyrosine. Instead of using ATP, we used its non-hydrolysable analog AMPPNP to stabilize the ternary complex in order to validate whether the enzyme-substrate complex can be detected by FRET between mCitrine and an acceptor fluorophore. FRET was measured by both intensity based fluorescence spectrometry and FLIM.

FRET occurs between donor and acceptor fluorophores and gives rise to a reduction of the donor fluorescence intensity and concomitantly to the increase of acceptor fluorescence intensity (Padilla-Parra and Tramier 2012). FRET could be detected by measuring donor emission intensity at a fixed wavelength as a function of time upon association of the

substrate peptide to EphA3c-mCit. The formation of transient ES-complexes was detected as a sharp drop in donor emission intensity upon substrate addition, displaying the quenching effect due to FRET. However, this apparent FRET signal is independent of the phosphorylation reaction catalyzed by EphA3c-mCit since the donor intensity was not recovered as expected from the disassociation of the Cy3.5-substrate upon phosphorylation (Figure 3.4a yellow). To exclude the bleed-through effects in the steady state emission scan experiment, the steady-state spectrum of acceptor was subtracted from the spectrum of the donor-acceptor mixture (Figure 3.4b dashed line). After the subtraction, the spectra only showed a minor acceptor signal, which might be ascribed to sensitized emission mixed with donor fluorescence bleed-through.

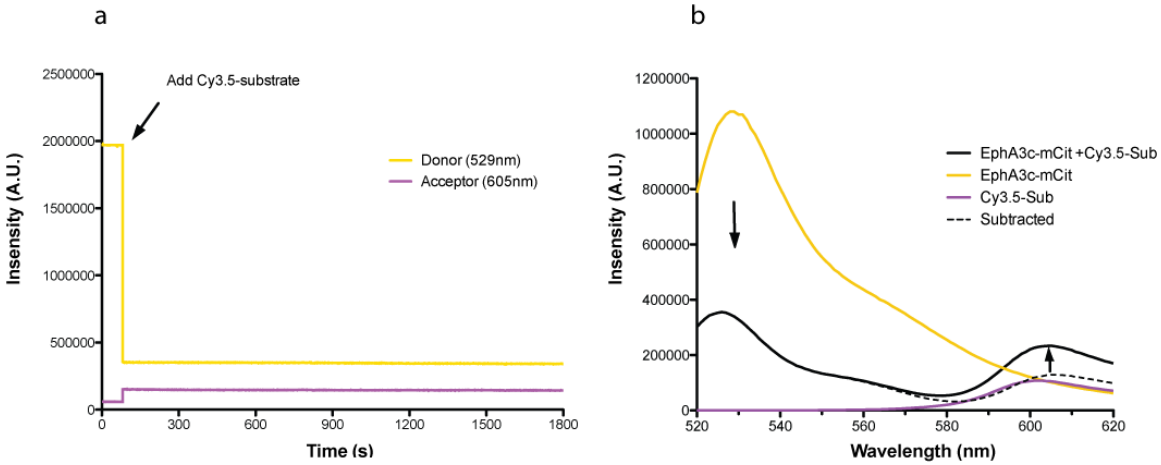

Figure 3.4, Intensity based FRET for observing EphA3 kinase substrate complex formation. a) 5 µM of purified recombinant EphA3c-mCit were pre-incubated with reaction buffer containing 10 mM ATP in a 50 µl cuvette. Emission intensity for both donor (529 nm, yellow) and acceptor (605 nm, purple) were measured with excitation at 470 nm. When the intensity for both channels were steady, 1 µl of concentrated Cy3.5-Substrate was added into the cuvette to achieve the final concentration of 35 µM and start the reaction. Quenching of mCitrine fluorescence and increased emission of Cy3.5 were observed upon excitation at 470 nm. However the FRET from the transient ES complex was independent of EphA3c phosphorylation reaction, as the intensity for both channels did not change after the addition of Cy3.5-substrate. b) The emission spectrum (520-620 nm) of samples containing 5 µM of purified recombinant EphA3c-mCit, 35 µM Cy3.5-substrate and a

mixture of those two in the presence of 10mM AMPPNP were scanned with 470 nm excitation. The quenching effect was observed for the donor (yellow) channel. After the subtraction of acceptor (red) from the mixture spectrum (black solid), there is a small residual signal in the acceptor channel (dashed line, after subtraction). More details can be found in the method section.

The FLIM technique measures the excited-state lifetime of the donor which fluorescence can be selectively detected by the narrow band pass filters of the FLIM instrument. Therefore, higher concentrations of acceptor tagged substrate could be applied to reach the maximum amount of enzyme-substrate complexes. With FLIM-FRET, we first validated the possibility of observing the formation of ES intermediates in solution.

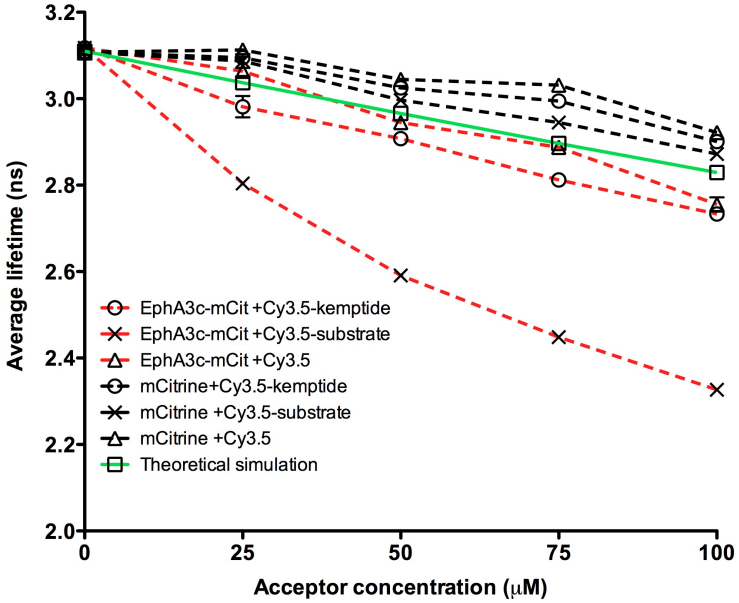

Figure 3.5 Concentration dependent kinase-substrate interactions in steady-state observed by FLIM-FRET. 10 μM of EphA3c-mCitrine was mixed with the indicated concentration of Cy3.5-substrate (dashed red line with cross) in the presence of 1mM of AMPPNP. The other samples with different combinations (mCitrine as donor or, Cy3.5-kemptide, Cy3.5 as acceptor) as indicated in the graph were mixed under the same conditions and measured as negative controls. The dashed red line represents EphA3-mCit as the donor and the dashed black line represents mCitrine as the donor. The green solid line is the theoretically computed curve for acceptor concentration quenching. The error bar represents the standard deviation from three measurements.

The same amount of purified recombinant EphA3c-mCit was mixed with different amounts of Cy3.5-substrate in the presence of AMPPNP. Since AMPPNP could not be hydrolyzed for the phosphorylation reaction, the ordinarily transient ES intermediate was stabilized and the FRET signal from the ES complex could be easily detected using FLIM. FRET in the ES complex was determined by the significant reduction of the donor fluorescence lifetime, where the amount of ES-AMPPNP ternary complex is correlated to the reduction in donor fluorescence lifetime (Figure 3.5 dashed red line with crosses). The donor fluorescence lifetimes of the control samples, such as the mixture of EphA3c-mCit with free Cy3.5 dye exhibited only a small change that is consistent with concentration quenching. The high concentration of free Cy3.5 indeed induced a detectable drop of the donor fluorescence lifetime that is consistent with the theoretically computed curve based on the average distance in solution between the donor and acceptor fluorophores at high concentration (Figure 3.5 green solid line) (Lakowicz 2006). This result argues that the quenching effect by the acceptor concentration has to be considered when a highly concentrated acceptor is applied to measure ES intermediates. However, we cannot exclude other trivial possibilities that affect the donor fluorescence lifetime such as the inner filter effect (Lakowicz 2006).

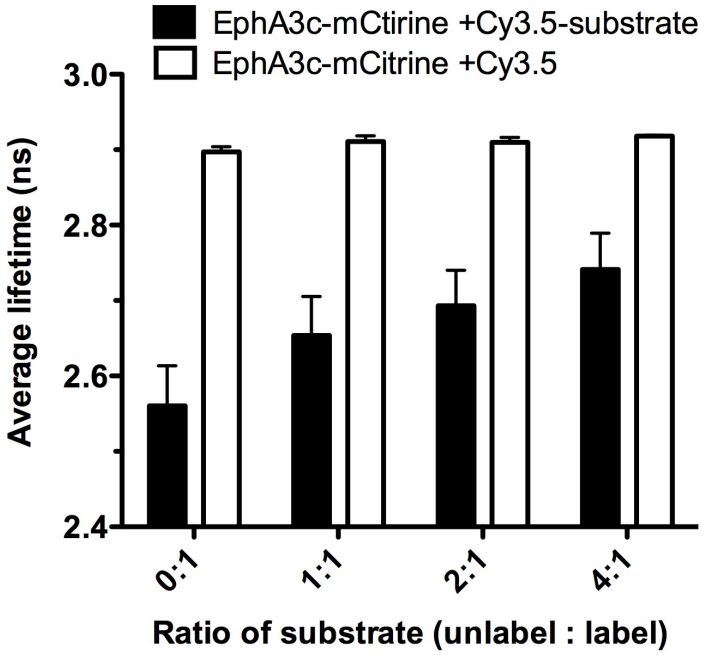

Figure 3.6, Validation of the specificity of the FLIM-FRET signal. To prevent binding of the Cy3.5-substrate (100 μM) to the EphA3c-mCit substrate-binding site, unlabeled peptide substrate was premixed with Cy3.5-substrate peptide at different ratios (4:1, 2:1, 1:1, 0:1). 1 μM EphAc-mCitrine in reaction buffer with 1 mM AMPPNP was added into those mixtures and incubated at room temperature for 30 minutes. 10 μl samples were placed on the coverslip and the EphA3c-mCit fluorescence lifetime in the presence of Cy3.5-substrate was measured (black column). The EphA3c-mCit mixtures with free Cy3.5 dye under the same condition (white column) were measured as controls. Error bar represents SD from three experiments.

To further prove that the specificity of the FRET signal as measured by FLIM reports on the binding of the Cy3.5-substrate to the active site, we introduced the unlabeled substrate peptide into the ES mixture described above. The competition with the unlabeled substrate peptide should lead to a reduced occupancy of the substrate-binding site in EphA3c-mCit by the Cy3.5-substrate. A recovery of the average donor fluorescence lifetime was observed that was dependent on the amount of unlabeled substrate peptide in the mixture (Figure 3.6, black column) which shows that FRET indeed occurs between EphA3c-mCit and the Cy3.5-substrate bound to the active site.

Fluorescence correlation spectroscopy (FCS) records fluorescence intensity fluctuations in the small volume with high temporal resolution (Breusegem, Levi et al. 2006). Therefore, we also applied this technique as an independent observation of enzyme substrate interactions by monitoring FRET signals with the donor intensity fluctuations. The addition of ATP allows the initiation of the phosphorylation reaction, which leads to the rapid turnover of ES intermediates toward the final phosphorylated substrate products (Figure 3.2b). The phosphorylated protein substrate disassociates from the EphA3c-mCit kinase binding pocket and results in the reduction of the FRET signal which is detectable by the enhanced count rate per molecule (intensity correlated)(Figure 3.7a, red column) and increased average lifetime (Figure 3.7a, red dot) of the donor fluorophore. The count rate and the lifetime of the negative control with the EphA3c-mCit and mCherry mixture were not affected by the addition of ATP.

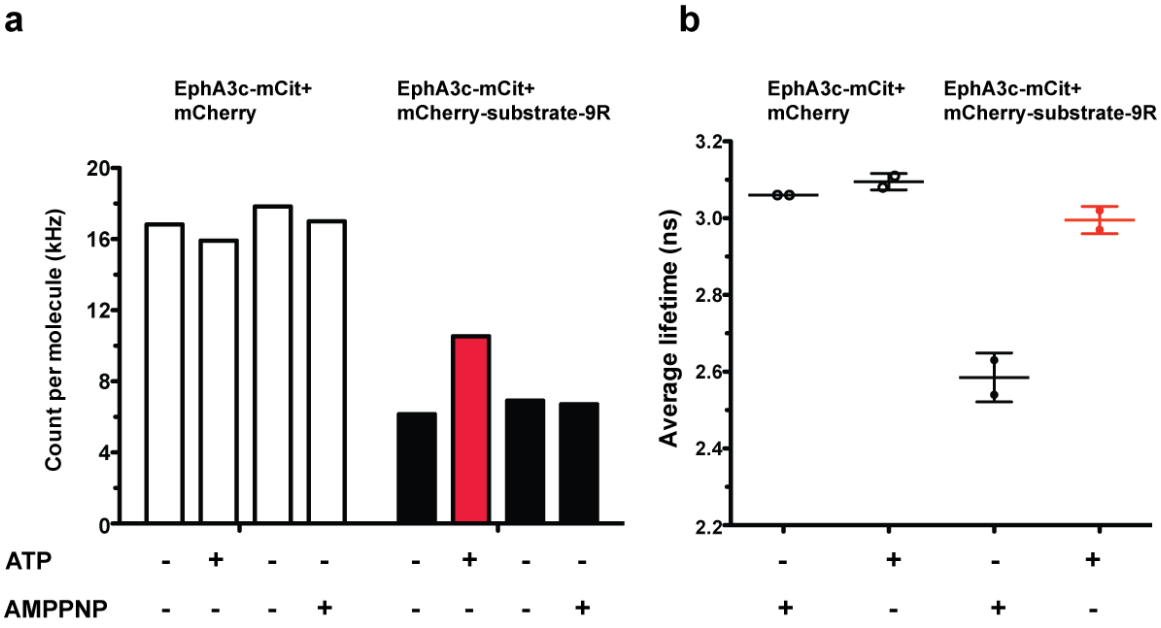

Figure 3.7 Observation of transient and stable ES intermediates. a) 50 nM of EphA3c-mCit was mixed with 30 μM mCherry-substrate-9R in the presence of AMPPNP or ATP as indicated. The count rate from each donor molecule was calculated by ConfoCor3 software (LSM510 Carl Zeiss

microscopy). b) The same samples mentioned above in panel (a) were also used for FLIM measurement as previously described. The red color indicates the changed intensity and lifetime after the addition of ATP.

3.1.4 Monitoring the ES-intermediate at steady-state by FLIM in vitro

The molecular system of phosphotyrosine (pTyr)-based signal transduction transmits extracellular/cellular regulatory information to downstream target proteins in the cytoplasm. Both RTKs and PTPs are involved in maintaining the steady-state level of tyrosine phosphorylation at each time point in living cells. It has been reported that PTP1B modulates signaling and enzymatic activity of the EphA3 RTK spatially and thereby affects functions such as cell positioning during normal and oncogenic development (Nievergall, Janes et al. 2010). We had shown that the interaction between EphA3c-mCit and Cy3.5-substrate could be detected by FLIM *in vitro*. We wanted to show that we could observe the ES intermediate also at steady-state in a cyclic phosphorylation/dephosphorylation reaction (Figure 3.8).

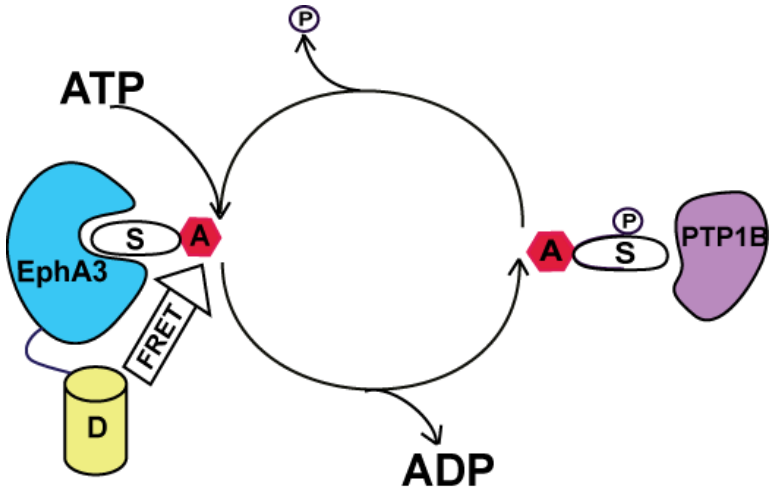

Figure 3.8, Monitoring steady-state ES-intermediate in a cyclic phosphorylation/ dephosphorylation reaction by FRET. The donor YFP (yellow) fused to the EphA3 catalytic domain (cyan), Cy3.5 (red) labeled tyrosine containing synthetic substrate peptide (S) and ATP form a transient ternary complex. The substrate binds to the kinase active site and FRET occurs, which can

be monitored by FLIM. After catalysis, the reaction product dissociates from EphA3, resulting in a loss of FRET. The substrate is dephosphorylated by PTP1B (magenta) and re-associated with EphA3 kinase.

As illustrated in the schematic diagram shown in Figure 3.8, we established a reconstituted system with purified recombinant proteins and synthetic peptide substrates. The basic system includes reaction buffer, EphA3c-mCit and Cy3.5-substrate. Addition of ATP to this basic mixture leads to the phosphorylation and disassociation of the Cy3.5-substrate and therefore increases the average donor lifetime, which is consistent with results from the mCherry-substrate-9R (Figure 3.7b, Figure 3.9b). To generate the phosphorylation cycle, excess ATP and different amounts of purified PTP1Bc were sequentially added to the basic mixture and the average donor fluorescence lifetime of those samples was measured within 5 minutes. The amount of PTP1Bc in the reaction mixture dictates the de-phosphorylation reaction rate, and consequently affects the amount of ES complex at steady-state by providing un-phosphorylated Cy3.5-substrates to EphA3c-mCit (Figure 3.9a). There was a turning point (0.04/1 PTP1Bc to EphA3c-mCit ratio) where the average donor fluorescence lifetime increased again when an excess of PTP1Bc was presented to the reaction mixture. One possibility is that the excess of PTP1B counter-acts the auto-phosphorylation of EphA3c-mCit on the juxtamembrane segment (JMS) and activation loop (AL), thereby inactivating the enzyme (Figure 3.9a).

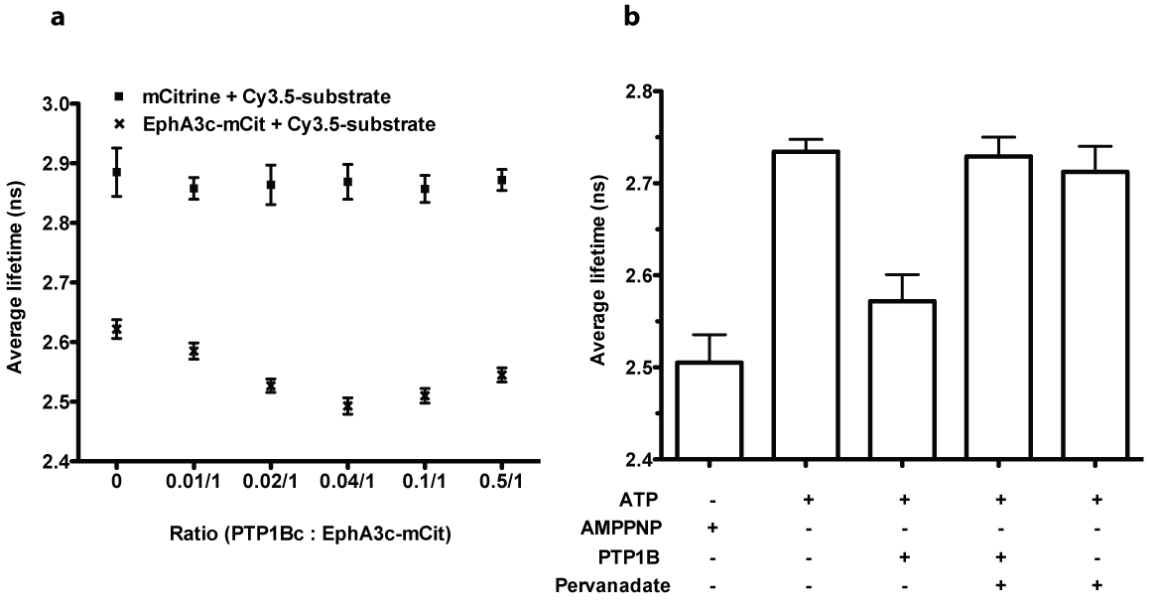

Figure 3.9, Probing the ES-intermediate with FLIM in a steady-state phosphorylation cycle maintained by EphA3c-mCit and PTP1Bc. a) PTP1Bc titration. Different amounts (molar ratio to EphA3c-mCit is indicated) of PTP1Bc were mixed with 10 μM EphA3c-mCit, 100 μM Cy3.5-substrate and 10 mM ATP in reaction buffer. The average donor lifetime was measured 5 minutes after the addition of PTP1Bc. Purified mCitrine was used as the negative control of which the fluorescence lifetime was not influenced by the addition of PTP1Bc. b) As described above, 10 μM EphA3c-mCit, 100 μM Cy3.5-substrate and 10 mM ATP were mixed in a reaction buffer for *in vitro* FLIM measurements. Addition of 0.4 μM of PTP1Bc lowers the fluorescence lifetime of EphA3c-mCit as in panel (a). Addition of the phosphatase inhibitor pervanadate (1 mM) abolishes dephosphorylation by PTP1Bc and leads to the loss of ES-intermediates and recovery of the donor fluorescence lifetime whereas the inhibitor itself had no effect. Substitution of ATP with AMPPNP resulted in a lower average fluorescence lifetime as previously described. Error bar represents SD from three experiments.

These observations from *in vitro* experiments raise the possibility that the EphA3 receptor tyrosine kinase substrate interaction could be visualized in cells by FLIM as described in the next section. We have shown here that this interaction is concentration dependent as the donor fluorescence lifetime is anti-correlated to the acceptor concentration. Additionally, this interaction could be interrupted by unlabeled substrate peptides. In agreement with the FLIM data, the fluorescence intensity (counts per molecule measured by FCS) of

EphA3c-mCit also changed owing to the replacement of AMPPNP with ATP, which initialize the phosphorylation reaction and change the amount of ES intermediates. Furthermore, the average donor fluorescence lifetime measured at the different phosphorylation equilibrium states demonstrate the possibility of monitoring the interplay between EphA3 kinase and PTP1Bc by ES imaging.

3.2 Characterization of EphA3 receptor tyrosine kinase and substrate interaction in vivo

Biochemical reactions are based on the fundamental physico-chemical processes of molecule binding, association, conformational change, diffusion and catalysis (Jares-Erijman and Jovin 2003). In living cells, the complex background of spatially organized intertwined reactions restricts the interpretation of catalysis with classic biochemistry theory on homogenous reactions. Functional fluorescence imaging of fluorescently tagged enzymes in living cells enables us to study their regulation in this complex context. Our *in vitro* results have validated the principle of ES imaging to monitor catalysis of EphA3 kinase. We were therefore in a position to apply this approach to study the regulation of EphA3 RTK catalytic activity in living cells.

3.2.1 Introduction of the acceptor conjugated substrate into living cells

The FRET signal from the ES complex can only be identified by FRET-FLIM at a certain substrate concentration range close to the *Km* of EphA3 kinase-substrate interaction. However, neither the overexpressed mCherry-substrate nor cell penetration peptides (CPPs) mediated mCherry-substrate-9R transportation (data not shown) could bring the acceptor substrate concentration up to the range in which we detected the notable FRET signal from the ES complex. Alternative methods to deliver non-permeable exogenous substances into cells are mechanical transduction methods such as microinjection.

Microinjection achieves high transduction efficiency and it controls delivery dosage and timing precisely, therefore it has been widely used in many research fields (Zhang and Yu 2008). Nevertheless, the injection itself causes a physical stress to cells which requires proper controls to ensure that the injection does not significantly affect cell function and viability (Zhang and Yu 2008).

In this work, microinjection was applied for the transduction of Cy3.5-substrate peptide into Cos-7 cell transiently expressing full length EphA3-mCitrine. All the injected cells were left on the microscope stage or in the incubator for at least half an hour to reach the relative steady-state and only those cells that survived the injection were used for further experiments.

The group of cells injected with Cy3.5-substrate had a much lower average donor fluorescence lifetime of the EphA3-mCitrine than those injected with Cy3.5 free dye (Figure 3.10, Figure 3.11). After microinjection of Cy3.5-substrate, Cos-7 cells transiently expressing EphA3-mCitrine WT, 2YF or 2YE exhibited different distributions of fluorescence lifetimes of the mCitrine. In contrast to WT, the 2YE mutant had the highest proportion of ES complexes as evident from the lowest average mCitrine fluorescence lifetime. This is possibly due to the more accessible substrate binding site as a result of the tyrosine (Y) to glutamic acid (E) substitution. The 2YE mutant has the negatively charged amino acid in the JMS that mimics the phosphorylation of the tyrosine that leads to the disordered structure of the JMS with enhanced substrate accessibility and kinase activity (Wybenga-Groot, Baskin et al. 2001; Tara, John et al. 2009). Accordingly, the tyrosine (Y) to phenylalanine (F) substitution mimics the un-phosphorylated JMS that interacts with the N- and C-lobe of the EphA3 kinase domain, thereby auto-inhibiting the kinase activity. Because of their less accessible active site, 2YF mutants exhibit a higher average donor fluorescence lifetime for

mCitrine than 2YE. Interestingly, WT EphA3-mCitrine expressing cells show an average donor fluorescence lifetime between that of the two mutants. The average donor fluorescence lifetime of WT EphA3-mCitrine was closer to that of the 2YF mutant (slightly lower than 2YF). Taken together, these results indicate that the EphA3 RTK WT was auto-inhibited in starved Cos-7 cells.

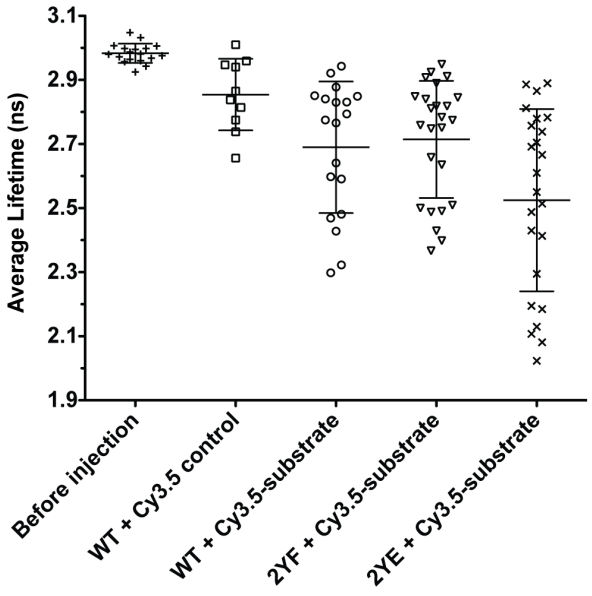

Figure 3.10, Comparison of the EphA3-mCitrine average donor fluorescence lifetime at steady-state after microinjection. Cos-7 cells transiently expressing EphA3-mCitrine (WT or 2YF, 2YE mutant) were starved for at least 4 hours before microinjection. Free Cy3.5 dye was microinjected into the WT cells as the negative control. Two tyrosine residues (596, 602) in the juxtamembrane segments (JMS) were substituted by either phenylalanine (2YF) or glutamic acid (2YE) to modulate the accessibility of substrate binding site in the EphA3 kinase domain. Error bar represents the standard deviation from the data set.

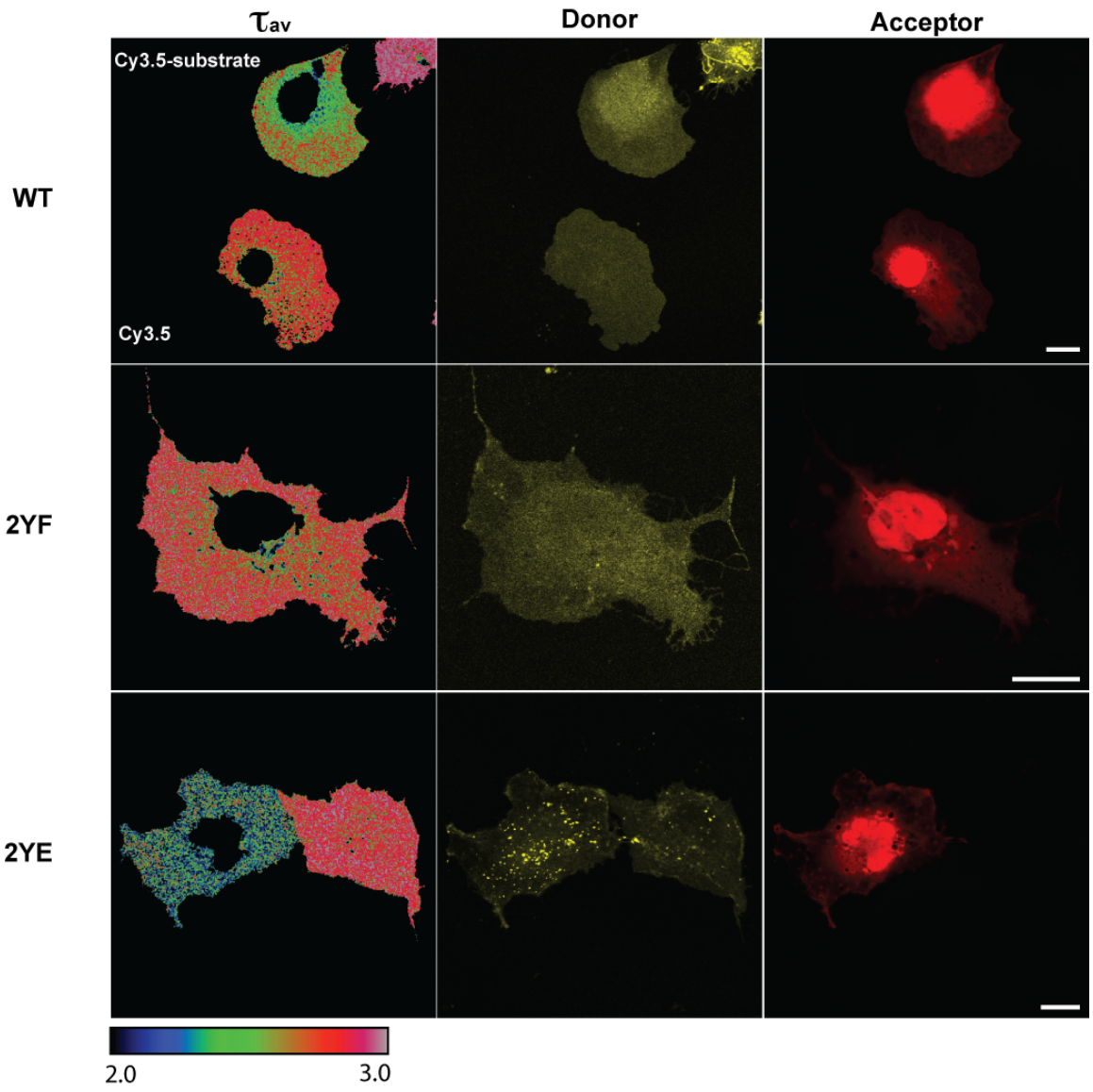

Figure 3.11, Spatial distribution of the EphA3-mCitrine (WT&MT) average donor lifetime at steady-state after microinjection. Cos-7 cells transiently expressing EphA3-mCitrine (WT or 2YF, 2YE mutant) were starved for at least 4 hours before microinjection. Free Cy3.5 dye (lower cell in the upper panel) was microinjected into the WT cells as the negative control. The rest of WT, 2YF and 2YE expressing cells were microinjected with Cy3.5-substrate. The cells were allowed to recover for 30 minutes before FLIM data acquisition. The nuclear area was masked in the analysis to omit the dominating concentration quenching effect. Scale bar: 20 μm, rainbow color bar: 2.0 to 3.0 ns.

3.2.2 EphA3 RTK substrate interaction upon ephrin-A5 stimulation

Oligomerization rather than dimerization of ephrin-A5 is required for the stimulation of cells expressing EphA3 RTK (Binns, Taylor et al. 2000). To achieve this with soluble ligands, Fc-fusion proteins of the soluble ephrin-A5 extracellular domain were clustered by anti-Fc antibody cross-linking. Addition of pre-clustered ephrin-A5 triggers the assembly of EphA3 clusters, therefore allowing intermolecular auto-phosphorylation of several key tyrosine residues (Binns, Taylor et al. 2000). Briefly, the switch to an active conformation involves a coordinated phosphorylation of the JMS and kinase domain tyrosine residues to relieve the distortion of the N-terminal catalytic kinase lobe leading to a conformation where the substrate has access to the active site (Wybenga-Groot, Baskin et al. 2001).

To investigate this regulatory mechanism in living cells, Cos-7 cells transiently expressing EphA3-mCitrine were microinjected with Cy3.5-substrate and, 1 hour later, stimulated with pre-clustered ephrinA5-Fc ligand. Initial binding of Cy3.5-substrate to the EphA3 RTK was observed as a significantly reduced average donor fluorescence lifetime, 5 minutes after microinjection (Figure 3.12 a,b). The amount of ES complexes further increased over 60 minutes as shown in a further drop in average donor fluorescence lifetime of 70 ps. In some microinjected cells, EphA3 RTK clustering could be observed after this period. This suggests a possible stress response upon microinjection of cells that activate the EphA3 receptors or that an excess of Cy3.5-substrate shifts the conformational equilibrium toward the active state by stabilizing the “open” catalytically active conformation by interaction with the active site.

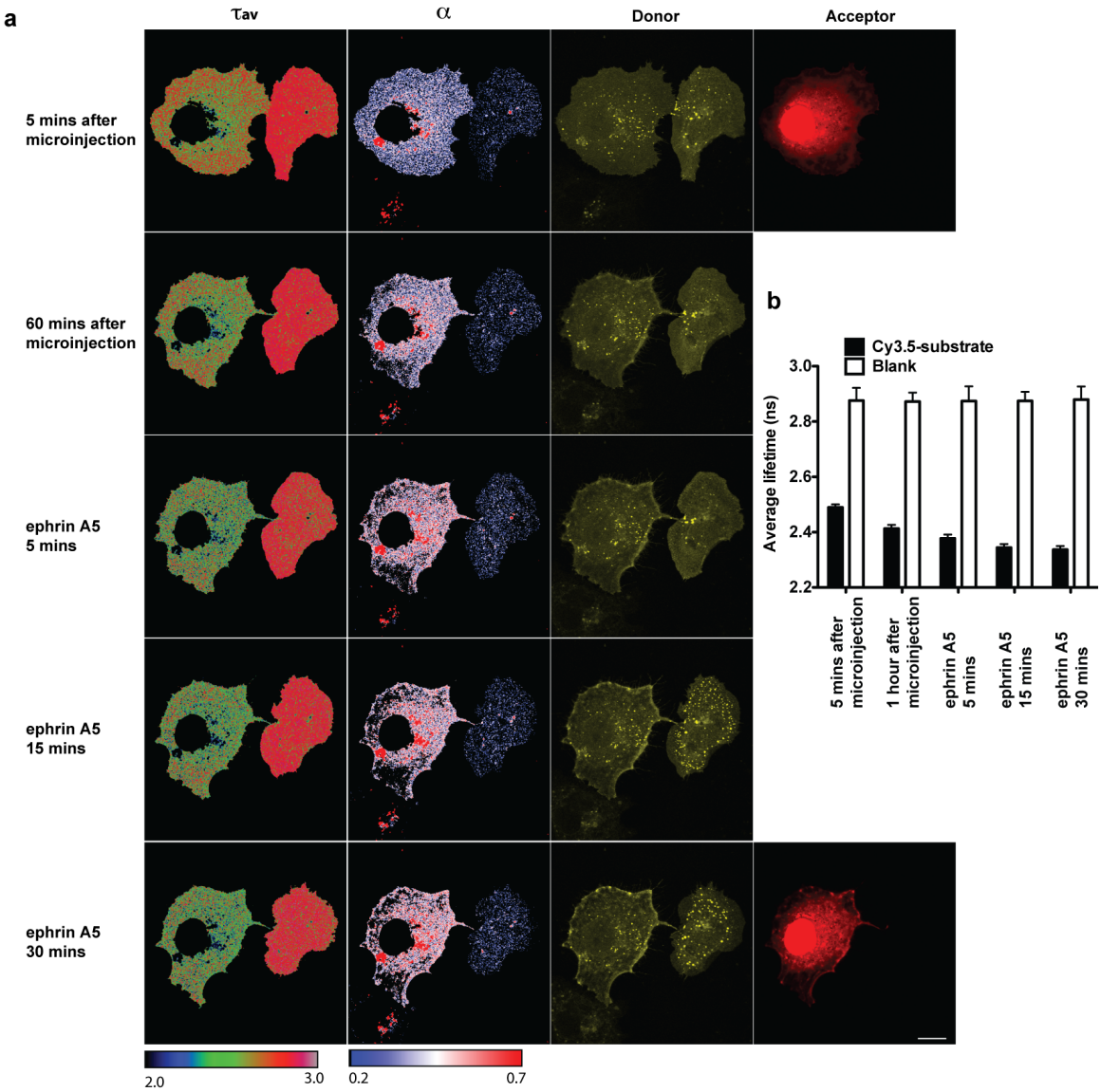

Figure 3.12 ephrin A5 stimulation activates EphA3 RTK kinase. a) Cos-7 cells transiently expressing EphA3-mCitrine (WT) were starved for 5-7 hours and microinjected with Cy3.5-substrate (left cell). 1 hour after injection, the pre-clustered EphrineA5 ligand was added to stimulate the cells as previously described (Nievergall, Janes et al. 2010). For each sample, the fluorescence intensity of mCitrine (donor), the fluorescence intensity of Cy3.5 (acceptor), the spatial distribution of the mean fluorescence lifetime (τ_{av}) in nanoseconds is shown. The fraction of EphA3-mCitrine interacting with substrate (α) as computed from global analysis is also shown. Scale bar: 20 μm; b) Average fluorescence lifetime (τ_{av}) of mCitrine in Cy3.5-substrate microinjected cell (solid column; Cy3.5-substrate) and non-injected cell (empty column; blank). Error bar represents SD from the FLIM data fitting.

A further reduction of the average mCitrine fluorescence lifetime could be ovserved after addition of pre-clustered ephrin-A5-Fc to the cells (Figure 3.12a,b). This suggests that the ephrin-A5 ligand enhances EphA3 RTK clustering and thereby increasing the substrate accessibility of the active site. Notably, ligand-induced endocytosis of the receptor was less pronounced in the substrate-injected cell. This result suggests that ES imaging can be used for studying the relation between EphA3 conformation and catalysis in living cells. Care should be however taken in interpreting receptor trafficking and cellular responses because the microinjection of the fluorescent substrate causes a serious perturbation of cell physiology.

3.2.3 Kinase/phosphatase cycles in the regulation of EphA3 activity in cells

Similar to other RTKs, the activation of EphA3 involves a change in the balance between tyrosine kinase and phosphatase activities that maintain the steady-state level of EphA3 tyrosine phosphorylation. Inhibition of the phosphatase activity shifts this balance towards the tyrosine kinase activity, leading to phosphorylation of the receptor and its full activation. To date, several PTPs have been implicated with Eph signaling. For example, changes in PTP1B expression significantly affect duration and amplitude of EphA3 phosphorylation and its biological response (Wimmer-Kleikamp, Nievergall et al. 2008; Nievergall, Janes et al. 2010). This activation process of Eph, incorporating the phosphorylation of JMS and kinase domain (KD) tyrosine residues, emphasizes that a tight threshold level of phosphorylation is required for Eph activation.

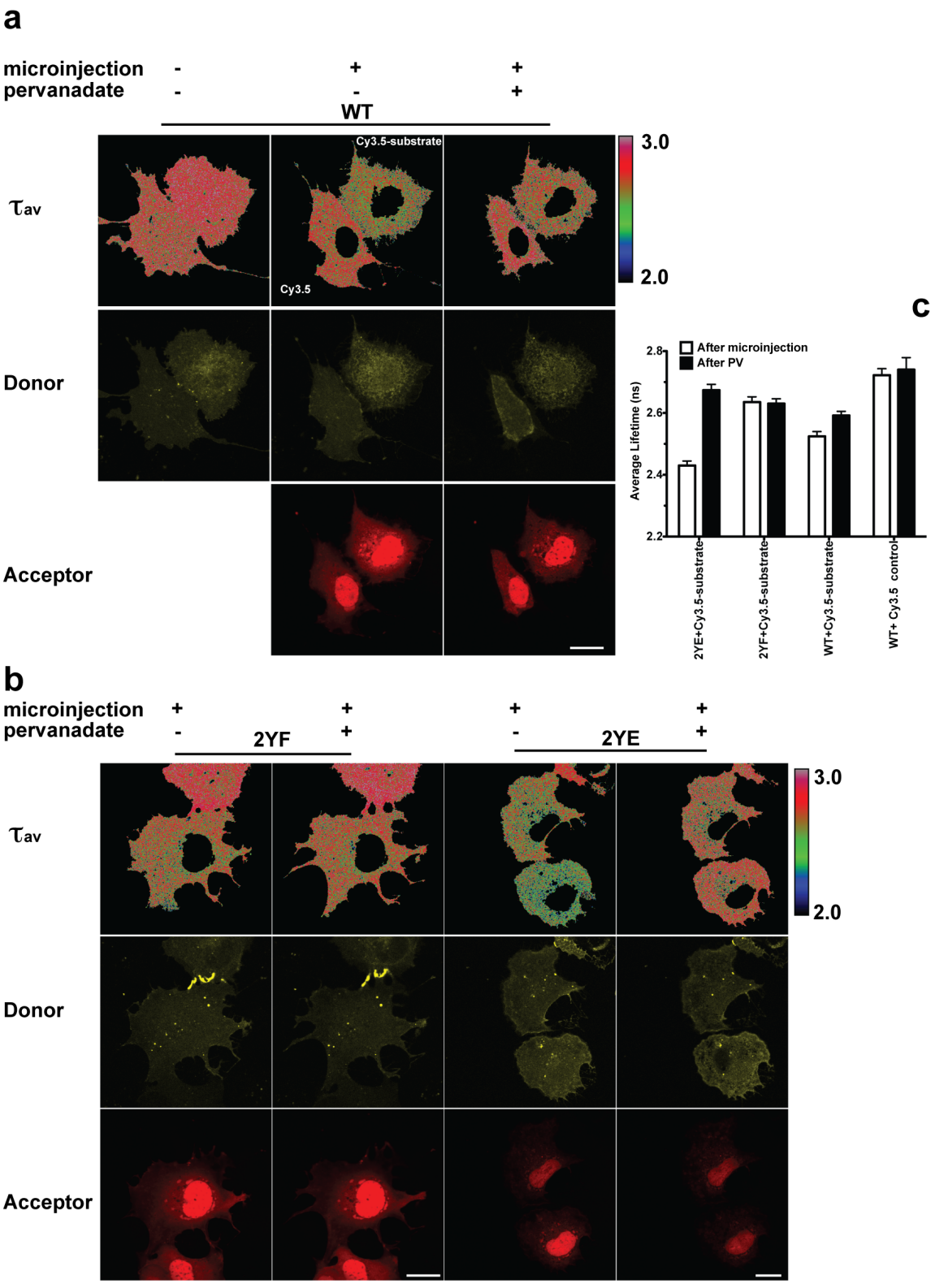
a
microinjection - + +
pervanadate - - +
WT
τav
Donor
Acceptor
Cy3.5-substrate
Cy3.5
3.0
2.0
c
After microinjection
After PV
Average Lifetime (ns)
2.8
2.6
2.4
2.2
2YE+Cy3.5-substrate
2YF+Cy3.5-substrate
WT+Cy3.5-substrate
WT+ Cy3.5 control
b
microinjection + + + +
pervanadate - + - +
2YF
2YE
τav
Donor
Acceptor
3.0
2.0

Figure 3.13, The phosphatase inhibitor pervanadate perturbs the steady-state phosphorylation level of the EphA3 substrate. a) Cos-7 cells transiently expressing EphA3 (WT)-mCitrine were microinjected with Cy3.5-substrate (right) or Cy3.5 alone (left). After 30-60 minutes recovery time the phosphatase inhibitor pervanadate (PV, 1 mM final concentration) was added. For each sample, the fluorescence intensity of mCitrine (donor) and Cy3.5 (acceptor), the spatial distribution of the mean fluorescence lifetime (τ_{av}) in nanoseconds is shown. Scale bar represents 15 μm. b) Cos-7 cells expressing EphA3-mCitrine 2YE or 2YF mutants were microinjected with Cy3.5-substrate. Cells were treated by PV as described above. c) The mean fluorescence lifetime (τ_{av}) of the EphA3-mcitrine (WT, 2YF or 2YE) expressing cells after microinjection (white column) and after 1 mM PV treatment (black column) were quantified respectively and plotted in the column bar format. Error bar represents SD from the FLIM data fitting and scale bar represents 20 μm.

The non-phosphorylated Eph JMS considerably distorts the N-lobe of the catalytic kinase domain and disrupts the active site conformation. Phenylalanine replacement of the tyrosines in the JMS results in severe loss of ephrin-induced kinase activation, suggesting the involvement of these tyrosine residues in the regulation of Eph activation. To clarify the JMS regulatory mechanism of EphA3 activation in living cells, Cos-7 cells transiently expressing EphA3-mCitrine with JMS regulation-deficient mutations, such as EphA3 (2YF)-mCitrine (tyrosine-to-phenylalanine) and EphA3 (2YE)-mCitrine (tyrosine-to-glutamic acid), were microinjected with Cy3.5-substrate.

We have shown that those mutants possess different binding efficiencies to the substrate in Cos-7 cells (Figure 3.10). It was previously shown that those mutants also possess different kinase activities and phosphorylation levels in cell lysates (Davis, Walker et al. 2008; Shi, Yue et al. 2010). Remarkably, inhibition of phosphatases by pervanadate for 1 hour has different influences on the donor fluorescence lifetime of mCitrine fused to the different mutants of EphA3 in Cy3.5-substrate microinjected cells (Figure 3.13a,b,c): 2YF remained the same, whereas 2YE and WT increased (Figure 3.13c). The 2YE possesses a negatively charged JMS that mimics the disordered JMS upon phosphorylation resulting in a relieved auto-inhibition of the kinase catalytic activity. When phosphatases are inhibited by

pervanadate, the dephosphorylated Cy3.5-substrate is depleted, leading to an empty binding pocket and an increased 2YE EphA3-mCitrine fluorescence lifetime (Figure 3.13b,c). In contrast, the ordered JMS in the 2YF mutant prevents the kinase domain from the adopting a productive conformation that allows substrate binding. Depletion of substrate by phosphatase inhibition by pervanadate treatment has therefore no effect on the fluorescence time of this mutant EphA3-mCitrine (Figure 3.13b,c). Notably, the slightly lower donor lifetime of the EphA3-mCitrine WT after microinjection of Cy3.5-substrate suggests that part of the EphA3 RTKs adopt a catalytically active conformation in living cells in absence of ligand. The inhibition of phosphatases activity could stimulate the auto-phosphorylation of EphA3 in the JMS, whereby the acceptor adopts a catalytically competent conformation that phosphorylates and depletes the Cy3.5-substrate. This reduces the amount of ES complexes and enhances the average donor fluorescence lifetimes (Figure 3.13a,b,c). Cos-7 cells transiently expressing EphA3-Citrine microinjected with free Cy3.5 dye did not exhibit a notable effect on donor fluorescence lifetime upon the addition of pervanadate (Figure 3.13a,c), showing that the observed effects on the lifetime of EphA3-mCitrine in Cy3.5-substrate containing cells can be ascribed to changes in the amount of ES complexes.

4 Discussion

What is to date known about the regulation of enzymatic activities and protein-protein interactions has been gathered from years of research on biochemical experiments. However, if only classical biochemical methods are applied, cellular parameters such as enzyme/substrate compartmentalization, spatial distribution of natural regulators, and naturally occurring fluctuations of activity in time are neglected.

Our group has developed an approach for monitoring PTP1B enzyme substrate intermediates in living cells using FRET-FLIM (Yudushkin, Schleifenbaum et al. 2007). Despite the fact that the concept of enzyme-substrate (ES) imaging is generally straightforward, extending its usage to study kinases in living cells, specifically receptor tyrosine kinases (RTKs), has remained a challenge to date.

In this study, we applied the ES imaging approach to investigate the regulatory mechanisms of enzyme activity for a member of the Eph RTKs family, namely EphA3. In this assay, the enzyme was tagged with the monomeric donor chromophore Citrine, while the acceptor chromophore Cy3.5 was conjugated to a synthetic substrate (Figure 3.1a). The genetically coded EphA3-Citrine was transfected into living cells, while the synthetic substrate was microinjected. Upon formation of the transient enzyme-substrate complex, FRET could be observed and was measured quantitatively using FLIM.

The crystal structure of the EphA3 catalytic domain in complex with the synthetic peptide substrate used in this study has been resolved (Figure 4.1) (Tara, John et al. 2009). The calculated distance between the C-terminus of EphA3 kinase and the N-terminus of the substrate is about 29.1 angstrom, which is smaller than the R_0 (about 5.1 nm) value for YFP-Cy3.5 FRET pair (Figure 4.1). This provided the theoretical basis required to build and

validate the principle of FRET based ES imaging for EphA3 kinase substrate interactions, both in controlled *in vitro* conditions and more complex *in vivo* systems.

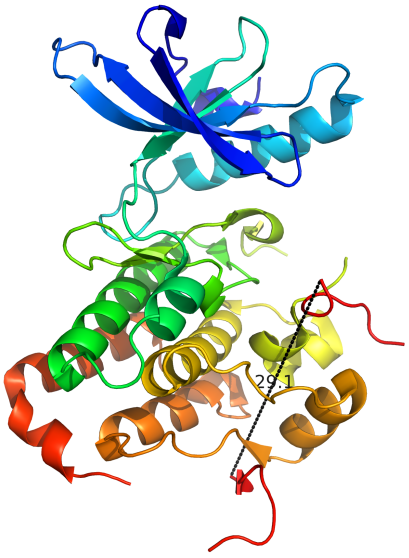

Figure 4.1 Structure of EphA3 kinase domain in complex with substrate (PDB: 3FY2). The crystal structure of the EphA3 kinase-substrate complex has been resolved (Tara, John et al. 2009) and the distance between the C-terminus of the kinase domain and the N-terminus of the substrate measured by MacPymol (Schrödinger LCC) is 29.1 angstrom which is smaller than the calculated R_0 (≈5.1 nm) for the mCitrine-Cy3.5 FRET pair (Sambrook and Russell.W 2001).

FLIM has several advantages as discussed in section 1.5.2. By using picoseconds pulsed lasers and gated photon counters, the precise excited-state lifetime of a fluorophore can be measured, and this relies on nano-environmental conditions such as hydrophobicity, pH, and FRET (Lakowicz 2006). FLIM can quantitatively detect FRET, independent of the fluorophore concentration. Thus, FRET-FLIM may be considered a valuable method for monitoring protein interactions, such as enzyme-substrate interactions, *in vivo.*

In this study we managed to directly monitor interactions between EphA3 RTK and its substrate using FLIM. The specificity of the observed FRET signal has been demonstrated in both *in vitro* and *in vivo* experiments. The application of this approach enables the

investigation of localized EphA3 RTK activity and its regulation in living cells. By comparing the formation of enzyme-substrate intermediates of wild type EphA3-mCitrine and JMS regulation-deficient mutants in Cos-7 cells, we were able to reveal the regulatory role of JMS phosphorylation towards EphA3 kinase active site accessibility in living cells.

4.1 Direct observation of Enzyme-Substrate complex via FRET-FLIM in vitro

In the presence of AMPPNP (ATP nonhydrolyzable analog), the ternary kinase-substrate-AMPPNP complex is trapped without catalysis. Therefore the observation of the FRET signal between purified recombinant EphA3c-mCit and synthetic Cy3.5-substrate peptide is more feasible than that of the complex in the presence of ATP. The FRET signal obtained from fluorescence spectrometry exhibited a significant quenching of donor intensity with negligible enhancement of the acceptor intensity. This may be due to the low quantum yield (QY) of Cy3.5 dye (QY≈0.15, according to the instruction from GE healthcare) and notable spectral bleed-through effect. We therefore decided to move to a superior technique, namely, FLIM to monitor the donor fluorescence lifetime. Donor fluorescence lifetime would be independent of its concentration and FLIM exhibits fewer artifacts in comparison to intensity-based FRET measurements. This enabled us to confirm that the donor intensity change was derived specifically from the FRET signal between the EphA3c-mCit and the Cy3.5-substrate.

The FRET signals might arise from both the formation of specific enzyme-substrate complexes and unspecific absorption of the substrate to EphA3c-mCit, thereby quenching the donor fluorescence. To rule out these non-specific effects, proper controls were required for the interpretation of the results. As opposed to the negative control samples (Figure 3.5), such as EphA3c-mCit with Cy3.5 free dye, the mixture of EphA3c-mCit with

Cy3.5-substrate in the presence of AMPPNP has a remarkably reduced average donor fluorescence lifetime and this reduction could be recovered by the addition of the competitive unlabeled "dark" substrate peptide. This indicates that the signals shown by FRET-FLIM were specifically derived from ES complexes (Figure 3.6). In contrast, the concentration quenching effects were observed at a different fluorescence lifetime range for negative controls, which is consistent with the theoretically computed model (Figure 3.5, green line). Moreover, the negative control is also not influenced by competition of the unlabeled substrate peptide, which further demonstrates the specificity of FRET signals from EphA3 kinase substrate interactions.

The molecular brightness of the donor fluorophore as measured by FCS suggested different amounts of ES complexes in the presence of ATP or AMPPNP (Figure 3.7). These different amounts of ES intermediate in the presence of ATP or AMPPNP have been confirmed by FRET-FLIM. The phosphorylation of substrates (either fused to mCherry or conjugated to Cy3.5) by EphA3c-mCit has been proven by assays such as western-blotting, pull-down and MALDI-TOF. Therefore, the amount of detected ES intermediate can be related to the catalytic turnover of the enzyme. The acceptor concentration-dependence of the donor fluorescence lifetime, together with the results on competition experiments using unlabeled peptide substrates suggests that FRET-FLIM can be applied to specifically measure this amount of ES complex in cells.

4.2 Phosphorylation equilibrium measured by FRET-FLIM both in vitro and in vivo

EphA3 phosphorylation and endocytosis are tightly controlled by PTP1B in both normal and cancer cell lines, thus regulating downstream cell morphological responses (Nievergall, Janes et al. 2010). PTP1B controls Eph receptor function by modulating the amplitude and

biological output of Eph/ephrin signaling (Nievergall, Janes et al. 2010). This phosphorylation dynamic is correlated to the auto-phosphorylation of EphA3 RTK in the JMS, which modulates the accessibility of the kinase active site.

A reconstituted system with purified recombinant EphA3c-mCit and PTP1Bc was established to observe EphA3 RTK phosphorylation in a catalytic cycle. The addition of PTP1Bc and ATP into the basic system was indeed able to generate a flux of Cy3.5-substrate between EphA3 and PTP1B. Dephosphorylation of the substrate by the phosphatase increased the amount of substrate for EphA3 and thereby the detected fraction of transient ES complex as shown by the lower donor fluorescence lifetime as compared to samples without PTP1Bc (Figure 3.9b). Interestingly, the maintenance of the ES complex by the substrate regenerating reaction of the phosphatase only took place in a certain concentration range. It has been reported that overexpression of PTP1B inhibits EphA3 internalization via its effective binding to phosphorylated EphA3 which competitively blocks access to the phosphorylated activation loop tyrosine required for endocytosis (Nievergall, Janes et al. 2010). A similar mechanism could explain the results from the *in vitro* reconstituted system. An excess of PTP1Bc could dephosphorylate tyrosine residues in the JMS of EphA3c-mCit and thereby inhibiting the kinase activity by the reduced substrate accessibility to the active site (Figure 3.9).

In living cells, the ES imaging principle for EphA3 kinase was demonstrated by direct monitoring interactions between mCitrine-tagged EphA3 RTK and Cy3.5-labeled substrate peptide using FRET-FLIM. About one hour after the microinjection of Cy3.5-substrate into Cos-7 cells transiently expressing EphA3-mCitrine, the ES intermediates reached a steady-state. The amount of EphA3-mCitrine RTK in transient steady-state ES complex reflects the accessibility of the kinase active site. The specificity of the FRET signal generated by ES

complex formation is also demonstrated by the comparison of the EphA3-Citrine RTK donor fluorescence lifetime after microinjection of Cy3.5-substrate or Cy3.5 free dye. The observed small decrease in donor fluorescence lifetime in the Cy3.5 dye-injected cells (Figure 3.10, 3.11) may be derived from the concentration quenching effects as previously discussed. Figure 3.11 shows an image containing two cells microinjected with two different reagents (either Cy3.5-substrate, upper cell or Cy3.5 free dye, bottom cell). From the specific drop of donor fluorescence lifetime in the cell microinjected with substrate, we can deduce that the FRET signal in the living cell is mainly caused by the formation of ES complexes, rather than as a result of a concentration quenching effect.

Previous reports suggested that an ordered activation loop (AL) in the structure is correlated with kinase activity and that the phosphorylation of the JMS modulates the transition between ordered and disordered AL. The EphA3 (2YF) mutant structure exhibited typical conformation of an inactive kinase in terms of the JMS ordering and the AL disordering (Davis, Walker et al. 2008) whereas the structure of EphA3(2YE) that mimics a phosphorylated JMS is still unknown. In EphA3 these two tyrosine residues (Y596 and Y602) have different functions in the regulation of catalytic activity. The single Y602F mutation did not exhibit lower catalytic activity and the Y596F mutant was only partially active with respect to the wild type EphA3 (Davis, Walker et al. 2008). Nevertheless, a contribution of these JMS tyrosine residues to the regulatory mechanism of EphA3 was suggested based on the properties of the double mutant (Y596F, Y602F), which was a much poorer enzyme as compared to the single tyrosine mutants. This is consistent with phosphorylation profiling of the EphA3 auto-phosphorylation by western blotting (Davis, Walker et al. 2008; Shi, Yue et al. 2010).

Different distributions of donor fluorescence lifetimes have been found with EphA3-mCitrine WT, 2YF and 2YE after microinjection of Cy3.5-substrates (Figure 3.10). The group of 2YF mutants (2.714±0.183 ns) exhibited a similar average donor fluorescence lifetimes to that of the WT (2.69± 0.206 ns), whereas the average donor fluorescence lifetimes of the group of 2YE mutants (2.525±0.2844 ns) were significantly lower. These different behaviors of the two mutants indicate their various binding affinities to Cy3.5-substrate, which suggest that most of the WT was auto-inhibited after starvation. Several different PTPs are involved in the maintenance of the EphA3 RTK phosphorylation state (Wimmer-Kleikamp, Nievergall et al. 2008) in living cells, where the opposing de-phosphorylation activity of phosphatases is in all probability more efficient than in an *in vitro* reconstituted system. Therefore, the different responses to the PTP inhibitor perturbation in living cells could represent the differential kinase activity of the WT and MTs (further discussed in section 4.3).

It has been suggested that the phosphorylation of the JMS exhibits a threshold that must be exceeded in order to induce receptor activation (Binns, Taylor et al. 2000; Davis, Walker et al. 2008). In starved cells, the auto-phosphorylation of EphA3 was suppressed for WT, 2YE and 2YF. It is possible that all their catalytic activities were inhibited and none of them could pass the threshold, which would enable the catalytic substrate conversion. As compared to 2YF and WT, the active site of the 2YE mutant has a more accessible active site because of its released disordered JMS. Consequently, more ES complexes were detected by FLIM. This phosphorylation threshold assumption in living cells is based on the fact that the EphA3 kinase activity is relatively low in the starved EphA3 WT and MTs expressing cells.

4.3 Phosphatase inhibition reveals the JMS regulatory mechanism for EphA3 RTK substrate accessibility in living cells

The first obvious consequence of EphA3 RTK activation is the auto-phosphorylation of cytoplasmic tyrosine residues, two of which are located in the juxtamembrane segment (Y596, Y602). A third (Y779) is located in the kinase activation-loop, whereas a fourth tyrosine (Y701) has no significant effect on kinase activity (Vearing and Lackmann 2005; Davis, Walker et al. 2008). Phosphorylation of the first three tyrosines is required for full enzyme activity. The crystal structure of EphA3 JMS and kinase domains revealed a dual inhibition mechanism, in which not only phosphorylation of the activation loop tyrosine, but also of the two juxtamembrane tyrosine residues, is necessary to relieve structural constraints that block substrate access to the kinase domain (Wybenga-Groot, Baskin et al. 2001; Davis, Walker et al. 2008). It is noteworthy that the replacement of these two tyrosines with phenylalanine (2YF) resulted in the loss of auto-phosphorylation and reduction of the response to ephrin-A5 involved cell migration inhibition (Davis, Walker et al. 2008; Shi, Yue et al. 2010). However, disordering of the JMS through phosphorylation results in only minor changes in the overall structure and orientation of the N- or C-terminal lobe (Davis, Walker et al. 2008). The 2YF mutant mimics the dephosphorylated JMS which was observed as the ordering conformation (Figure 4.2a) (Davis, Walker et al. 2008).

Our results suggest that the 2YF mutant has similar substrate accessibility as the EphA3 WT in non-stimulated cells, while the 2YE mutant seems to possess a conformation where the active site is accessible to substrates (Figure 3.10, 3.11). Treatment with the generic phosphatase inhibitor pervanadate perturbed the phosphorylation equilibrium as maintained by the PTPs and increased EphA3 phosphorylation (Nievergall, Janes et al. 2010). We have shown that this perturbation increased the donor fluorescence lifetime in

the reconstituted phosphorylation cycle because of substrate depletion (Figure 3.9a,b). Using ES imaging, different responses were observed for WT and MTs upon phosphatases inhibition. With the addition of pervanadate, the WT and 2YE mutant donor fluorescence lifetimes increased, whereas the 2YF mutant and Cy3.5 injected WT control cells remained unchanged (Figure 3.13).

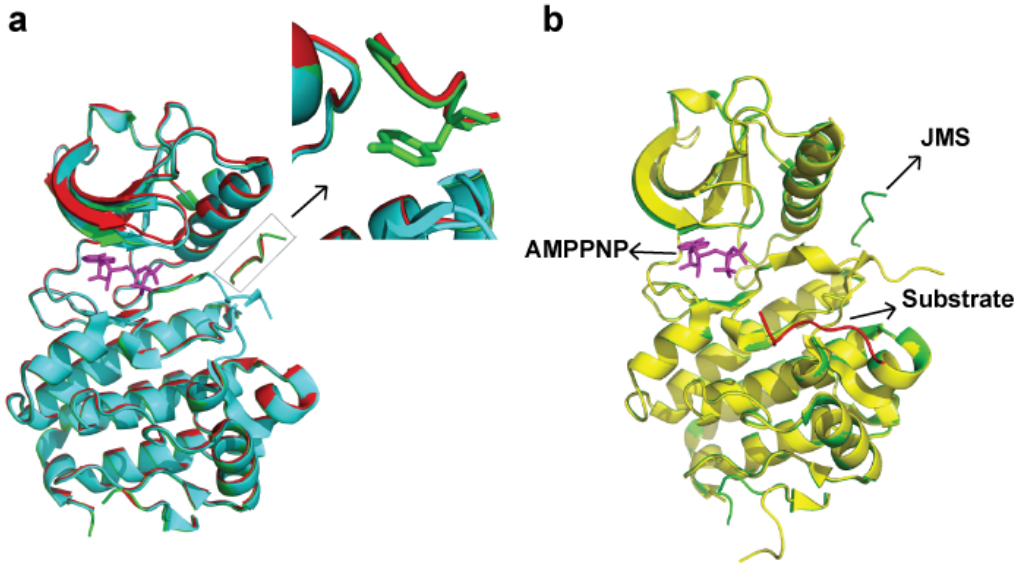

Figure 4.2 Crystal structure alignments reveal JMS regulation of EphA3 kinase (PDB: 2Q07, 2Q09, 2Q0I, 3FY2). a) Resolved structures of dephosphorylated EphA3 kinase domain (2Q07, green), phosphorylated EphA3 kinase domain (cyan, 2Q09) and EphA3 kinase domain 2YF mutant (red, 2Q0I) are aligned by MacPymol software (Schrödinger LCC). The phosphorylation affects EphA3 kinase structures mainly in the JMS and AL region. Dephosphorylated kinase domain and 2YF mutant possess an ordered JMS (zoomed figure), which suppresses their kinase activities (Davis, Walker et al. 2008). b) The structure of dephosphorylated EphA3 kinase domain (green, 2Q07) is aligned with the complex structure of phosphorylated EphA3 kinase domain and the OPTYF substrate (yellow, 3FY2). Interactions between the EphA3 kinase domain and the OPTYF substrate do not affect large conformational changes in the N- or C-terminal lobes of the kinase (Tara, John et al. 2009). The substrate peptide (red) and ordered JMS peptide (green) interact with different regions of the kinase domain.

As described in section 1.3.2, the protein phosphorylation reaction includes substrate binding, phosphoryl transfer and product release. Mutations introduced to the JMS might

affect the phosphorylation reaction in different ways. Inhibition of phosphatase increased the EphA3 auto-phosphorylation of Y596 and Y602 in the JMS whose disordering regulates both the AL conformation and the phosphorylation reaction rate. In the substrate injected EphA3 (WT) expressing cells, the FRET signal fluctuation upon perturbation is caused by both substrate accessibility adjustment and changes in catalytic activity. Phosphorylation of the JMS not only increases substrate binding (more ES complex, lower fluorescence lifetime) but also promotes catalysis (less ES intermediates, higher fluorescence lifetime). These opposing effects on the donor fluorescence lifetime might be dominated by catalysis when the net kinase activity is dramatically increased by the treatment of cells with pervanadate thereby resulting in an enhancement of donor fluorescence lifetime (Figure 3.13a,c).

The 2YF mutant restricts the accessibility of the active site for substrate. Thus, the donor fluorescence lifetime of 2YF mutants in living cells that were microinjected with substrate reflects only its substrate accessibility (Figure 3.13b,c). For the 2YE mutant, it is likely that the negative charge given by the glutamic acid residue substitution in the JMS restored EphA3 kinase activity to the fully activated state. In living cells, the catalytic activity of PTPs, such as PTP1B and SHIP2, is much higher than that of EphA3 kinases. The resulting fast dephosphorylation of the substrate maintains a high amount of transient ES intermediates as for example observed for the EphA3c/PTP1Bc cycle *in vitro* (Figure 3.9b). Without extra stimulation, a large fraction of 2YE mutants formed ES complexes in cells which points at a full accessibility of the active site (Figure 3.10). Therefore, we propose that the donor fluorescence lifetime measured by 2YE ES imaging mainly reflects its catalytic turnover rate. The other, more unlikely, possibility is that the 2YE mutants have a slower catalytic rate than the wild type enzyme, which stabilizes the ES complex in a subset of molecules with the open conformation

Former reports have shown that the wild type EphA3 RTK has basal kinase activity (Shi, Yue et al. 2010). EphA3 kinase WT should therefore exhibit a donor fluorescence lifetime that is in between that of the 2YE (active) and 2YF (inactive) mutants, after injection of Cy3.5-substrate. The observed distribution of donor fluorescence lifetimes of the WT enzyme was however similar to that of the 2YF mutant. This discrepancy may have occurred as a result of the following: first, the donor fluorescence lifetime of EphA3 WT exhibited a large variance that was depended on the amount of injected substrate. This suggests that a sub-population of EphA3 had an active conformation. It also seems likely that the 2YF undergoes this conformational "breathing" mechanism (the AL was phosphorylated by endogenous EphA3 in Cos-7 cells) and the temporarily relieved auto-inhibition also allows substrate binding to the kinase. Therefore, the WT adopts a JMS regulated intermediate conformation between the relatively more accessible kinase active site and the mainly constrained kinase domain. Second, experiments have shown that ephrin-A5 stimulation further increases the EphA3 RTK WT phosphorylation level (Nievergall, Janes et al. 2010). This indicates that the EphA3 RTK was only partially activated before stimulation, which supports our assumption that the majority of EphA3 RTK WT possesses the auto-inhibited conformation and reduced substrate accessibility.

Interestingly, the structural alignment of dephosphorylated EphA3 kinase and EphA3 kinase-substrate complex has revealed that the substrate peptide and ordered JMS peptide interact with a different region of the EphA3 kinase domain (Figure 4.2b). This implicates that the JMS might not regulate the substrate binding directly. Davis, Walker et al. proposed a model in which the activation of EphA3 kinase occurs mainly through communication of activity state from the JMS to the AL through Tyr742, Ser768 and subtle changes in regions of the enzyme that are important for catalysis (Davis, Walker et al. 2008). Possibly,

structurally invisible regions of disordered JMS and AL cooperatively affect the substrate binding and phosphoryl transfer processes.

4.4 ephrin-A5 ligand stimulation enhances the EphA3 RTK substrate interaction in living cells

Activation of EphA3 by ephrin-A5 leads to the formation of large receptor clusters that expand laterally through Eph-Eph interactions. This signaling cluster propagation is ephrin-independent, which might enable the amplification of an initially small signal generated by cell contact and Eph-ephrin binding (Wimmer-Kleikamp, Janes et al. 2004; Pitulescu and Adams 2010).

With ES imaging we have studied the regulation of conformational dynamics of EphA3 RTK in living cells. However, excess injected Cy3.5-substrate interferes with the biological function of EphA3 RTK and thereby affects the related cell morphology. Interactions between EphA3 RTK and the substrate peptide lead to EphA3 RTK clustering about 1 hour after microinjection but without ligand stimulation (Figure 3.12a, WT; 3.13b, 2YE). This clustering might be caused by enhancement of kinase activity or ephrin-independent signaling (Wimmer-Kleikamp, Janes et al. 2004) or by the mechanical perturbation from microinjection. One of other possibilities can be that the injected substrate traps the active conformation in a fluctuating enzyme that explores all conformations. This will require a K_{cat}, which is much lower than the rate of conformational transition. Also, Cy3.5-substrate interacting with the kinase active site possibly restricts its interaction to other downstream target proteins and could competitively block access to the phosphorylated activation loop tyrosine that is required for endocytosis (Nievergall, Janes et al. 2010; Pitulescu and Adams 2010).

The addition of antibody cross-linked ephrin-Fc ligand further enhances EphA3 RTK cluster and more ES complexes are observed as evident from the decreased average donor fluorescence lifetime and the increased apparent FRET efficiency (Figure 3.12).

Interestingly, ES complexes initially concentrated on the plasma membrane and further extended throughout the cytoplasm after ephrin-A5 stimulation. It is possible that physical-chemical mechanisms such as free diffusion, reaction-diffusion, or active transport contribute to this process (Grecco, Schmick et al. 2011). The activated EphA3 upon ephrin-A5 stimulation undergoes endocytosis and transmits signals from the plasma membrane to other cytosolic compartments.

The ephrin-A5 stimulation increases the auto-phosphorylation level and changes the substrate accessibility of the kinase active site. It has been reported that the addition of 1 mM pervanadate enhances the EphA3 phosphorylation level more efficiently than ephrin-A5 stimulation (Wimmer-Kleikamp, Nievergall et al. 2008). Compared to the pervanadate inhibition, ephrin-A5 stimulation is only a moderate kinase activity perturbation. Activation of EphA3 RTK changes the phosphorylation equilibrium to a level that may not be detectable with the current ES imaging approach. Furthermore, the kinase phosphorylation reaction is typically transient and rapid, and the kinase activity might change on only a short time scale. Thus with current FRET-FLIM techniques, we can detect changes in ES intermediates but the sampling rate of FLIM might be too low to monitor the transient ES complex transitions during EphA3 signaling.

5 Summary and Outlook

Within this thesis, a direct approach to observe kinase-substrate interaction was developed to understand dynamic behaviors of EphA3 kinase in living cells. However, the known generally high *Km*-value for the peptide substrate, the acceptor concentration quenching effect and the photo acquisition time required for FLIM remained the obstacles for its wide application. Further mutagenesis and biochemical assays are required to assist the interpretation of the EphA3 RTK activity regulatory mechanism.

1. To overcome the low binding affinity of the kinase substrate, the EPHOPT substrate (encoding KQWDNYEp-YIW) with better binding affinity can be applied for EphA3 ES imaging despite the extra-phosphorylated tyrosine in the sequence.
2. Using a protein substrate containing the distal contact region could increase the binding affinity to RTK and stabilize the ES complex. Therefore, less acceptor labeled substrate is required to generate the detectable FRET signals with fewer disturbances to the cellular signal transduction.
3. Single molecule FRET (smFRET) has a time resolution in the ms range. The combination of smFRET and ES imaging may enable us to visualize the rapid phosphorylation turnover and obtain kinetic parameters for kinase catalysis. Nevertheless, up to date, smFRET is mainly used for the investigation of surface-immobilized protein-protein interactions, and its application for the cell-based assays is highly challenging.
4. A genetically encoded intra-molecular FRET-based biosensor can also be applied for ES imaging. The ERK2 ES sensor developed by Thies Klüßendorf (Klüßendorf 2011) proves the principle of this concept. In this strategy, the enzyme and the substrate are fused into an integrated protein, thus the probability of forming an ES complex

is increased with the high local substrate concentration. Crystal structure assisted molecular design, screening and optimization are required for this application.

5. Recombinant and purified EphA3c (2YF)-mCit and EphA3c (2YE)-mCit would allow us to characterize interactions between Cy3.5-substrate and MTs in a controlled *in vitro* system.
6. Observation, by ES imaging, of EphA3 RTK substrate interactions with different mutants, such as Y592F, Y602F single mutation and 2YF, K653R triple mutation, can further extend our understanding of the molecular regulatory mechanism of EphA3 RTK in living cells.
7. The application of ES imaging for other RTKs shall also be considered.

References

Adams, J. A. (2001). "Kinetic and Catalytic Mechanisms of Protein Kinases." Chemical Reviews **101**(8): 2271-2290.

Barford, D., A. J. Flint, et al. (1994). "Crystal structure of human protein tyrosine phosphatase 1B." Science **263**(5152): 1397-1404.

Bastiaens, P. I. and R. Pepperkok (2000). "Observing proteins in their natural habitat: the living cell." Trends Biochem Sci **25**(12): 631-637.

Bialy, L. and H. Waldmann (2005). "Inhibitors of Protein Tyrosine Phosphatases: Next-Generation Drugs?" Angewandte Chemie International Edition **44**(25): 3814-3839.

Binns, K. L., P. P. Taylor, et al. (2000). "Phosphorylation of Tyrosine Residues in the Kinase Domain and Juxtamembrane Region Regulates the Biological and Catalytic Activities of Eph Receptors." Mol. Cell. Biol. **20**(13): 4791-4805.

Breusegem, S. Y., M. Levi, et al. (2006). "Fluorescence correlation spectroscopy and fluorescence lifetime imaging microscopy." Nephron Exp Nephrol **103**(2): e41-49.

Brown, G. C. and B. N. Kholodenko (1999). "Spatial gradients of cellular phospho-proteins." FEBS Lett **457**(3): 452-454.

Cabrita, L. D., W. Dai, et al. (2006). "A family of E. coli expression vectors for laboratory scale and high throughput soluble protein production." BMC Biotechnol **6**: 12.

Chandra, A., H. E. Grecco, et al. (2012). "The GDI-like solubilizing factor PDE[delta] sustains the spatial organization and signalling of Ras family proteins." Nat Cell Biol **14**(2): 148-158.

Cheng, H.-C., I. Matsuura, et al. (1993). "In vitro substrate specificity of protein tyrosine kinases." Molecular and Cellular Biochemistry **127**(1): 103-112.

Clegg, R. M. (2009). Chapter 1 Förster resonance energy transfer,ÄîFRET what is it, why do it, and how it's done. Laboratory Techniques in Biochemistry and Molecular Biology. T. W. J. Gadella, Elsevier. **Volume 33:** 1-57.

Davis, T. L., J. R. Walker, et al. (2008). "Autoregulation by the Juxtamembrane Region of the Human Ephrin Receptor Tyrosine Kinase A3 (EphA3)." Structure **16**(6): 873-884.

Deribe, Y. L., T. Pawson, et al. (2010). "Post-translational modifications in signal integration." Nat Struct Mol Biol **17**(6): 666-672.

Eckhart, W., M. A. Hutchinson, et al. (1979). "An activity phosphorylating tyrosine in polyoma T antigen immunoprecipitates." Cell **18**(4): 925-933.

Förster, T. (1948). "Zwischenmolekulare Energiewanderung und Fluoreszenz." Annalen der Physik **437**(1-2): 55-75.

Gerritsen, H. C., A. V. Agronskaia, et al. (2009). Chapter 3 Time domain FLIM: Theory, instrumentation, and data analysis. Laboratory Techniques in Biochemistry and Molecular Biology. T. W. J. Gadella, Elsevier. **Volume 33:** 95-132.

Giepmans, B. N. G., S. R. Adams, et al. (2006). "The Fluorescent Toolbox for Assessing Protein Location and Function." Science **312**(5771): 217-224.

Grecco, H. n. E., M. Schmick, et al. (2011). "Signaling from the Living Plasma Membrane." Cell **144**(6): 897-909.

Himanen, J.-P. and D. B. Nikolov (2003). "Eph signaling: a structural view." Trends in Neurosciences **26**(1): 46-51.

Huang, B., M. Bates, et al. (2009). "Super-Resolution Fluorescence Microscopy." Annual Review of Biochemistry **78**(1): 993-1016.

Hubbard, S. R. (2004). "Juxtamembrane autoinhibition in receptor tyrosine kinases." Nat Rev Mol Cell Biol **5**(6): 464-471.

Hubbard, S. R. and J. H. Till (2000). "PROTEIN TYROSINE KINASE STRUCTURE AND FUNCTION." Annual Review of Biochemistry **69**(1): 373-398.
Hubbard, S. R., L. Wei, et al. (1994). "Crystal structure of the tyrosine kinase domain of the human insulin receptor." Nature **372**(6508): 746-754.
Hunter, T. (2009). "Tyrosine phosphorylation: thirty years and counting." Current Opinion in Cell Biology **21**(2): 140-146.
Hunter, T. and B. M. Sefton (1980). "Transforming gene product of Rous sarcoma virus phosphorylates tyrosine." Proceedings of the National Academy of Sciences **77**(3): 1311-1315.
Huyer, G., S. Liu, et al. (1997). "Mechanism of Inhibition of Protein-tyrosine Phosphatases by Vanadate and Pervanadate." Journal of Biological Chemistry **272**(2): 843-851.
Janes, P. W., E. Nievergall, et al. (2012). "Concepts and consequences of Eph receptor clustering." Seminars in Cell & Developmental Biology **23**(1): 43-50.
Janes, P. W., N. Saha, et al. (2005). "Adam Meets Eph: An ADAM Substrate Recognition Module Acts as a Molecular Switch for Ephrin Cleavage In trans." Cell **123**(2): 291-304.
Jares-Erijman, E. A. and T. M. Jovin (2003). "FRET imaging." Nat Biotech **21**(11): 1387-1395.
Jura, N., X. Zhang, et al. (2011). "Catalytic Control in the EGF Receptor and Its Connection to General Kinase Regulatory Mechanisms." Molecular cell **42**(1): 9-22.
Kapust, R. B., J. Tozser, et al. (2002). "The P1' specificity of tobacco etch virus protease." Biochem Biophys Res Commun **294**(5): 949-955.
Kholodenko, B. N. (2006). "Cell-signalling dynamics in time and space." Nat Rev Mol Cell Biol **7**(3): 165-176.
Klein, R. (2009). "Bidirectional modulation of synaptic functions by Eph/ephrin signaling." Nat Neurosci **12**(1): 15-20.
Klüßendorf, T. (2011). "Development of a FRET-Based Fluorescent Biosensor for ERK2 Activity." PhD dissertation from Max-Planck-Institut für molekulare Physiologie (http://hdl.handle.net/2003/28350).
Knighton, D., J. Zheng, et al. (1991). "Crystal structure of the catalytic subunit of cyclic adenosine monophosphate-dependent protein kinase." Science **253**(5018): 407-414.
Komatsu, N., K. Aoki, et al. (2011). "Development of an optimized backbone of FRET biosensors for kinases and GTPases." Molecular Biology of the Cell **22**(23): 4647-4656.
Kou, S. C., B. J. Cherayil, et al. (2005). "Single-Molecule Michaelis-Menten Equations." The Journal of Physical Chemistry B **109**(41): 19068-19081.
Krebs, E. G. and J. A. Beavo (1979). "Phosphorylation-Dephosphorylation of Enzymes." Annual Review of Biochemistry **48**(1): 923-959.
Krebs, E. G. and E. H. Fischer (1956). "The phosphorylase b to a converting enzyme of rabbit skeletal muscle." Biochimica et Biophysica Acta **20**(0): 150-157.
Kullander, K. and R. Klein (2002). "Mechanisms and functions of EPH and ephrin signalling." Nature Reviews Molecular Cell Biology **3**(7): 475-486.
Lackmann, M. and A. W. Boyd (2008). "Eph, a Protein Family Coming of Age: More Confusion, Insight, or Complexity?" Sci. Signal. **1**(15): re2-.
Lakowicz, J. R. (2006). "Principles of Fluorescence Spectroscopy, 4th edition."
Lemmon, M. A. and J. Schlessinger (2010). "Cell Signaling by Receptor Tyrosine Kinases." Cell **141**(7): 1117-1134.
Li, I., E. Pham, et al. (2006). "Protein biosensors based on the principle of fluorescence resonance energy transfer for monitoring cellular dynamics." Biotechnology Letters **28**(24): 1971-1982.

Li, M. Z. and S. J. Elledge (2007). "Harnessing homologous recombination in vitro to generate recombinant DNA via SLIC." Nat Methods **4**(3): 251-256.
Lieser, S. A., B. E. Aubol, et al. (2005). "Coupling phosphoryl transfer and substrate interactions in protein kinases." Biochimica et Biophysica Acta (BBA) - Proteins & Proteomics **1754**(1-2): 191-199.
Macdonald-Obermann, J. L. and L. J. Pike (2009). "The Intracellular Juxtamembrane Domain of the Epidermal Growth Factor (EGF) Receptor Is Responsible for the Allosteric Regulation of EGF Binding." Journal of Biological Chemistry **284**(20): 13570-13576.
McDonald, N. Q., J. Murray-Rust, et al. (1995). "The first structure of a receptor tyrosine kinase domain:a further step in understanding the molecular basis of insulin action." Structure **3**(1): 1-6.
Nievergall, E., P. W. Janes, et al. (2010). "PTP1B regulates Eph receptor function and trafficking." The Journal of Cell Biology **191**(6): 1189-1203.
Ostman, A., C. Hellberg, et al. (2006). "Protein-tyrosine phosphatases and cancer." Nat Rev Cancer **6**(4): 307-320.
Padilla-Parra, S. and M. Tramier (2012). "FRET microscopy in the living cell: Different approaches, strengths and weaknesses." BioEssays: n/a-n/a.
Parang, K. and P. A. Cole (2002). "Designing bisubstrate analog inhibitors for protein kinases." Pharmacology & Therapeutics **93**(2-3): 145-157.
Pasquale, E. B. (2008). "Eph-Ephrin Bidirectional Signaling in Physiology and Disease." Cell **133**(1): 38-52.
Pasquale, E. B. (2010). "Eph receptors and ephrins in cancer: bidirectional signalling and beyond." Nat Rev Cancer **10**(3): 165-180.
Patwardhan, P. and M. D. Resh (2011). "Myristoylation and Membrane Binding Regulate c-Src Stability and Kinase Activity." Mol. Cell. Biol. **30**(17): 4094-4107.
Peters, G. n. H., S. Branner, et al. (2003). "Enzyme kinetic characterization of protein tyrosine phosphatases." Biochimie **85**(5): 527-534.
Pitulescu, M. E. and R. H. Adams (2010). "Eph/ephrin molecules - a hub for signaling and endocytosis." Genes & Development **24**(22): 2480-2492.
Purushottam, M. D., H. Nai-Mu, et al. (2005). "Protein Tyrosine Phosphatases and their Inhibitors." Current Medicinal Chemistry **12**(1): 1-22.
Roskoski, J. R. (2004). "Src protein-tyrosine kinase structure and regulation." Biochemical and Biophysical Research Communications **324**(4): 1155-1164.
Sambrook, J. and D. Russell.W (2001). Molecular Cloning A Laboratory Manual 3rd edition.
Schultz, C. (2007). "Molecular tools for cell and systems biology." HFSP Journal **1**(4): 230-248.
Shi, G., G. Yue, et al. (2010). "EphA3 functions are regulated by collaborating phosphotyrosine residues." Cell Res **20**(11): 1263-1275.
Smock, R. G. and L. M. Gierasch (2009). "Sending Signals Dynamically." Science **324**(5924): 198-203.
Tara, L. D., R. W. John, et al. (2009). "Structural recognition of an optimized substrate for the ephrin family of receptor tyrosine kinases." FEBS Journal **9999**(9999).
Tarrant, M. K. and P. A. Cole (2009). "The Chemical Biology of Protein Phosphorylation." Annual Review of Biochemistry **78**(1): 797-825.
Taylor, S. S. and G. Ghosh (2006). "Protein kinases: Catalysis and regulation." Current Opinion in Structural Biology **16**(6): 665-667.
Taylor, S. S., E. Radzio-Andzelm, et al. (1995). "How do protein kinases discriminate between serine/threonine and tyrosine? Structural insights from the insulin receptor protein- tyrosine kinase." The FASEB Journal **9**(13): 1255-1266.

Tiganis, T. and A. M. Bennett (2007). "Protein tyrosine phosphatase function: the substrate perspective." Biochem J **402**(1): 1-15.
Ubersax, J. A. and J. E. Ferrell Jr (2007). "Mechanisms of specificity in protein phosphorylation." Nature reviews. Molecular cell biology **8**(7): 530-541.
Vearing, C. J. and M. Lackmann (2005). ""Eph receptor signalling; dimerisation just isn't enough"." Growth Factors **23**(1): 67-76.
Verveer, P. J., O. Rocks, et al. (2006). "Imaging Protein Interactions by FRET Microscopy: FRET Measurements by Acceptor Photobleaching." Cold Spring Harbor Protocols **2006**(6): pdb.prot4598.
Verveer, P. J., F. S. Wouters, et al. (2000). "Quantitative imaging of lateral ErbB1 receptor signal propagation in the plasma membrane." Science **290**(5496): 1567-1570.
Vintonyak, V. V., A. P. Antonchick, et al. (2009). "The therapeutic potential of phosphatase inhibitors." Current Opinion in Chemical Biology **13**(3): 272-283.
Walther, K. A., B. Papke, et al. (2011). "Precise measurement of protein interacting fractions with fluorescence lifetime imaging microscopy." Molecular BioSystems **7**(2): 322-336.
Wang, Y., J. Y. Shyy, et al. (2008). "Fluorescence proteins, live-cell imaging, and mechanobiology: seeing is believing." Annu Rev Biomed Eng **10**: 1-38.
Westheimer, F. (1987). "Why nature chose phosphates." Science **235**(4793): 1173-1178.
Wiesmann, C., K. J. Barr, et al. (2004). "Allosteric inhibition of protein tyrosine phosphatase 1B." Nat Struct Mol Biol **11**(8): 730-737.
Wiesner, S., L. E. Wybenga-Groot, et al. (2006). "A change in conformational dynamics underlies the activation of Eph receptor tyrosine kinases." EMBO J **25**(19): 4686-4696.
Wiley, H. S. and P. M. Burke (2001). "Regulation of Receptor Tyrosine Kinase Signaling by Endocytic Trafficking." Traffic **2**(1): 12-18.
Wimmer-Kleikamp, S. H., P. W. Janes, et al. (2004). "Recruitment of Eph receptors into signaling clusters does not require ephrin contact." Journal of Cell Biology **164**(5): 661-666.
Wimmer-Kleikamp, S. H., E. Nievergall, et al. (2008). "Elevated protein tyrosine phosphatase activity provokes Eph/ephrin-facilitated adhesion of pre-B leukemia cells." Blood **112**(3): 721-732.
Wybenga-Groot, L. E., B. Baskin, et al. (2001). "Structural Basis for Autoinhibition of the EphB2 Receptor Tyrosine Kinase by the Unphosphorylated Juxtamembrane Region." Cell **106**(6): 745-757.
Xu, W., S. C. Harrison, et al. (1997). "Three-dimensional structure of the tyrosine kinase c-Src." Nature **385**(6617): 595-602.
Yudushkin, I. A., A. Schleifenbaum, et al. (2007). "Live-cell imaging of enzyme-substrate interaction reveals spatial regulation of PTP1B." Science **315**(5808): 115-119.
Zhang, S. and Z.-Y. Zhang (2007). "PTP1B as a drug target: recent developments in PTP1B inhibitor discovery." Drug Discovery Today **12**(9,Äì10): 373-381.
Zhang, X., J. Gureasko, et al. (2006). "An Allosteric Mechanism for Activation of the Kinase Domain of Epidermal Growth Factor Receptor." Cell **125**(6): 1137-1149.
Zhang, Y. and L.-C. Yu (2008). "Single-cell microinjection technology in cell biology." BioEssays **30**(6): 606-610.
Zhang, Z. Y. (2002). "Protein tyrosine phosphatases: structure and function, substrate specificity, and inhibitor development." Annu Rev Pharmacol Toxicol **42**: 209-234.
Zhuang, G., S. Hunter, et al. (2007). "Regulation of EphA2 Receptor Endocytosis by SHIP2 Lipid Phosphatase via Phosphatidylinositol 3-Kinase-dependent Rac1 Activation." Journal of Biological Chemistry **282**(4): 2683-2694.

Acknowledgements

Firstly, I would like to thank my supervisor, Prof. Philippe Bastiaens, for giving me the opportunity to work with this challenging project in his laboratory. Thank you for the valuable hours of discussion and sharing your knowledge and experiences.

I am very appreciated that Prof. Roland Winter agrees to be my second examiner.

Thank-you to Dr. Hernan Grecco, for your helpful discussions, for the assistance as the physicist, and for the continuous supports no matter which project I was working on.

My team player, Ola Sabet, your continuous input, extensive helps with troubleshooting all aspects of my project and social life encouraged me to keep calm and carry on, thank you!

I would like to thank many current and past members from Bastiaens' lab including my lovely office team Justine Mondry, Martin Bierbaum, Kirstin Walther, Christian Schmees, Sina Koch, Zeta Xouri, Katrin Prost; The "ES" imaging fighter Thies Klüßendorf, Eulashini Chuntharpursat; The yeast group Christina Hecker, Johann Jarzombek, Lisa Karajannis, Ali Kinkhabwala; The football team Pedro Roda-Navarro, Björn Papke, Márton Gelléri, Sven Fengler, Rahul Ravindran; My microscopy teachers Mark Hink, Piet Lommerse, Nachiket Vartak, Anchal Chandra, Franziska Thorwirth; And many others, Joaquim Mendes, Malte Schmick, Hong-mei Han, Jenny Ibach, Leif Dehmelt, Peter Verveer, Prof. Frank Wehner, Eli Zamir, Markus Grabenbauer, Kondaiah Mogandi, Dina Truxius, Maja Sinn, Jens Christmann et al., to create the friendly working atmosphere in the department.

Thank-you to the lab mamas, Kirsten Michel, Hendrike Schütz, Jutta Luig, Anette Langerak, Petra Glitz and lab cousin Sven Müller, Michael Schulz, Lisaweta Roßmannek for your invaluable work to maintain the running lab.

I would like to thank Dr. Astrid Krämer and Tanja Forck for helping me to arrange the appointment with the boss and to organize documents for me to deal with the administrative affairs in Germany.

I would also like to thank Prof. Roger Goody, Yao-wen Wu, Qi-ang Li, Zhong Guo from department III and Gemma Triola, Long Yi, Ai-min Yang from department IV for their scientific discussion and technique assistance.

I want to thank the IMPRS to give me the finance support for my study.

Last but not the least, thank-you to my family. My wife, Yong-xiang Chen, is also my collaborator for the peptide substrate synthesis and characterization. Thank you is not enough to express my feeling, let me seal it with kiss. To my parents and parents in law, thank you for your understanding and to be patient. I am sorry that I have been away for too long and that I cannot be there when you need me. I am coming home soon.

Abbreviation

Aa	amino acid
AMPPNP	Adenosine 5’-(β,γ-imido)triphosphate
ATP	adenosine triphophate
bp	base pair
BSA	bovine serum albumine
C-terminal	carboxy-terminal
Da	Dalton
ddH_2O	double distilled water
DMEM	Dulbecco's modied Eagle's medium
DNA	deoxyribonucleic acid
dNTP	deoxynucleotide-5'-triphosphate
E. coli	epidermal growth factor
EGFP	enhanced green fluorescent protein
ES	enzyme-substrate
ESI-MS	electrospray ionization mass spectrometry
FCS	fluorescence correlation spectroscopy
FLIM	fluorescnet lifetime imaging microscopy
FPLC	fast protein liquid chromatography
FRET	forster resonance energy transfer
h	hour
HPLC	high-performance liquid chromatography
Km	michaelis menten constant
L	liter
MALDI-TOF MS	matrix-assisted laser desorption ionisation time of flight mass spectrometry
min	minute
MT	mutant
N-terminal	amine terminal
PTP	protein tyrosine phosphatase
RTK	Receptor tyrosine kinase
s	sencod
SLIC	sequence and ligation independent cloning
WT	wild type

Supplementary materials

Materials

Chemicals

2-Mercapto-ethanol	SERVA Electrophoresis GmbH
2'-deoxyadenosine-5'-triphosphate (dATP)	Invitrogen Life Technologies
2'-deoxycytidine-5'-triphosphate (dCTP)	Invitrogen Life Technologies
2'-deoxyguanosine-5'-triphosphate (dGTP)	Invitrogen Life Technologies
2'-deoxythymidine-5'-triphosphate (dTTP)	Invitrogen Life Technologies
Acetonitrile	Fluka Analytical
Adenosin-5'-triphosphate (ATP)	Sigma-Aldrich
Ammonium persulfate (APS)	SERVA Electrophoresis GmbH
Ampicillin sodium salt	SERVA Electrophoresis GmbH
Bromphenolblue	Sigma-Aldrich
Cy3 -NHS ester	GE healthcare
Cy3.5 -NHS ester	GE healthcare
Dimethyl sulfoxide (DMSO)	SERVA Electrophoresis GmbH
Disodium hydrogen phosphate (Na_2HPO4)	Merck KG
Dithiothreitol (DTT)	Fluka Analytical
DPBS	PAN
Ethanol	J.T.Baker
Ethidium bromide (10 mg/ml)	Fisher Scientific
Ethylenediaminetetraacetic acid (EDTA)	Fluka Analytical
Glycerol	GERBU Biotechnik GmbH
Imidazole	Merck KG
Isopropanol	J.T.Baker
Isopropyl β-D-thiogalactopyranoside (IPTG)	AppliChem GmbH
Kanamycine sulfate	GERBU Biotechnik GmbH
Magnesium chloride ($MgCl_2$)	Merck KG/J.T.Baker
Methanol	AppliChem GmbH
Monodispersed silicon particles (SiO_2-F-1434)	microparticles GmbH
Monopotassium phosphate (KH_2PO_4)	J.T. Baker
N-(2-Hydroxyethyl)Piperazine-N'-ethane-2-	GERBU Biotechnik GmbH
N,N,N',N'-Tetramethylene-diamine (TEMED)	Sigma-Aldrich
Phorbol-12-myristat-13-acetat (PMA)	AppliChem GmbH
Phosphatase Inhibitor Cocktail 1	Sigma-Aldrich
Phosphatase Inhibitor Cocktail 2	Sigma-Aldrich
Potassium chloride (KCl)	J.T.Baker
RedSafe (20,000x)	CHEMBIO
Sodium chloride (NaCl)	Fluka Analytical
Sodium dodecyl sulfate (SDS)	SERVA Electrophoresis GmbH

Sulfonic acid (HEPES)	GERBU Biotechnik GmbH
Trifluoroacetic acid (TFA)	Carl Roth GmbH
Tris-base	Carl Roth GmbH
Tris-HCl	J.T. Baker
Triton X-100	SERVA Electrophoresis GmbH
Tween 20	SERVA Electrophoresis GmbH
UltraPure™ Agarose	Invitrogen Life Technologies
Yeast extract	Fluka Analytical

Enzymes

AgeI-HF	New England Biolabs Inc.
BamH I	New England Biolabs Inc.
DpnI	New England Biolabs Inc.
EcoRI-HF	New England Biolabs Inc.
EcoRV	New England Biolabs Inc.
HindIII	New England Biolabs Inc.
NaeI Turbo™	Promega
NdeI	New England Biolabs Inc.
NotI	New England Biolabs Inc.
Paq5000 DNA polymerase	Agilent Technologies
Pfu Ultra High-Fidelity DNA polymerase	Stratagene
Phusion High-Fidelity DNA Polymerase	New England Biolabs Inc.
SalI	New England Biolabs Inc.
SfoI	New England Biolabs Inc.
Shrimp alkaline phosphatase (SAP)	New England Biolabs Inc.
Taq DNA polymerase	New England Biolabs Inc.
XhoI	New England Biolabs Inc.
XmaI	New England Biolabs Inc.

Antibody and Protein

Anti Phospho tyrosine pY72	
Anti-α-Tubulin	Sigma Aldrich
Anti-Eph receptor A2+A3+A4 (phospho Y588 + Y596) antibody (ab62256)	Abcam
Anti-EphA3	Abcam
Anti-Fc tag	Chembiochem
Ephrin-A5-Fc (Recombinant human chimera, 374-EA)	R&D systems
IRDye R• 680 donkey anti-rabbit IgG	LI-COR Biosciences
IRDye R• 680 goat anti-rabbit IgG	LI-COR Biosciences
IRDye R• 800CW donkey anti-mouse IgG	LI-COR Biosciences
IRDye R• 800CW goat anti-mouse IgG	LI-COR Biosciences

Plasmids

Supplementary Table 1, plasmids list

Plasmids name	Inserts	Resistance	Annotations
pEFBOS-EphA3	EphA3 wt full length	Amp	Provided by Prof. Martin Lackmann
pET24a-LIC-9R-mCherry-Substrate	poly-Arg , EphA3c substrate	Kan	For expressing recombinant 9R-mCherry-substrate
pET24a-LIC-C1 (SfoI)	SfoI site and TEV protease site	Kan	For N-terminal insertion
pET24a-LIC-EphA3c-mCitrine	Catalytic domain of EphA3	Kan	For expressing recombinant EphA3c-mCitrine
pET24a-LIC-mCitrine-EphA3c	Catalytic domain of EphA3	Kan	For expressing recombinant mCitrine-EphA3c
pET24a-LIC-N1 (NaeI)	NaeI site and TEV protease site	Kan	For C-terminal insertion
pET24a-LIC-PTP1Bc	Catalytic domain of PTP1B	Kan	For expressing recombinant PTP1Bc
pET24a(+)		Kan	Novagen
pmCherry-C1		Kan	Clontech
pmCherry-N1		Kan	Clontech
pmCitrine-C1		Kan	Clontech
pmCitrine-N1		Kan	Clontech
pmCitrine-N1-EphA3(2YE)-mCitrine	Full length EphA3 2YE mt with C-ternimal fused mCitrine	Kan	For mamalian cell expression
pmCitrine-N1-EphA3(2YF)-mCitrine	Full length EphA3 2YF mt with C-ternimal fused mCitrine	Kan	For mamalian cell expression
pmCitrine-N1-EphA3(3YF)-mCitrine	Full length EphA3 3YF mt with C-ternimal fused mCitrine	Kan	For mamalian cell expression
pmCitrine-N1-EphA3(wt)-mCitrine	Full length EphA3 wt with C-ternimal fused mCitrine	Kan	For mamalian cell expression
pmEGFP-C1		Kan	Clontech
pmEGFP-N1		Kan	Clontech

Amp: Ampicillin; Kan: Kanamycin,

Bacterial Strains

Name	Supplier	Resistance	Annotations
BL21 (DE3)	Novagen		Transformed plasmids containing T7 promoter driven expression are repressed until IPTG induction of T7 RNA polymerase from a lac promoter
BL21 (DE3) Rosseta	Novagen	Cam	As above, the extra rare codons AGG, AGA, AUA, CUA, CCC, and GGA are supplemented
XL-10 Golden	Stratagene	Tet, Cam	Routine used competent cells. Allows high transformation with large plasmid inserts

Tet, Tetracycline; Cam: Chloramphenicol.

Oligonucleotides

If it is not specially mentioned, all the oligonucleotides were purchased from Eurofins MWG Operon in HPSF (High Purity Salt Free) form.

Cell line

Name	Origin	Morphology	Supplier
COS-7	African green monkey kidney	Fibroblast	ATCC
Hela	Human cervical adenocarcinoma	Epithelial	ATCC
MDCK	Female cocker spaniel kidney	Epithelial	ATCC

Buffers

Protein purification

Buffer A: 50 mM Tris-HCl (pH8.0), 500 mM NaCl, 10% Glycerol

Buffer B: 50 mM Tris-HCl (pH8.0), 500 mM NaCl, 10% Glycerol, 500 mM Imidazol

Buffer C: 50 mM Tris-HCl (pH8.0), 150 mM NaCl, 10% Glycerol

Enzyme assay buffer

Kinase assay buffer: 20mM Tris-HCl (pH8.0), 150 mM NaCl, 10 mM $MgCl_2$, 0.1% TritonX-100

2×Phosphatase assay buffer: 50mM Bis-Tris propane (pH7.5), 50 mM NaCl, 2.5 mM EDTA, 2 mM TCEP and 0.025% NP-40.

Cell culture

1×PBS (pH 7.4): 137 mM NaCl, 10 mM Na_2HPO_4, 2.6 mM KCl, 1.8 mM KH_2PO_4

LB medium (Luria-Bertani Medium): 10 g tryptone, 5 g yeast extract, 10 g NaCl dissolve in 1 liter of deionized H2O. Sterilized by autoclaving for 20 minutes at 15 psi; For LB plate, add 15g/liter agar before autoclaving. Allow the medium to cool to 50-60°C before adding antibiotics. Mix the medium by swirling and plates can then be poured directly from the flask.

TB medium (Terrific Broth Medium): 10 g tryptone, 24 g yeast extract, 4 ml glycerol dissolved in 900 ml of deionized H2O. Sterilized by autoclaving for 20 minutes at 15 psi. Allow the solution to cool to 60°C or less, and then add 100 ml of sterile solution of 0.17 M KH_2PO_4, 0.72 M K_2HPO_4.

Imaging medium: DMEM without phenolred (PAN) +4.5 g/L glucose+ stabil L-Glutmin +sodium pyruvate +25 mM Hepes sterilized by filtration.

SDS PAGE and Western Blotting

5×SDS sample buffer: 250 mM Tris-HCl (pH6.8), 50% glycerol, 10% (w/v) SDS, and 500mM dithiothreitol (DTT), 0.5% bromophenol blue.

1×Tris-glycine electrophoresis buffer: 25 mM Tris-base, 192 mM glycine, 0.1% SDS

Resolving gel buffer: 1.5 M Tris-HCl (pH 8.8)

Stacking gel buffer: 1 M Tris-HCl (pH 6.8)

1×TBST: 100 mM Tris-HCl (pH 7.4), 150 mM NaCl, 0.1 % Tween 20

Transfer buffer: 25 mM Tris-base, 192 mM glycine, 0.1% SDS, 20% methanol

Staining buffer: dissolving 2.5 g of Coomassie Brilliant Blue R-250 with 500 ml methanol, 100 ml glacial acetic acid and 100 ml H_2O. fliter the solution through a Whatman No. 1 filter to remove any insoluble particles.

Destaining buffer: 500 ml methanol, 100 ml glacial acetic acid and 100 ml H_2O till 1 liter.

Biochemical kits

100x BSA (10mg/ml)	New England Biolabs Inc.
1kb/ 100bp ladder	Invitrogen Life Technologies
2-log DNA ladder	New England Biolabs Inc.
6x DNA gel loading buffer	Novagen
BigDye Terminator v3.1 cycle sequencing kit	Applied Biosystems
Bradford reagent	Sigma Aldrich
DyeEx 2.0 Spin kit	QIAGEN
NucleoBond Xtra Maxi EF kit	Macherey-Nagel GmbH & Co. KG.
QIAprep Spin Miniprep kit	QIAGEN
QIAquick Gel Extraction kit	QIAGEN
QIAquick PCR Purification kit	QIAGEN
QuikChange XL Site-Directed Mutagenesis kit	Stratagene

The others

1x TAE buffer: 40 mM Tris/Acetate (pH 7.5), 20 mM NaOAc, 1 mM EDTA

Borosilicate glass capillaries: 1.2 mm O.D. ×0.94mm I.D., GC120TF-10, Harvard Apparatus, Kent, UK

Instruments

Biochemistry and cell culture insturments

96 well plates reader	Thermo Fisher Scientific Inc
Äkta purifier	GE Healthcare
AutoFlow 5810 CO2 water jacketed incubator	NuAire Laboratory Equipment Supply
Cell biability analyzer Vi-Cell XR	Beckman Coulter GmbH
Centrifuge 5424	Eppendorf AG
Centrifuge 5810 R	Eppendorf AG

Chromatography Cabinet for Äkta-Systems, Unichromat 1500	UniEquip GmbH
Dry block heating systems QB04	Grant Instruments Ltd
Electrophorsis chamber	Carl Roth GmbH
Emulsi Flex-C5 Homogenizer	Avestin Inc
Gel-Doc XR system	Bio-Rad Laboratories, Inc.
Gene Pulser & Pulse controller	Bio-Rad Laboratories, Inc.
Ice machine	ZIEGRA Eismaschinen GmbH
Incubator 1500 with 37C	Flow Laboratories Inc
Incubator shaker I26	New Brunswick Scientific
Incubator with 16C WTB	Binder GmbH
Innova 400 incubator sharker	New Brunswick Scientific
Knick pH meter 766	Calimetic
Laboratory balance 1574	Sartorius AG
Licor infared imaging system, Odyssey	LI-COR Biosciences GmbH
Milli-Q Q-POD	Millipore Co
Nanodrop sepectrophotometer ND-1000	PEQLab Biotechnologie GmbH
PCR master cycler epgradient	Eppendorf AG
Power Pac HC high current power supply and chamber	Bio-Rad Laboratories, Inc.
Precisa 62A balance	PESA Waagen GmbH
Refrigerated centrifuge 5417R	Eppendorf AG
Safe Imager	Invitrogen
Sonopuls HD2200	BANDELIN electronic GmbH & Co. KG
Sorvall Discovery 100	Thermo Fisher Scientific Inc
Sorvall RC 6+ centrifuge	Thermo Fisher Scientific Inc
Sorvall RC-5B, refrigerated super speed centrifuge	Dupont Instruments
Sorvall rotor with swing bucket AH-629	Dupont Instruments
Spectrophotometer DU800	Beckman Coulter GmbH
Thermoshaker TS1	Biometra

Microscopy and related instruments

Climate chamber	EMBL
FluoView 1000	Olympus
Inject man NII	Eppendorf AG
Leica lght microscpy DM IRB	Leica Microsystems GmbH
Leica sp5	Leica Microsystems GmbH
LSM 510 meta	Carl Zeiss
P-97 Flaming/Brown Micropipette Puller	Sutter Instrument Co.
Picoharp	Picoquant

S. Figure1, High resolution HPLC and accurate LCMS of peptide substrate

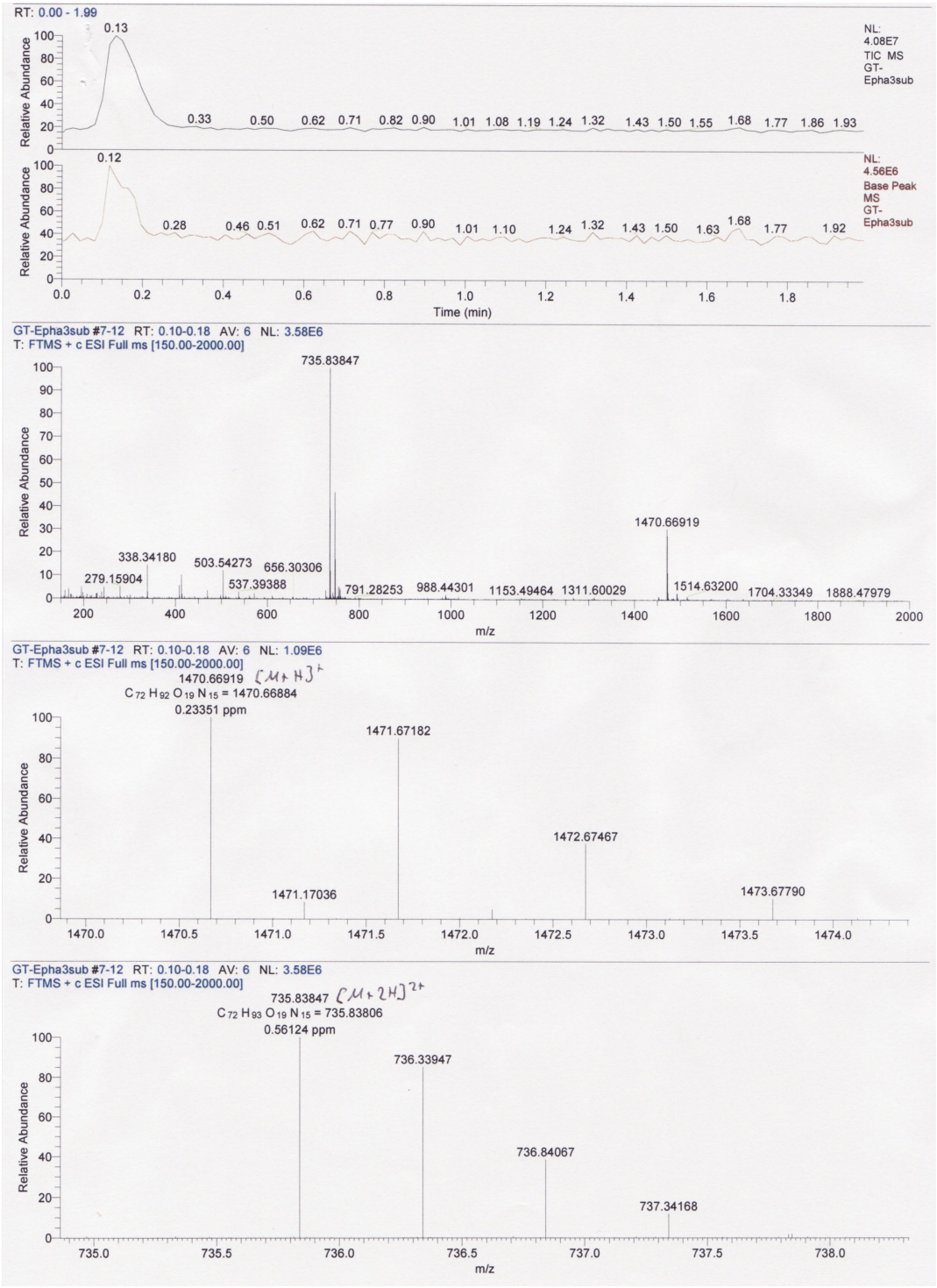

HR-ESIMS: *m/z*: calcd for $C_{72}H_{92}N_{15}O_{19}$: 1470.66939 $[M+H]^+$, found 1470.66919 $[M+H]^+$

S. Figure2, ESI-MS analysis of Cy3.5 labeled peptide substrate

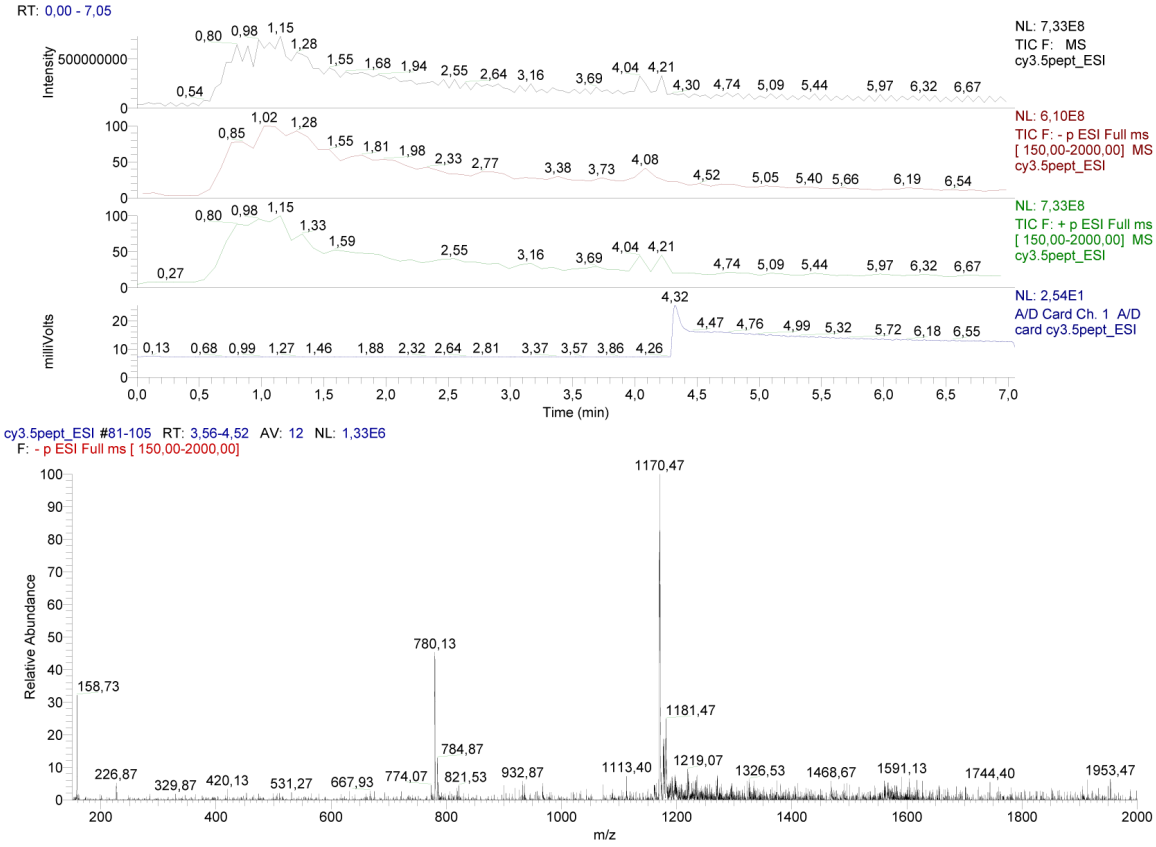

ESI-MS: m/z: calcd for $C_{111}H_{129}N_{17}O_{32}S_4$: 1170.39 $[M+2H]^+$, found 1170.47 $[M+2H]^+$ and 780.13 $[M+3H]^+$.

Publications

1. van Wijk, S. J. L., E. Fiskin., Mateusz, P., Francesco, P., **Hou. J**, et al. (2012). "Fluorescence-Based Sensors to Monitor Localization and Functions of Linear and K63-Linked Ubiquitin Chains in Cells." Molecular cell **47**(5): 797-809.
2. Grecco, H. E., P. Roda-Navarro., Andreas, G., **Hou. J**, et al. (2010). "In situ analysis of tyrosine phosphorylation networks by FLIM on cell arrays." Nature Method **7**(6): 467-472.
3. Cheng, F., **Hou. J**, et al. (2010). "Functional interaction between MutL and 3'-5' Exonuclease X in Escherichia coli." Archives of Biochemistry and Biophysics **502**(1): 39-43.
4. Wang, T., Xiang. Y., **Hou. J**, et al. (2008). "ABP41 is Involved in the Pollen Tube Development via Fragmenting Actin Filaments." Molecular Plant **1**(6): 1048-1055.
5. Fan, X., **Hou. J**, et al. (2004). "Identification and Characterization of a Ca^{2+}-Dependent Actin Filament-Severing Protein from Lily Pollen." Plant Physiology **136**(4): 3979-3989.